SECURITY CLASSIFICATION OF THIS PAGE

# REPORT DOCUMENTATION PAGE

| | |
|---|---|
| 1a. REPORT SECURITY CLASSIFICATION<br>Unclassified | 1b. RESTRICTIVE MARKINGS |
| 2a. SECURITY CLASSIFICATION AUTHORITY | 3. DISTRIBUTION/AVAILABILITY OF REPORT<br>Approved for distribution and unlimited public release |
| 2b. DECLASSIFICATION/DOWNGRADING SCHEDULE | |
| 4. PERFORMING ORGANIZATION REPORT NUMBER(S)<br>Report 5 | 5. MONITORING ORGANIZATION REPORT NUMBER(S) |
| 6a. NAME OF PERFORMING ORGANIZATION<br>Department of Chemical Engineering<br>University of Illinois<br>6b. OFFICE SYMBOL (If applicable) | 7a. NAME OF MONITORING ORGANIZATION<br>Office of Naval Research |
| 6c. ADDRESS (City, State and ZIP Code)<br>Urbana, Illinois 61801 | 7b. ADDRESS (City, State and ZIP Code)<br>Arlington, Virginia 22217 |
| 8a. NAME OF FUNDING/SPONSORING ORGANIZATION<br>8b. OFFICE SYMBOL (If applicable) | 9. PROCUREMENT INSTRUMENT IDENTIFICATION NUMBER<br>N00014-82-K-0324 |
| 8c. ADDRESS (City, State and ZIP Code) | 10. SOURCE OF FUNDING NOS.<br>PROGRAM ELEMENT NO.: NR 657-728 / PROJECT NO. / TASK NO. / WORK UNIT NO. |
| 11. TITLE (Include Security Classification) Studies of the Wall Shear Stress in a Turbulent Pulsating Pipe Flow --Unclassified | |
| 12. PERSONAL AUTHOR(S)<br>Mao, Zhuo-Xiong and Thomas J. Hanratty, Project Supervisor | |
| 13a. TYPE OF REPORT<br>Progress<br>13b. TIME COVERED<br>FROM 1981 TO 1984 | 14. DATE OF REPORT (Yr., Mo., Day)<br>1984, September, 24<br>15. PAGE COUNT<br>172 |
| 16. SUPPLEMENTARY NOTATION | |
| 17. COSATI CODES<br>FIELD / GROUP / SUB. GR. | 18. SUBJECT TERMS (Continue on reverse if necessary and identify by block number)<br>Wall shear stress, turbulence, pulsating flow, unsteady flow |

19. ABSTRACT (Continue on reverse if necessary and identify by block number)

See reverse side

| | |
|---|---|
| 20. DISTRIBUTION/AVAILABILITY OF ABSTRACT<br>UNCLASSIFIED/UNLIMITED ☐ SAME AS RPT. ☐ DTIC USERS ☐ | 21. ABSTRACT SECURITY CLASSIFICATION |
| 22a. NAME OF RESPONSIBLE INDIVIDUAL | 22b. TELEPHONE NUMBER (Include Area Code)<br>22c. OFFICE SYMBOL |

DD FORM 1473, 83 APR EDITION OF 1 JAN 73 IS OBSOLETE.

SECURITY CLASSIFICATION OF THIS PAGE

# Studies of the Wall Shear Stress in a Turbulent Pulsating Pipe Flow

Measurements are presented of the time variation of the wall shear stress caused by the imposition of a sinusoidal oscillation on a turbulent pipe flow. The amplitude of the oscillation is small enough that a linear response is obtained and the dimensionless frequency, $\omega^+$, is large compared to that studied by most previous investigators. The most striking feature of the results is a relaxation effect, similar to what has been observed for flow over a wavy surface, whereby the phase angle characterizing the temporal variation of the wall shear stress undergoes a sharp change over a rather narrow range of $\omega^+$. At $\omega^+$ larger than the median frequency of the turbulence there appears to be an interaction between the imposed flow oscillation and the turbulence fluctuations in the viscous sublayer, which is not described by present theories of turbulence.

# STUDIES OF THE WALL SHEAR STRESS IN A TURBULENT PULSATING PIPE FLOW

PREPARED BY
ZHUO-XIONG MAO
THOMAS J. HANRATTY, PROJECT SUPERVISOR

FOR
THE OFFICE OF NAVAL RESEARCH, ARLINGTON, VA 22217
CONTRACT NOOO14-82-K-0324
PROJECT NR 657-728

REPORT 5

DEPARTMENT OF CHEMICAL ENGINEERING
UNIVERSITY OF ILLINOIS
URBANA, ILLINOIS
61801

SEPTEMBER, 1984

# STUDIES OF THE WALL SHEAR STRESS IN A TURBULENT PULSATING PIPE FLOW

Prepared by

Zhuo-Xiong Mao
Thomas J. Hanratty, Project Supervisor

for

The Office of Naval Research, Arlington, VA 22217
Contract N00014-82-K-0324
Project NR 657-728

Report 5

Department of Chemical Engineering
University of Illinois
Urbana, Illinois
61801

September, 1984

TABLE OF CONTENTS

# LIST OF FIGURES

Figure | Page

# CHAPTER 1. INTRODUCTION

The imposition of a sinusoidal oscillation, of amplitude $a_o$ and angular frequency $\omega$, on the mean flow through a circular pipe causes a periodically varying pressure and velocity field. If the amplitude is small enough a linear response is obtained for which

$$\frac{dp}{dx} = \frac{d\bar{p}}{dx} + a_o \left|\frac{d\hat{p}}{dx}\right| \cos(\omega t), \tag{1.1}$$

$$u = \bar{u}(y) + a_o \left|\hat{u}(y)\right| \cos(\omega t + \theta_u(y)), \tag{1.2}$$

with x being the distance in the flow direction, y, the distance from the wall and t, the time. The time mean pressure gradient and the time mean velocity of the undisturbed flow are designated by $\frac{d\bar{p}}{dx}$ and $\bar{u}(y)$; and the amplitudes of the oscillations, by $a_o \left|\frac{d\hat{p}}{dx}\right|$ and $a_o\left|\hat{u}(y)\right|$. These oscillations in the velocity field give rise to oscillations in the shear stress at the wall,

$$\tau_w = \bar{\tau}_w + a_o \left|\hat{\tau}_w\right| \cos(\omega t + \theta_{\tau_w}), \tag{1.3}$$

with $\theta_{\tau_w} = \lim_{y\to 0} \theta_u(y)$. This thesis presents the results of experiments with a fully developed pipe flow in which $\left|\hat{\tau}_w\right|$ and $\theta_{\tau_w}$ are related to $\left|\frac{d\hat{p}}{dx}\right|$.

The experiments were conducted at high enough frequencies so that over most of the flow field inertia is dominant; that is,

$$\rho \frac{\partial u}{\partial t} = -\frac{\partial p}{\partial x}. \tag{1.4}$$

A solution of (1.4) for a sinusoidally varying pressure gradient gives

$$\omega\rho \left|\hat{u}\right| = \left|\frac{d\hat{p}}{dx}\right| , \tag{1.5}$$

and

$$\theta_u = -\frac{\pi}{2} \tag{1.6}$$

Equation (1.5) reveals that, for this high frequncy range, even small oscillations in the volumetric flow can cause oscillations in the pressure gradient many times larger than the mean pressure gradient.

Close to the wall turbulent and viscous stresses become important so that u is related to the pressure gradient through the eqation

$$\rho \frac{\partial u}{\partial t} = -\frac{\partial p}{\partial x} + \mu \frac{\partial^2 u}{\partial y^2} + \frac{\partial \tau^{(t)}}{\partial y} \quad . \tag{1.7}$$

The principal theoretical problem in predicting how the oscillations in the wall shear stress are related to the oscillations in the pressure gradient is the determination of how an oscillating pressure gradient affects the turbulence. The experiments therefore provide a test of closure methods that predict $\tau^{(t)}$ close to a wall.

The motivation for this work has come from studies of the wall shear stress variation along a solid wavy surface over which a turbulent fluid is flowing. It was found, in these experiments, that the amplitude and phase angle characterizing the periodic variation of the shear stress along the wavy surface depend on the wave number, $\alpha = 2\pi/\lambda$, and that this dependency could be scaled by using the kinematic viscosity, $\nu$, and the friction velocity, $u^*$. Of most interest was the discovery of a sharp change in phase angle with increasing dimensionless wave number at $\alpha^+ \approx .0005 \sim .001$.

The interpretation of these results depends on the prediction of the wave-induced variation of the Reynolds stress in the viscous wall region ($0 \leq y^+ \leq 40$). The turbulence modeling differs from that for flow over a flat plate in that the waves induce a periodic variation of the streamline curvature and of the pressure gradient at the surface. Thorsness, Morrisroe and Hanratty (1978) and Abrams and Hanratty (1984) have suggested that the observed behavior of the phase angle is primarily associated with the influence of wave-induced pressure gradient. They argue that at small $\alpha^+$ an equilibrium situation exists whereby the flow behaves similarly to that observed in gradually expanding or converging channels. Regions of the wave surface with a favorable pressure gradient experience a damping of the turbulence in the viscous wall region; regions with an unfavorable pressure gradient experience an enhancement of the turbulence. As $\alpha^+$ increases the pressure gradient varies so rapidly along the wave surface that the turbulence in the viscous wall region does not respond immediately. There is a relaxation from an equilibrium turbulence to a frozen turbulence, manifested by the sharp change in the phase angle with increasing $\alpha^+$.

The principal goal of the present experiments was to investigate the above interpretation by carrying out studies of the influence of a rapidly varying pressure gradient on the behavior of the viscous wall region, without having to deal with additional complications associated with streamline curvature. Of particular interest is the determination of whether the variation of $\theta_{\tau_w}$ with $\omega^+$ shows the same relaxation phenomenon observed for flow over wavy surfaces.

In order to meet the above objective it was necessary to design the experiment so that $\omega^+$ was of the same order as the median frequency of

the turbulent velocity fluctuations in the vicinity of the wall ($\approx .01 \times 2\pi$). At the same time, it was desirable to avoid the use of imposed oscillations of unrealistically high frequency. This was done by using a system which has low frequency turbulence; i.e., water flow in a 19.4 cm pipe. Sinusoidal oscillations with frequencies of 0.325 Hz and 0.625 Hz were introduced into the system with a plunger type pump. The amplitudes of the oscillations were made small enough that the pressure gradient and wall shear stress varied sinusoidally with time. The shear stress variation at the wall was measured with electrochemical probes mounted flush with the wall. It was not possible to design this experiment so that the frequency response of the probe did not have to be taken into account. An advantage of using the electrochemical method is that an analytical, rather than an experimental, scheme can be used to correct for frequency response.

A number of previous investigators have studied the influence of controlled flow oscillations on turbulent flows. An excellent review has recently been presented by Carr (1981). The work presented in this thesis differs in that attention is focused on the wall shear stress variation and on high values of $\omega^+$. Previous investigators have found that the influence of the oscillations on the mean velocity profile is small and that their effect on turbulence is felt principally in the region close to the wall. For this reason, there exists a need for measurements of the wall shear stress oscillations. In most previous studies accurate velocity measurements were not made close enough to the wall to determine the time varying velocity gradient at the wall. Recently, Tu and Ramaprian (1983) reported on direct measurements of the wall shear stress with flush mounted wall heat transfer probes.

These were at values of $\omega^+$ too low to observe the relaxation phenomenon in which we are interested. In addition, there are uncertainties about these results since no attempt was made to take into account the frequency response of the probe.

The measurements of the velocity gradient at the wall in this study confirms previous findings by a number of researchers that the mean flow field is actually not affected by the imposed flow oscillation. The measurements in this work have also verified the assumption that there exists a linear response of the wall shear stress to the imposition of a small amplitude flow oscillation. Moreover, it is found that the relative phase and amplitude which characterize this response can be correlated by a single parameter $\omega^+$, which combines the effects of frequency and Reynolds number in the range of variables studied.

The most striking feature of the results is a relaxation effect, similar to what has been observed for flow over a wavy surface, whereby the phase angle characterizing the temporal variation of the wall shear stress undergoes a sharp change over a rather narrow range of $\omega^+$. At $\omega^+$ larger than the median frequency of the turbulence, there appears to be an interaction between the imposed flow oscillation and turbulence fluctuations in the viscous sublayer, which is not described by present theories of turbulence.

# CHAPTER 2. LITERATURE SURVEY

Unsteady laminar flows in simple cases were solved analytically or asymptotically. These solutions are summarized by Schlichting (1979). G. Stokes (1851) and later Lord Rayleigh (1911) considered flow over an infinite flat plate which executes linear harmonic oscillations parallel to itself--Stokes second problem. Th.Sexl (1930) and S. Uchida (1956) treated the case of flow through a pipe under the influence of a periodic pressure gradient. An unique parameter $\Omega = \sqrt{\frac{\omega}{\nu}}\, r_o$ was found to characterize periodic laminar flow in the pipe, where $\omega$ is angular frequency, $\nu$, kinematic viscosity and $r_o$, radius of the pipe. At very low values of $\Omega$, the velocity profile of the oscillation component is in phase with the imposed variation of pressure gradient and behaves like that in steady state flow with the same mean flow rate. At very large values of $\Omega$, the oscillation flow field moves like a solid body in the core region of the pipe and varies rapidly close to the wall. For this case the phase of the oscillation velocity lags of the pressure gradient by 90° in the center of the pipe, but only by 45° at the neighborhood of the wall. This indicates that for high frequencies viscous effect plays an important role in the wall region and that the outer flow can be considered as inviscid.

Because the complexities and difficulties encountered in experimental studies of unsteady turbulent flow, researches in this area were rarely seen in literature a decade ago. Interest in this area has been growing rapidly in recent years. Partially, this is because results from such studies are needed in solving many urgent engineering problems. More importantly, this recent interest can be associated with

the development of instrumentation and the availability of new techniques of data acquisition and processing. Researchers have been mainly concentrated on three subjects: Oscillating flow at transitional Reynolds number, turbulent boundary flow over flat plate under periodic exitation of free stream flow, and turbulent oscillating pipe flow.

In this chapter, a brief survey of studies on these subjects will first be presented. Then, studies in a relevant field, turbulent flow over wavy surfaces, will be discussed. Finally, what has been learned from these studies, and what are still unclear or controversial points will be summarized.

## 2.1 Oscillating Flow at Transitional Reynolds Numbers

Experience with steady flows subjected to spatial pressure gradients has shown that pressure gradients can have a significant effect on the critical Reynolds number. In an unsteady flow, one would intuitively expect that the effects of unsteadyness on the flow structure will be stronger on flows in the neighborhood of transition than on flows at very large Reynolds numbers. This is because the transition process can be sensitive to the strong acceleration/deceleration occurring in the unsteady flow.

Gerrard (1971) studied pulsating flow at a mean flow Reynolds number of 3370 in a pipe of diameter 3.81 cm with an amplitude of oscillation 0.57 of mean and a period of 12.2 s. A sheet of dye was produced by electrolysis from a fine wire stretched across the diameter. Cinephotography was used to record the motion of dyes and to find the velocity profile. The most significant information obtained from the experiment was that the flow was laminarized during the acceleration phase of flow cycle.

Ramaprian & Tu (1980) found a similar phenomenon in their experiments, in which oil flow was used in a circular pipe at a mean Reynolds number of about 2100. Two frequencies (1.75 Hz and 0.057 Hz) were studied with an amplitude 30% of the mean flow. Instantaneous velocities were measured by using laser-Doppler anemometry (LDA). They observed that flow oscillation increased the critical Reynolds number and, under certain conditions, even brought about laminarization of the flow.

Shemer & Wygnaski (1981) approached the problem differently. They compared the responses of laminar and turbulent air flow to an imposed oscillation at the same mean Reynolds number 4,000. The undisturbed flow was laminar, and turbulence was triggered artificially by inserting a cylinder into the pipe. The hot wire anemometer was used to measure the instantaneous velocity. They found that turbulent flow responded to an imposed pressure variation differently from laminar flow for the same Reynolds number and the same pressure variation. They argued that the frequency parameter $\Omega$ no longer controls the flow because the relevant viscosity is no longer $\nu$ but turbulent eddy viscosity $\nu_t$, which is orders of magnitude larger than $\nu$. The effective $\Omega$ is thus much lower. They also observed a partial laminarization of the trubulent flow during the acceleration of the flow. The time averaged Reynolds stress $-\overline{u'v'}$ and the phase averaged Reynolds stress $-<u'v'>$ were measured with an x-wire. It was observed that $-\overline{u'v'}$ was independent of the flow oscillation and that the phase of $-<u'v'>$ lagged behind the pressure variation.

There have been some efforts to consider the stability of time periodic flows. Davis (1976) reviewed research works in this area. The term unstable for a basic periodic state is defined by Davis as

a situation for which a disturbance experiences net growth over each modulation cycle. A state for which every disturbance decays at every instant is defined as stable. The most interesting result coming from these studies is that there may be a state which is neither unstable nor stable; i.e., the basic state is subject to a disturbance that grows during part of the cycle, that attains an appreciable amplitude, that decays during another part of the cycle. This type flow is called transiently stable by Davis. Both theoretical and experimental works indicate that Stokes layers are stable to small disturbances but are apparently unstable to disturbances of large amplitude. For a fully developed pipe flow, Sarphaya (1966) found that the critical Reynolds number increases with increasing amplitude until it reaches a peak value, after which it falls to values below the critical Reynodls number for steady flow. More works need to be done in this area.

## 2.2 Periodic Turbulent Boundary Flow Over Flat Plate

The first experimental study on periodic turbulent boundary flow over a flat plate was done by Karlsson in 1959. Amplitudes of the sinusoidal oscillation up to 34% of the mean velocity and frequencies ranging from 0 to 48 cycles/sec were used in a boundary layer wind tunnel with zero pressure gradient. The hot wire was used to measure the mean velocity, the amplitude of in- and out-of phase components of the first harmonic of the periodic oscillation, and the intensity of higher harmonics and turbulence. One of the most remarkable results of his work is that effects due to non-linear interactions between turbulence and the oscillation, even for oscillation amplitude

as large as 34% of the free stream velocity, are so small that the effect of the oscillation on the mean flow is negligible.

The group at ONERA/CERT in France has done extensive studies on a turbulent boundary layer subjected to sinusoidal free-stream oscillations. Cousteix et al. (1977) used hot-wire anemometers to measure time averaged and phase averaged velocity profiles as well as turbulent intensity and shear stress across the boundary layer. They found that the general behavior of the boundary layer and that the structure of the turbulence were not fundamentally affected by the unsteadiness of the flow. A quasi-steady approximation, combined with a mixing length model, was used to describe unsteady flow at small Strouhal number. Later, Cousteix et al. (1981,1982) extended the range of their experiments so that they covered Strouhal numbers from 1.5 to 18. They confirmed that the mean flow field is not affected by the unsteady effects, even up to a Strouhal number 18. An interesting finding is that the main parameters of boundary layer like displacement and momentum thickness $\delta_1$, $\theta$ ... oscilate as Strouhal number increases. Direct measurements of the wall shear stress was done by using a modified hot wire gauge. They found that the law of the wall is not valid for evaluating wall shear stress if the Strouhal number is larger than 5.

Parikh et al. (1981,1982) and Jayaraman et al. (1982) designed a test section in which the boundary layer was subjected to a sinusoidally varying, adverse, free-stream gradient. In the upstream of the test section, a trubulent boundary layer grew under steady, zero-pressure gradient conditions. This provided a well-defined inlet condition to

the test section, which is especially important for computation of the flow. The imposed oscillation frequencies used in their experiments covered a range from quasi-steady ($f \cong 0$) to values approaching the bursting frequency. The relative amplitudes of oscillations were 5% and 25% of mean free stream velocity at the end of the test section. The laser Doppler velocimeter was used to measure the phase averaged velocity profiles and turbulent intensities. Again, they found the time averaged flow field is essentially unaffected by the imposed unsteadiness and considered this a consequence of two observations: (a) The time-averaged Reynolds stress distribution across the boundary layer is unaffected; and (b) the Reynolds stresses arising from the organized velocity fluctuations under imposed oscillation are negligible compared to the Reynolds stresses due to the random fluctuations. However, the periodic flow was observed to be very strongly dependent on the frequency of the excitation. At high frequencies of oscillation, the boundary layer thickness and turbulent Reynolds stress were found to become frozen over the oscillation cycle while they were observed to have significant variation over the cycle at low frequencies. The steady form of the law of the wall was found not to be valid for the phase averaged velocity profile at high frequencies. The authors argued that the Strouhal number based on the streamwise distance in the test section and the local mean free-stream velocity is a very important parameter for the periodic velocity.

The unsteady separating turbulent boundary layer over a flat plate has been studied extensively by Simpson et al. (1981,1983a,1983b). The hot-wire anemometer, the laser Doppler velocimeter and a thermal flow direction probe were used to measure the effects of the sinusoidal

unsteadiness of the free-stream velocity on the separating turbulent boundary layer at low oscillation frequency.

The measurements showed that, upstream of any flow reversal or backflow, the flow behaves in a quasi-steady manner. The semi-logarithmic law-of-the-wall velocity profile was found to be valid at each phase of the cycle. The phase and the amplitude of phase averaged velocity was found close to the values in the free-stream. However, downstream of the detachment, large variations of the amplitude and phase of the phase averaged velocity and the phase averaged turbulent properties were observed across the boundary layer. They considered that unsteady effects produce a hysteresis in relationships among flow parameters. The effect of unsteadiness was described by the authors in the following way: As the free-stream velocity, during a cycle, begins to increase, the detached shear layer decreases in thickness, and the fraction of time that the flow moves downstream $\hat{r}_{pu}$ increases as backflow fluid is washed downstream. As the free-stream velocity nears the maximum value in a cycle, the increasingly adverse pressure gradient causes progressingly greater near wall backflow at downstream locations while $\hat{r}_{pu}$ remains high at the upstream part of the detached flow. After the free-stream velocity begins to decelerate, the detached shear layer grows in thickness and the location where flow reversal begins moves upstream. Higher oscillation frequencies were found to enhance this hysteresis phenomenon.

## 2.3 Periodic Trubulent Pipe (or Channel) Flow

Lu (1973) studied the effects of pulsations on a fully developed turbulent pipe flow of water in a range of Reynolds numbers from 16,000 to 81,600, with amplitudes from 0 to 0.17 of mean flow rate and frequencies

from 0 to 1.5 Hz. The hot-film anemometer was used to measure the velocity profiles and turbulent intensities. It was found that, when the pulsating amplitude is small compared to the mean velocity the Reynolds number and the dimensionless pulsating frequency are two important parameters to characterize the flow, whereas, when the amplitude is not small, the pulsating amplitude becomes an additional parameter. The time averaged flow field was found not be affected by the unsteadiness. They suggested that a quasi-steady model can be used to predict periodic flow at low oscillation frequency.

Achary and Reynolds (1975) made measurements of periodic turbulent air flow in a channel by using a hot-wire anemometer. The Reynolds number, based on channel half width, was 13,800; the amplitudes were 2.4% and 3.6% of the channel centerline mean velocity; the oscillation frequencies were 24 Hz and 40 Hz respectively. The data show that the periodic velocity is constant over most of the flow, with all the intersting effects occurring in a region very close to the wall. The turbulent Reynolds stress perturbations were found to be out of phase with the strain-rates, indicating a viscoelastic type of repsonse. An interesting finding is the strange difference between the 25 Hz data and 40 Hz data. They suggested that there might be an interaction between the turbulence and the imposed oscillation since the data 40 Hz was taken at a frequency close to the "bursting frequency". Several closure models were developed by the authors for the purpose of predicting the experimental results. The models were not satisfactory. However, they revealed several key features which need to be incorporated in a successful model.

Misushina et al. (1973) made comprehensive experimental studies of the velocity profiles, turbulent intensities and auto-correlations in a

2 cm turbulent pipe flow with imposed oscillation frequencies from 0.125 Hz to 1.32 Hz and a time averaged Reynolds number $10^4$. Electrochemical probes were used to measure the instantaneous velocity and the turbulent intensity. The bursting period was measured by determining the delay time of the location of the maximum in the auto-correlation curve of velocity fluctuations. The authors suggested that turbulent pulsating flows can be classified into two groups by means of a critical period of pulsation, which is equal to the maximum time between bursts. When the periods of pulsation are longer than the critical period, the velocity profiles are similar to those for steady flow and the intensity of turbulent fluctuations don't vary in a cycle. For shorter periods, the velocity profiles are different from those for steady flow and the intensity of turbulent fluctuations oscillates in a cycle with its phase about 180° different from that of the phase averaged velocity. Later Mizushina et al. (1975) investigated the effects of pulsations on the bursting phenomenon. They claimed that if the pulsating period is in the range of the burst period, turbulence is generated near the wall by the flow pulsation. Then, the generated turbulence propagates radially to the centre-line of the tube. The mean propagation time of the generated turbulence from the origin to the centre-line of the tube agrees well with the mean burst period of steady turbulent flow and is independent of the pulsation period. In the experiment, they found that when pulsation period is less than the mean burst period, the turbulent intensity oscillates near the wall and is frozen to its steady state value in the central region of the pipe. This was interpreted by the authors to mean that the oscillation induced intensity near the wall doesn't have time to penetrate to the center in a period.

Ohmi et al. (1976) reported experimental results on the velocity distribution in pulsating turbulent pipe flow. They found that the time-averaged distribution in pulsating flow agrees well with that of steady flows, and that the oscillating velocity profiles can be described by approximate solutions derived from a four-region model for a steady turbulent flow. They further (1978) solved the fundamental equation for pulsating turbulent flow numerically by using this four-region eddy viscosity model. The calculation indicates that a quasi-steady treatment, i.e., a time dependent friction velocity, should be applied at low oscillation frequencies. The numerical results also suggest that the effect of large Reynolds number could be similar to that of low frequency on the oscillating flow field.

Kirme (1979) used the laser Doppler velocimeter to measure velocities in pulsating turbulent pipe flow. He pointed out that there might be a small region of backflow near the wall for some combinations of flow parameters. For a larger Reynolds number, higher frequencies and amplitudes of oscillation are needed to form these zones. Kirme also reported that an eddy viscosity model based on turbulent kinetic energy can not predict the pulsating flow correctly.

Kita et al. (1980) proposed a fluctuating eddy viscosity model for Reynolds stress, based on a five region model in steady turbulent flow, and compared it with experimental data. They suggested that a modified Strouhal number $\Omega/\sqrt{Re^*}$, where $\Omega = \sqrt{\frac{\omega}{\nu}}\, r_0$ and $R_e^* = \frac{u^* d}{\nu}$, characterizes the volumetric flow rate, while $\Omega/R_e^*$ is an important parameter near the wall. Their experimental data show no effect of oscillation on the time-mean velocity profile.

Binder and Kuney (1982) measured periodic velocity oscillations near the wall in a turbulent pulsating channel water flow. They reported that with a proper optical arrangement it was possible to use LDV to make measurements as close as 0.25 mm from the wall corresponding to $y^+ \tilde{=} 2$ for $\bar{u}_c = 17.5$ cm/s. The results showed that the mean flow and the mean turbulent intensity were not affected by the forced oscillation. The amplitude and the phase shift profiles of the periodic component approximately follow the laminar Stokes solution at high frequency. At low frequencies, the phase shift near the wall decreases to slightly negative values while the amplitude remains close to the Stokes solution. The phase averaged longitudinal trubulent intensity was not found to be simply proportional to the velocity oscillations. The authors argued that in the region near the wall the Stokes thickness $\ell_s^+$ nondimensionalized with the mean viscous sublayer thickness is an important parameter needed to characterize turbulent pulsating flow.

Ramaprian and Tu (1982,1983a,1983b) reported detailed experimental data on the instantaneous velocity and wall shear stress at a mean Reynolds number 50,000 in a fully developed turbulent pipe flow in which the volumetric flow rate was varied sinusoidally with frequencies 0.5 Hz and 3.6 Hz, and amplitudes 64% and 15% of the mean flow rate respectively. In contrast to most other researchers, they concluded from their data that both the time mean velocity profiles and the time mean turbulent intensities are affected by the imposed unsteadiness. They considered that these effects are caused by the combination of high oscillation frequency (approaching the bursting frequency) and large amplitude. The phase averaged turbulent intensity data showed that at high frequency

the turbulent intensity remains frozen throughout the cycle in the outer region and that at lower frequency it experiences significant variation. The authors also reported the results of direct measurement of wall shear stress in turbulent pulsating flow with flush mounted hot film gauges. The phase shifts of the wall shear stress were found to be of the order of 10 degrees in their experimental range. However, since they didn't consider the frequency response of the probe, serious errors could be present in the results obtained at high frequency. They suggested a modified Strouhal number $\frac{\omega d}{u^*}$, which uses friction velocity instead of bulk mean velocity, to characterize unsteady turbulent flow. With this parameter, they classified turbulent pulsating flow into five regimes, based on the histogram of the intervals between the bursts measured by Mizushina et al.

## 2.4 Turbulent Flow Over a Solid Wavy Surface

A relevant field to the pulsating flow is turbulent flow over a wavy surface. The spatial periodic variation of the solid boundary causes changes of pressure in the fluid field and of shear stress along the wall. For small enough wave amplitudes a linear response is obtained whereby the functions describing the pressure and shear stress variation have a single harmonic. Abrams et al. (1981) presented necessary conditions for a linear response.

A review of the measurements of wall shear stress and pressure profiles over a solid wavy surface is given by Abrams (1984).

The analysis carried out by Thorsness et al. (1978) indicates that the phase angle characterizing the shear stress variation at the wall is a unique function of a wave number, $\alpha^+ = 2\pi\nu/\lambda u^*$, made dimensionless

with the kinematic viscosity, $\nu$, and the friction velocity, $u^*$. The amplitude of the shear stress variation, made dimensionless by using $\nu$ and $u^*$, is found to vary linearly with $a_0 u^*/\nu$, where $a_0$ is the amplitude of the wave. The ratio of these two dimensionless amplitudes is also an unique function of $\alpha^+$. To predict the phase shift and amplitude of the wall shear stress, the principal problem is the specification of the wave induced Reynolds stresses. Thorsness (1975) tried several models and found that the mixing length model of Loyd et al. (1970) did the best job in accounting for the influence of wave induced variations of the turbulence properties. This model predicts a sharp variation of phase shift of the wall stress in a narrow range of $\alpha^+$. However, his experimental data didn't cover a large enough range of conditions to show this variation.

Abrams (1984) extended the experimental range by using the same wavelength $\lambda$ = 2 inches, and by increasing the maximum value of $u^*$ by a factor of four. The experimental data indeed show a sharp change in the phase shift of the wall shear stress for $6 \times 10^{-4} < \alpha^+ < 10^{-3}$. The interpretation of this observation is the relaxation effect of turbulent flow in the viscous wall region, associated with the wave-induced variation of the pressure gradient. The physical process underlying this phenomenon is not yet understood. Although, the author tried a k-$\varepsilon$ model to introduce the relaxation in a more natural way, the calculated results couldn't describe the data any better. His work also indicates that the wave induced variation of pressure gradient has a more important effect on the turbulence in the viscous sublayer than the wave induced variations of streamline curvature.

## 2.5 Summary of the State of Art

Due to large efforts made in the last decade, many experimental and some computational results have been published. Nevertheless, turbulent pulsating flow is still not understood.

Most of the data have shown that the time mean flow field is unaffected by the imposed oscillation. Only the data reported by Ramaprian and Tu indicate a slight effect of oscillation on the time mean velocity profile and on the time mean turbulent intensity. One can at least get an impression that the mean flow field is not sensitive to the imposed unsteadiness.

Nevertheless, the phase averaged velocity field is strongly dependent on the characteristics of the external excitation, especially of the oscillation frequency. The response of turbulent flow to an imposed oscillation is qualitatively similar to that of laminar flow. At very low frequency, the velocity profile for both flows at each instant is the same as that in a steady flow with the same flow rate. At high frequency, the periodic velocity component for both flowsis flat in the center of the pipe and has a rapid change near the wall. However, the response of these two flows are quantitatively very different. For example, the frequency parameter $\Omega = \sqrt{\frac{\omega}{\nu}}\, r_0$, which characterizes the laminar periodic flow, is no longer a suitable parameter for the turbulent case. Although several frequency parameters have been suggested for characterizing turbulent pulsating flow, no definite conclusion can be deduced. Moreover, the amplitude of the imposed oscillation and the mean Reynolds number are other important factors affecting the turbulent pulsating flow. Their effects, especially when they combine with the effect of frequency, are not yet understood.

There are some data on the phase averaged intensity of turbulent fluctuations reported in the literature. It seems that the phase averaged intensity oscillates around the mean value at low frequency, while at high frequency it varies only near the wall and is frozen to the mean value in the region away from the wall. The phase of the intensity variation also shifts from that of the velocity, indicating that there is no simple relation between the turbulent properties and the rate of strain.

The effects of the imposed oscillation on the turbulent structure are not clear. Most of the existing data for the Reynolds stress are calculated from the measurement of the velocity profile by using the momentum balance equation. The large possible errors in data obtained in such manner make it difficult to come to any definite conclusions. A strong interation between the turbulent and the imposed oscillations at some resonant frequency, anticipated by several researchers, is still not substantiated.

The response of the flow in near wall region is very important for understanding turbulent pulsating flow. Because the inertial effect is much less in this region than in the outer flow, the data near the wall offer a good test for turbulent models used to predict the flow. However, few reliable measurements have been made in this region. At high frequencies, the layer, in which the periodic velocity has spatial variation, is so thin that measurement of its properties is not feasible. Therefore, the wall shear stress measurements in the present study are needed to obtain a better understanding of a turbulent pulsating flow.

# CHAPTER 3. THEORY

In this chapter, a theoretical framework for the description of turbulent pipe flow with a superimposed organized sinusoidal excitation is presented. The flow field is decomposed into three components: the time mean flow, an oscillation flow and the turbulent fluctuations. The equation governing the oscillation flow is derived and solved numerically by applying several turbulent models based on the eddy viscosity concept. Then, the phase and the amplitude characterizing the variation of shear stress at the wall are calculated at different flow conditions. The results are compared with experimental data in Chapter 5.

## 3.1 Triple Decomposition and the Phase Average

In steady turbulent flow, the problem is attacked by decomposing flow variables into time mean values and turbulent fluctuations. The term "steady" means the time mean values are independent of time. When an organized unsteadiness is imposed on the system, this additional component, which is a deterministic function of time, has to be included. Following Hussain and Reynolds (1970), the problem can be formulated as

$$E(\underline{x},t) = \overline{E}(\underline{x}) + \tilde{E}(\underline{x},t) + E'(\underline{x},t), \tag{3.1}$$

where $\overline{E}(\underline{x})$ is the time mean value of $E(\underline{x},t)$ at a given location $\underline{x}$, $\tilde{E}(\underline{x},t)$, the organized response component due to the imposed excitation and $E'(\underline{x},t)$, the turbulent fluctuation.

In order to separate the three components of a flow variable, two different averaging procedures are employed; i.e., a time average and an

ensemble average. The time average is conventionally used in steady turbulent studies, and is defined as

$$\overline{E}(\underline{x}) = \lim_{T\to\infty} \frac{1}{T} \int_0^T E(\underline{x},t)\, dt \tag{3.2}$$

In discrete form, the time average is the average of a large number of samples in a record of sufficiently long duration. That is

$$\overline{E}(\underline{x}) = \lim_{N\to\infty} \frac{1}{N} \sum_{i=1}^{N} E\,(\underline{x},t_i) \tag{3.3}$$

In practice, the total time duration in which all the samples were taken is large compared to the imposed excitation period and the longest turbulent fluctuation period.

The ensemble average is defined as the average over a large number of realizations of the same phenomenon and is expressed as

$$<E(\underline{x},t)> = \lim_{N\to\infty} \frac{1}{N} \sum_{i=1}^{N} E_i\,(\underline{x},t)\,, \tag{3.4}$$

where i identifies a particular realization. This procedure can be used to extract the organized flow component.

When the imposed excitation is periodic, the ensemble average is equivalent to a phase average. Each cycle is considered as a realization in the ensemble average. So, a phase average is defined as the average of samples from a large number of cycles at a fixed cycle angle.

$$<E(\underline{x},\theta)> = \lim_{N\to\infty} \frac{1}{N} \sum_{n=0}^{N-1} E(\underline{x},\theta + 2\pi n),\quad 0 \le \theta \le 2\pi, \tag{3.5}$$

where $\theta$ is the cycle phase angle. In practice, N is a large finite number.

By definition, phase averaging eliminates the term involving random turbulent fluctuations, namely,

$$< E(\underline{x},\theta) > = \overline{E}(\underline{x}) + \tilde{E}(\underline{x},\theta) \ , \tag{3.6}$$

and the time average of $< E(\underline{x},\theta) >$ eliminates the oscillation component,

$$\overline{< E(\underline{x},\theta) >} = \overline{E}(\underline{x}) \ . \tag{3.7}$$

From the above expressions, the oscillation component and the turbulent fluctuations can be extracted from the flow variable as

$$\tilde{E}(\underline{x},t) = < E(\underline{x},t) > - \overline{E}(\underline{x}) \ , \tag{3.8}$$

and

$$E'(\underline{x},t) = E(\underline{x},t) - < E(\underline{x},t) > \ . \tag{3.9}$$

Figure 3.1 displays the relations among these components.

## 3.2 Governing Equation for the Oscillation Component

The governing equations for an incompressible flow of a Newtonian fluid in a circular pipe are given by the Nevier-Stokes equation in cylindrical coordinates,

$$\rho\left(\frac{\partial u}{\partial t} + v\,\frac{\partial u}{\partial r} + \frac{w}{r}\,\frac{\partial u}{\partial \theta} + u\,\frac{\partial u}{\partial x}\right) = -\,\frac{\partial p}{\partial x} + \mu\left[\frac{1}{r}\,\frac{\partial}{\partial r}\left(r\,\frac{\partial u}{\partial r}\right) + \frac{1}{r^2}\,\frac{\partial^2 u}{\partial \theta^2} + \frac{\partial^2 u}{\partial x^2}\right] , \tag{3.10}$$

$$\rho\left(\frac{\partial v}{\partial t} + v\,\frac{\partial v}{\partial r} + \frac{w}{r}\,\frac{\partial v}{\partial \theta} - \frac{w^2}{r} + u\,\frac{\partial v}{\partial x}\right) =$$

$$-\,\frac{\partial p}{\partial r} + \mu\left[\frac{\partial}{\partial r}\left(\frac{1}{r}\,\frac{\partial}{\partial r}\,(rv)\right) + \frac{1}{r^2}\,\frac{\partial^2 v}{\partial \theta^2} - \frac{2}{r^2}\,\frac{\partial w}{\partial \theta} + \frac{\partial^2 v}{\partial x^2}\right] , \tag{3.11}$$

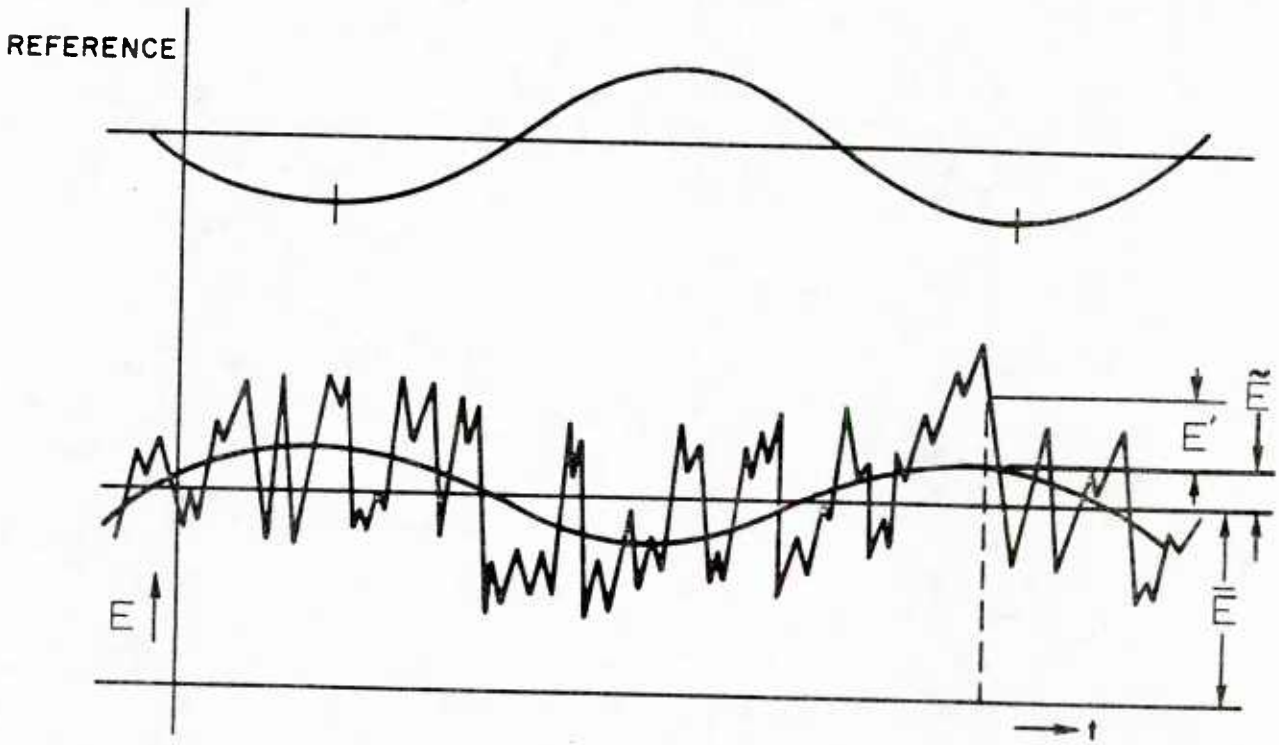


Figure 3.1 Time and phase averages

$$\rho\left(\frac{\partial w}{\partial t} + v\frac{\partial w}{\partial r} + \frac{w}{r}\frac{\partial w}{\partial \theta} + \frac{vw}{r} + u\frac{\partial w}{\partial x}\right) =$$

$$-\frac{1}{r}\frac{\partial p}{\partial \theta} + \mu\left[\frac{\partial}{\partial r}\left(\frac{1}{r}\frac{\partial}{\partial r}(rw)\right) + \frac{1}{r^2}\frac{\partial^2 w}{\partial \theta^2} + \frac{2}{r^2}\frac{\partial v}{\partial \theta} + \frac{\partial^2 w}{\partial x^2}\right] \qquad (3.12)$$

along with the continuity equation

$$\frac{1}{r}\frac{\partial}{\partial r}(rv) + \frac{1}{r}\frac{\partial w}{\partial \theta} + \frac{\partial w}{\partial x} = 0 \ , \qquad (3.13)$$

where u, v, and w are the velocity components in the axial direction x, the radial direction r and the angular direction $\theta$ respectively.

For turbulent pulsating flow, the triple decomposition is applied to these flow variables as,

$$\begin{aligned} u &= \bar{u} + \tilde{u} + u' \ , \\ v &= \bar{v} + \tilde{v} + v' \ , \\ w &= \bar{w} + \tilde{w} + w' \ , \\ p &= \bar{p} + \tilde{p} + p' \ . \end{aligned} \qquad (3.14)$$

If the flow is fully developed and symmetric in the angular direction, time averages of equations (3.10) to (3.14) are dramatically simplified. The components of velocities such as $\bar{v}$, $\tilde{v}$, $\bar{w}$, $\tilde{w}$ vanish. The equation describing the time mean flow becomes

$$0 = -\frac{d\bar{p}}{dx} - \frac{1}{r}\frac{d}{dr}\left(r\,\bar{\tau}^{(t)}\right) + \frac{\mu}{r}\frac{d}{dr}\left(r\frac{d\bar{u}}{dr}\right) \qquad (3.15)$$

To solve this equation, the Reynolds stress, $\bar{\tau}^{(t)} = -\rho\,\overline{u'v'}$, has to be specified in terms of $\bar{u}$ and r. This is the so called closure problem. In turbulent pulsating flow, one principal question is whether the time

mean turbulent property $\overline{u'v'}$ is affected by the imposed unsteadiness. If it is not affected, the closure method used for steady flow can be applied and the time mean velocity profile will be the same as that for steady flow. Otherwise, the time mean velocity profile in pulsating flows should show some differences from that in steady flow, and a new closure method needs to be developed.

In a similar way, the equation describing phase averaged flow is derived by phase averaging equations (3.10) to (3.13). It is given as

$$\rho \frac{\partial < u >}{\partial t} = - \frac{\partial < p >}{\partial x} - \frac{1}{r} \frac{\partial}{\partial r} (r < \tau^{(t)} >) + \frac{\mu}{r} \frac{\partial}{\partial r} \left( \frac{r \partial < u >}{\partial r} \right), \qquad (3.16)$$

where $< \tau^{(t)} > = -\rho < u'v' >$ is the phase averaged Reynolds stress.

The equation which governs the oscillation component is obtained by subtracting the mean flow equation (3.15) from the phase averaged equation of motion (3.16). This gives

$$\rho \frac{\partial \tilde{u}}{\partial t} = -\frac{\partial \tilde{p}}{\partial x} + \frac{1}{r} \frac{\partial}{\partial r} [ r (< \tau^{(t)} > - \bar{\tau}^{(t)}) ] + \frac{\mu}{r} \frac{\partial}{\partial r} \left( r \frac{\partial \tilde{u}}{\partial r} \right) . \qquad (3.17)$$

In order to solve equation (3.17) the oscillation induced Reynolds stress $\tilde{\tau}^{(t)}$, which is defined as

$$\tilde{\tau}^{(t)} = < \tau^{(t)} > - \bar{\tau}^{(t)} \qquad (3.18)$$

has to be specified. This is done by following Boussinesq's (1877) concept of turbulent eddy viscosity, which relates Reynolds stress to the velocity gradient by an analogy with Newton's law of viscosity. The phase averaged Reynolds stress then can be written as

$$< \tau^{(t)} > = \rho < \nu_t \frac{\partial u}{\partial y} > . \qquad (3.19)$$

If it is assumed that the imposed small oscillation induces a variation of turbulent eddy viscosity $\tilde{\nu}_t$ around its time mean value $\overline{\nu}_t$, the oscillation induced Reynolds stress is expressed as

$$\tilde{\tau}(t) = \rho \left( \overline{\nu}_t \frac{\partial \tilde{u}}{\partial y} + \tilde{\nu}_t \frac{\partial \overline{u}}{\partial y} \right) , \tag{3.20}$$

if it is assumed that the second order term $\tilde{\nu}_t \frac{\partial \tilde{u}}{\partial y}$ is negligible. The time mean Reynold stress is written as

$$\overline{\tau}(t) = \rho \left( \overline{\nu}_t \frac{\partial \overline{u}}{\partial y} \right) . \tag{3.21}$$

## 3.3 Time Mean Flow

Most previous researchers have found that the time mean flow is not affected by imposed small amplitude flow oscillations. Experimental results on wall shear stress obtained in the present study also support this conclusion. Therefore, the time mean velocity profile is calculated by using the same eddy viscosity $\overline{\nu}_t$ that represents a steady flow. That is,

$$\overline{u} = \int_0^y \frac{(1 - y/r_0)\, \overline{u}^{*2}}{(\nu + \overline{\nu}_t)} \, dy \tag{3.22}$$

where $\overline{u}^*$ is the time mean friction velocity and $r_0$ is the radius of the pipe. An empirical equation proposed by Reichardt (1951) is used for the prediction of $\overline{\nu}_t$ in the core region:

$$\frac{\overline{\nu}_t}{\nu} = \frac{ky^+}{6} \left( 1 + \frac{r}{r_0} \right) \left[ 1 + 2 \left( \frac{r}{r_0} \right)^2 \right] , \tag{3.23}$$

where k is the von Karman constant, 0.4.

In the region close to the wall, the mixing-length theory is used so that

$$\bar{\nu}_t = \bar{\ell}^2 \frac{\partial \bar{u}}{\partial y} , \tag{3.24}$$

where $\bar{\ell}$, the mixing length characterizing the undisturbed flow, is described by the Van Driest function,

$$\bar{\ell} = ky\ [1 - \exp(-\bar{D}_m)] \tag{3.25}$$

The term $\bar{D}_m$ is a damping function defined as

$$\bar{D}_m = \frac{y\bar{\tau}_w^{1/2}}{\rho^{1/2}\nu A} \tag{3.26}$$

and $\bar{\tau}_w$ is the time mean shear stress at the wall. The Van Driest damping constant A is 26 for pipe flow. By combining (3.24) and (3.25), the eddy viscosity in the wall region can be expressed as

$$\frac{\bar{\nu}_t}{\nu} = 0.5 \left[-1 + \sqrt{1 + 4k^2y^{+2}(1 - \exp(-\bar{D}_m))^2\ (1 - y/r_0)}\right] \tag{3.27}$$

Figure 3.2 gives the radial variation of eddy viscosity, calculated from (3.23) and (3.27). It is seen that the change of the eddy viscosity from the near wall region to the outer flow is fairly smooth. The velocity profile calculated from (3.22) at Re = 23,000 is compared with the data measured by Nikuradse (1932) in Figure 3.3. The good agreement between the two indicates that the eddy viscosity model used in this study is able to describe the time mean flow field. Furthermore, the Van Driest formula is a continuous function from the wall through the viscous sublayer and into the fully developed turbulent region. This feature

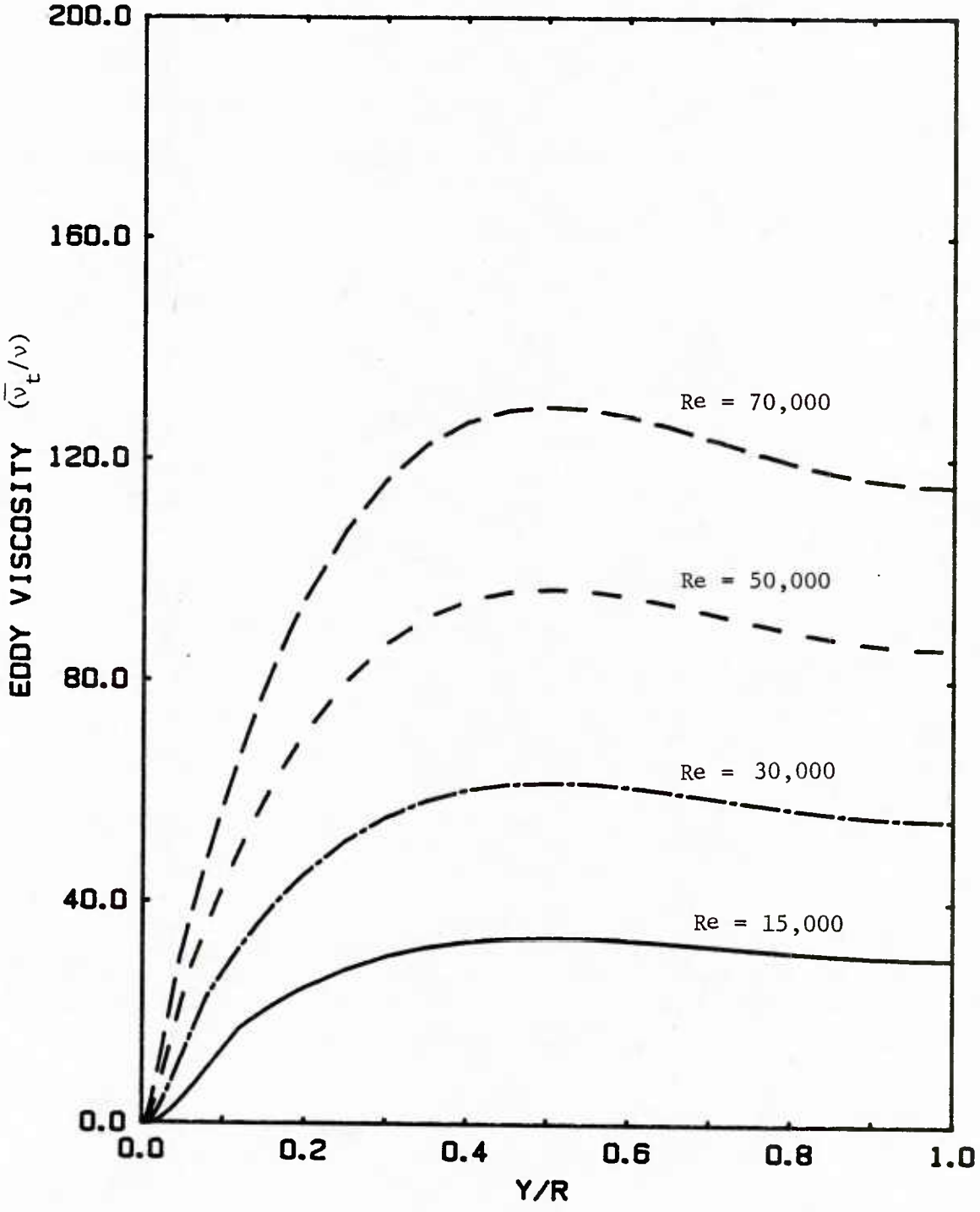


Figure 3.2 Turbulent eddy viscosity distribution for steady flows (calculated from (3.23) and (3.27))

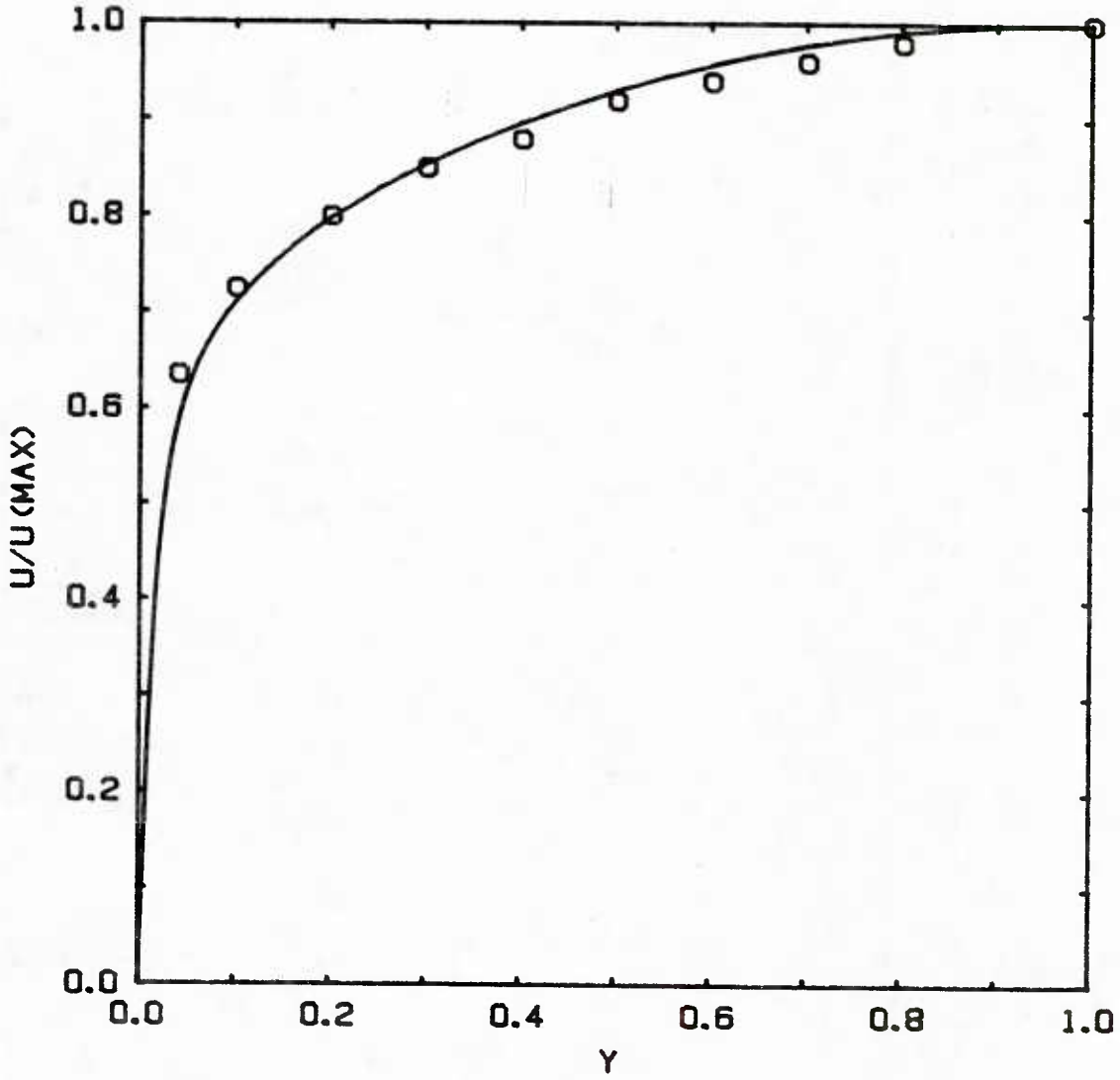


Figure 3.3 Time mean velocity profile of steady turbulent flow [Re = 23,000, data from Nikuradse (1932), — calculated from (3.22)]

is very important in modeling an oscillating flow for which the flow variation at high frequency case is confined to a thin layer near the wall.

### 3.4 Quasi-laminar Model (Model A) for the Induced Flow Oscillation

The simplest model for the induced flow oscillations involves the assumption that induced oscillations of the Reynolds stress are zero, $\tilde{\tau}(t) = 0$. This means that the induced oscillations in a turbulent flow will behave as the same as for a laminar pulsating flow, i.e.,

$$\frac{\partial \tilde{u}}{\partial t} = -\frac{1}{\rho}\frac{\partial \tilde{p}}{\partial x} + \frac{\nu}{r}\frac{\partial}{\partial r}\left(r\frac{\partial \tilde{u}}{\partial r}\right) \tag{3.28}$$

This equation has been solved by Th. Sexl (1930) and S. Uchida (1956) for a pressure gradient with sinusoidal variation in time,

$$-\frac{1}{\rho}\frac{\partial \tilde{p}}{\partial x} = a\cos\omega t\ . \tag{3.29}$$

The model is assumed to approximate the flow at very high frequencies, for the spatial variation of the imposed flow oscillations is confined to a very thin layer near the wall where turbulence has negligible effect. At high frequencies, $\Omega = \sqrt{\frac{\omega}{\nu}}\, r_0 >> 1$, the solution is given as

$$\tilde{u}(r,t) \doteq \frac{a}{\omega}\left\{\sin\omega t - \sqrt{\frac{r_0}{r}}\exp\left[-\sqrt{\frac{\omega}{2\nu}}\,(r_0 - r)\right]\right.$$

$$\left.\sin\left[\omega t - \sqrt{\frac{\omega}{2\nu}}\,(r_0 - r)\right]\right\}\ . \tag{3.30}$$

This equation shows that the oscillation component in the central portion of the pipe behaves as a solid body, i.e.,

$$\tilde{u}(t)\Big|_{r\to 0} = \frac{a}{\omega} \sin \omega t \ . \tag{3.31}$$

Only in the Stokes layer, of thickness

$$\delta_s = \sqrt{\frac{2\nu}{\omega}} \ , \tag{3.32}$$

does the velocity $\tilde{u}$ (r,t) change rapidly with distance y from the wall. The velocity gradient at the wall is obtained from (3.30) as

$$\frac{\partial \tilde{u}}{\partial y}\Big|_{y=0} \doteq \frac{a}{\omega\nu} \cos \left(\omega t - \frac{\pi}{4}\right) \ . \tag{3.33}$$

Certain phase relations are observed from these equations: The central velocity lags the pressure gradient by 90°. The velocity gradient at the wall lags by only 45°, i.e., the velocity gradient at the wall is 45° ahead of the central velocity.

Figure 3.4 shows the oscillation velocity profile at eight phases for laminar flow when the dimensionless frequency parameter $\Omega = 150$. The oscillation velocity component is made dimensionless with the amplitude of velocity at the center line. It is seen that the velocity is flat at $Y > 0.04$ for each instant. The changes of the velocity happen in a thin layer $Y < 0.04$. The crossover of the velocity profiles at different phases in the near wall region indicates the phase shift of the velocity. The frequency effects on the oscillation velocity can be easily seen in Figure 3.5 and Figure 3.6, where the amplitude and the phase of the oscillation component are plotted for four different $\Omega$. As $\Omega$ increases, the variation of the oscillation component is confined to a thinner

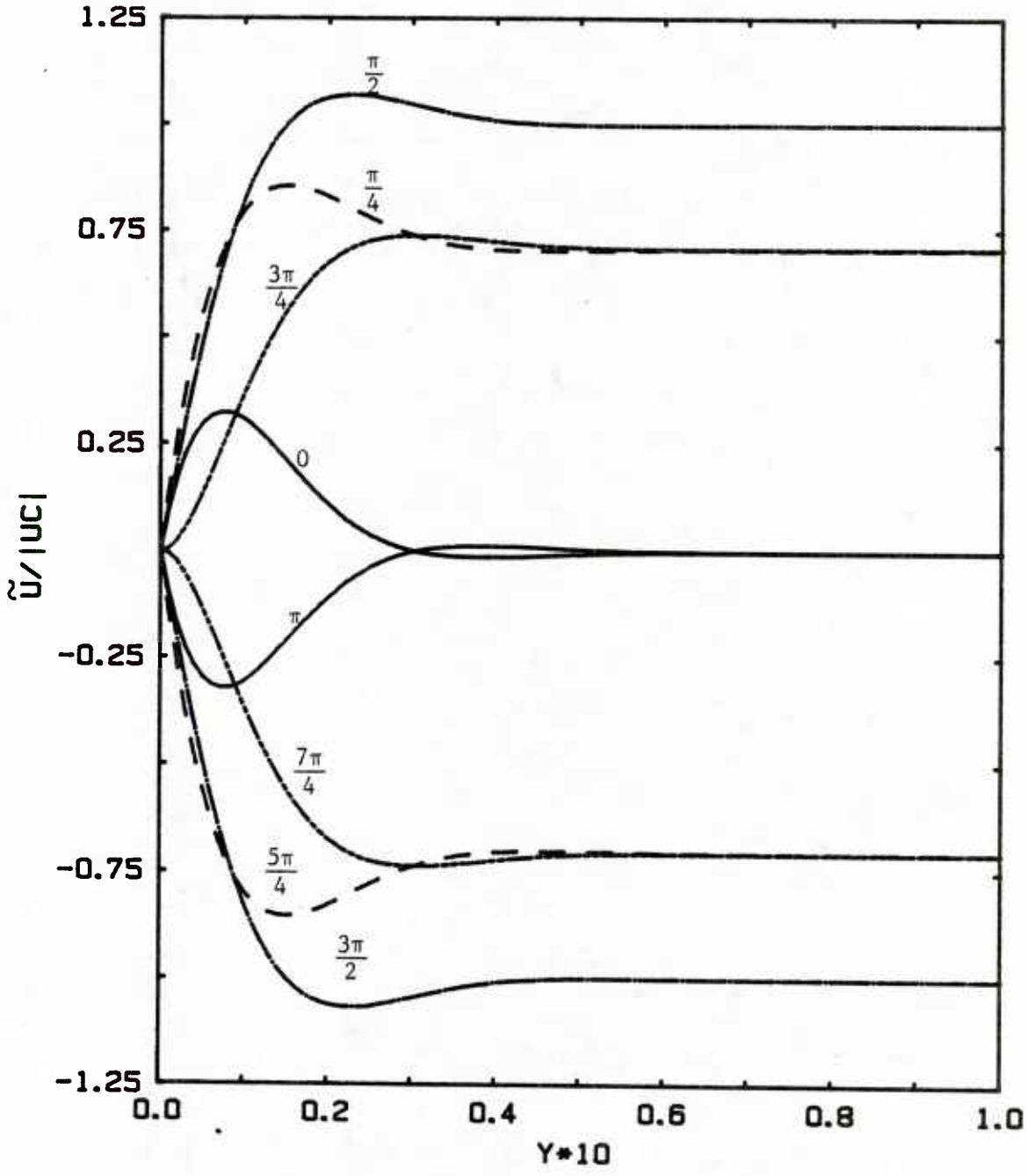


Figure 3.4 Oscillation velocity profile at different phases for laminar flow ($\Omega$ = 150)

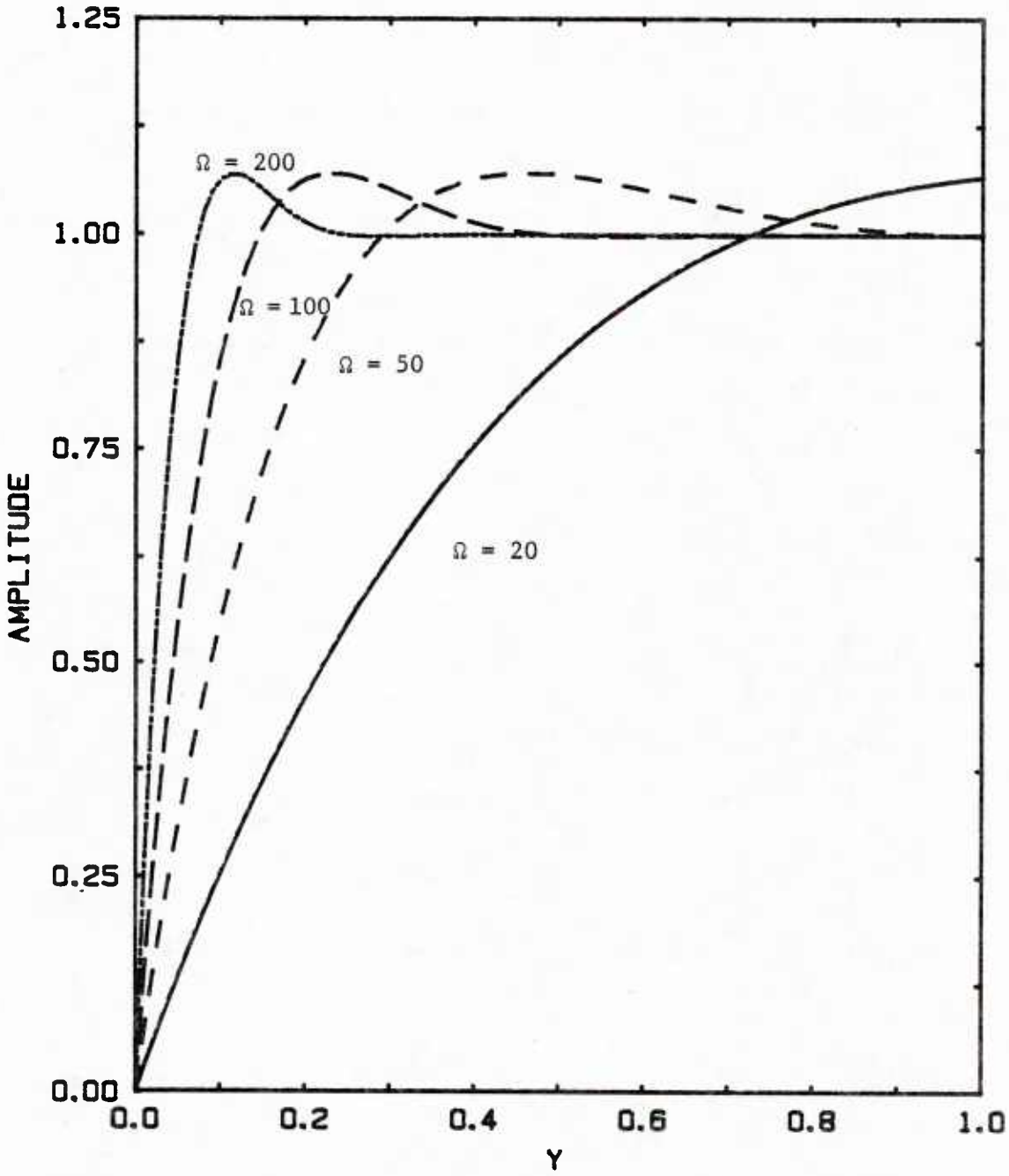


Figure 3.5 Amplitude profile of laminar oscillation flow at different Ω

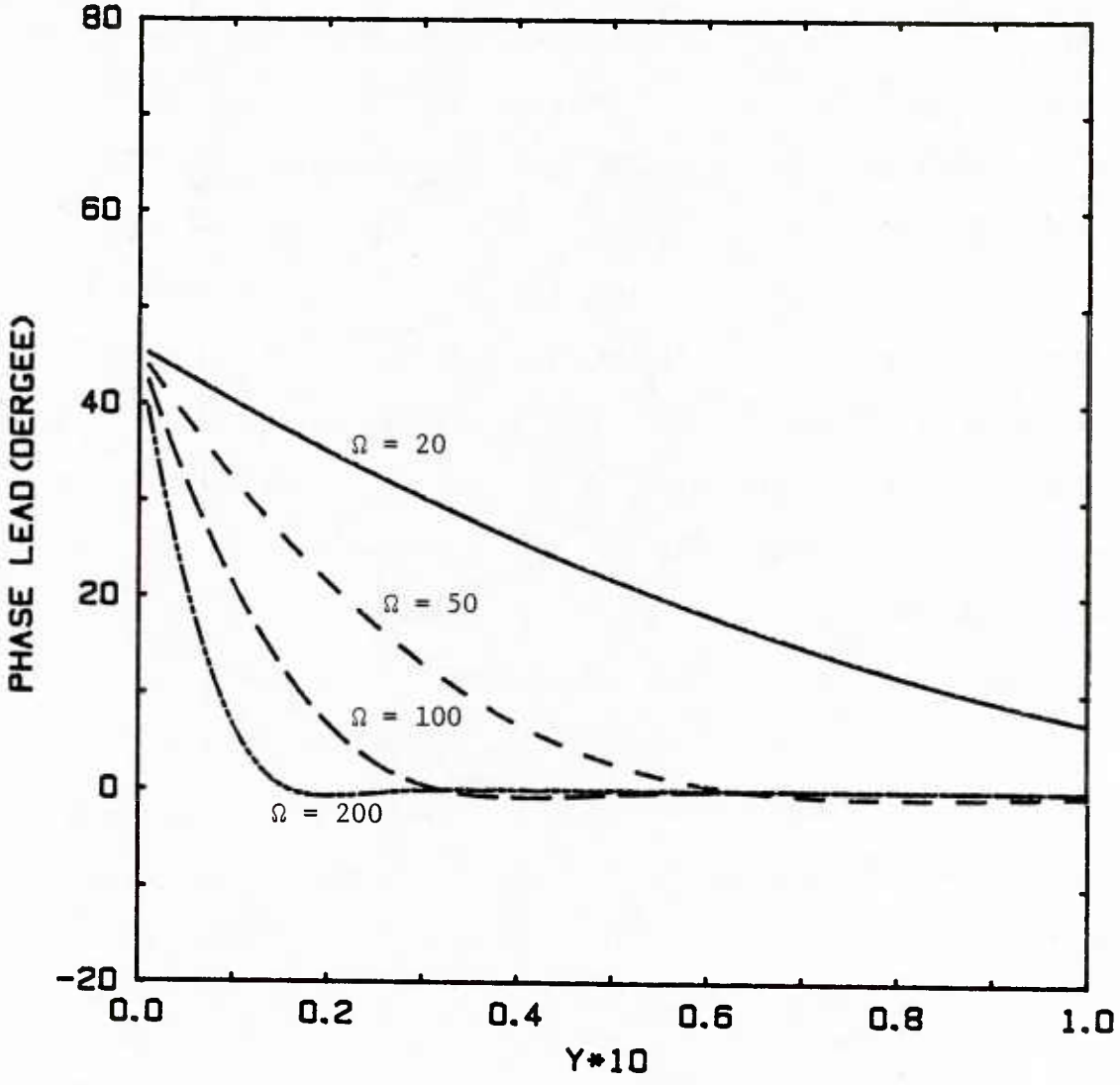


Figure 3.6 Phase profile of laminar oscillation flow at different Ω

region close to the wall. An interesting result is that the phase of the velocity near the wall is ahead of that in the center.

A physical interpretation of the behavior of the oscillation velocity in a laminar flow is given by Lighthill (1954) and Gerrard (1971). As the piston oscillates, the variation of pressure gradient is imposed on the flow. Due to inertia, the change of velocity lags behind that of pressure gradient. However, the inner part of the flow responds to the pressure gradient more rapidly than the outer flow since the inertia of the fluid is less here than at the pipe center. The vorticity, which is simply the radial gradient of velocity in a fully developed pipe flow, created at the wall diffuses into the flow. The relevant parameter $\Omega$ is a measure of the ratio of the tube radius to the distance vorticity diffuses in one period of oscillation. At high frequency the vorticity never has time to diffuse to the center region before being annulled by oppositely signed vorticity. This results in the flat distribution in the center part of the pipe. On the other hand, the sectional mean velocity must equal to the piston speed at each instant by the continuity condition of incompressible fluid. Retardation due to viscous effects near the wall is balanced by an acceleration over the rest of the cross section. This causes an overshoot of velocity at the outer part of the Stokes layer.

## 3.5 Hussain and Reynolds Model (Model B) for the Induced Flow Oscillations

If the effect of oscillation on turbulence is considered, i.e., $\tilde{\tau}^{(t)} \neq 0$, a simple way to relate the oscillation induced Reynolds stress to the induced velocity gradient is to assume that the eddy viscosity is specified only by mean flow field (Hussain and Reynolds, 1970). That is

$$\tilde{\tau}(t) = \rho \bar{\nu}_t \frac{\partial \tilde{u}}{\partial y} \quad . \tag{3.34}$$

The substitution of (3.34) into (3.17) gives

$$\frac{\partial \tilde{u}}{\partial t} = - \frac{1}{\rho} \frac{\partial \tilde{p}}{\partial x} + \frac{\nu}{r} \frac{\partial}{\partial r} \left[ r \left( 1 + \frac{\bar{\nu}_t}{\nu} \right) \frac{\partial \tilde{u}}{\partial r} \right] \quad . \tag{3.35}$$

where $\bar{\nu}_t$ is calculated by (3.23) and (3.27) for core and wall region, respectively.

## 3.6 Quasisteady Approximation for the Mixing Length (Model C)

The shortcoming of Model B is that it doesn't take account of the changes of eddy viscosity during the oscillation. To consider this, the mixing length is assumed to be given by

$$\ell = \bar{\ell} + \tilde{\ell} \quad , \tag{3.36}$$

where $\bar{\ell}$ is the mixing length for the undisturbed flow and $\tilde{\ell}$, the oscillation induced part. Then, the oscillation induced eddy viscosity can be expressed as

$$\tilde{\nu}_t = \bar{\ell}^2 \frac{\partial \tilde{u}}{\partial y} + 2\bar{\ell}\tilde{\ell} \frac{\partial \bar{u}}{\partial y} \quad , \tag{3.37}$$

where $\tilde{\ell}$ needs to be specified.

The Van Driest formula for the mixing length in (3.25) is for a steady flow with zero pressure gradient. The wall shear stress $\bar{\tau}_w$ is used in the damping factor since the shear stress is nearly constant in the region close to the wall. In flow over a wavy surface, the wave-induced pressure gradient can cause large variations of the shear stress through the viscous wall region which alter the production of turbulence.

Abrams and Hanratty (1984) took this into account by redefining the damping factor as

$$D_M = \frac{y\,\tau^{1/2}(y)}{\rho^{1/2}\nu A}\,, \tag{3.38}$$

where the local shear stress, $\tau(y)$, is used instead of the value at the surface, $\tau_w$. This formulation will predict a thickening of the viscous wall region in favorable pressure gradients since $\tau(y)$ is, then, less than the value at the surface $\tau_w$.

In a pulsating flow, the time variation of the pressure gradient also causes a large variation of shear stress in the viscous wall region. Therefore local phase averaged shear stresses $<\tau(y,t)>$ are used in the damping factor. The oscillation induced mixing length $\tilde{\ell}$ is then given as

$$\tilde{\ell} = \frac{1}{2}\,ky\,\frac{y^+}{A}\,\frac{\tilde{\tau}(y,t)}{\overline{\tau}(y)}\,\exp\,(-\,y^+/A), \tag{3.39}$$

where

$$\tilde{\tau}(y,t) = \tilde{\tau}^{(t)}(y,t) + \mu\,\frac{\partial\tilde{u}}{\partial y} \tag{3.40}$$

and

$$\overline{\tau}(y) = \overline{\tau}_w\,(1 - y/r_0)\,. \tag{3.41}$$

From (3.20), (3.37), and (3.39) to (3.41), the oscillation induced eddy viscosity is expressed as

$$\tilde{\nu}_t = \frac{\overline{\nu}_t + B\,(\nu + \overline{\nu}_t)}{(1 - B)\,\dfrac{\partial\overline{u}}{\partial y}}\,\frac{\partial\tilde{u}}{\partial y}\,, \tag{3.42}$$

where

$$B = k y \bar{\ell} \frac{y^+}{A} \left(\frac{\partial \bar{u}}{\partial y}\right)^2 \exp\left(- y^+/A\right)/\left[(1 - y/r_0)\, \bar{u}^{*2}\right] \qquad (3.43)$$

is a function of y, has a maximum near the wall and approaches to zero with increases of distance from the wall, as shown in Figure 3.7. The oscillation induced Reynolds stress, as described in (3.20), can be written as

$$\tilde{\tau}(t) = \rho\, \phi_1(y)\, \frac{\partial \tilde{u}}{\partial y}\,, \qquad (3.44)$$

with

$$\phi_1(y) = \frac{2\bar{\nu}_t + B\nu}{1 - B}\,. \qquad (3.45)$$

This model is a quasi-steady approximation. The mixing length, as well as the Reynolds stress, are directly associated with the instantaneous vleocity gradient in the same way as for a steady flow.

## 3.7 Relaxation Consideration of Pressure Gradient Effect (Model D)

Loyd, Moffat and Kays (1970) and Reynolds (1974), (1976) found that (3.26) with A = 25 does not correctly predict the effect of pressure gradient in equilibrium boundary layers. They therefore allowed A to be a function of the dimensionless pressure gradient $p^+ = \frac{dp}{dx}\, \nu/\rho u^{*3}$. For small $p^+$,

$$A = \bar{A}\, (1 + k_1\, p^+ + k_2 p^{+2} + \ldots)\,. \qquad (3.46)$$

with $k_1 = -30$ and $k_2 = 1.54 \times 10^3$.

For situations in which the pressure gradient is varying rapidly, Loyd *et al.*, (1970) suggest that the flow close to the wall sees an effective pressure gradient given by the equation

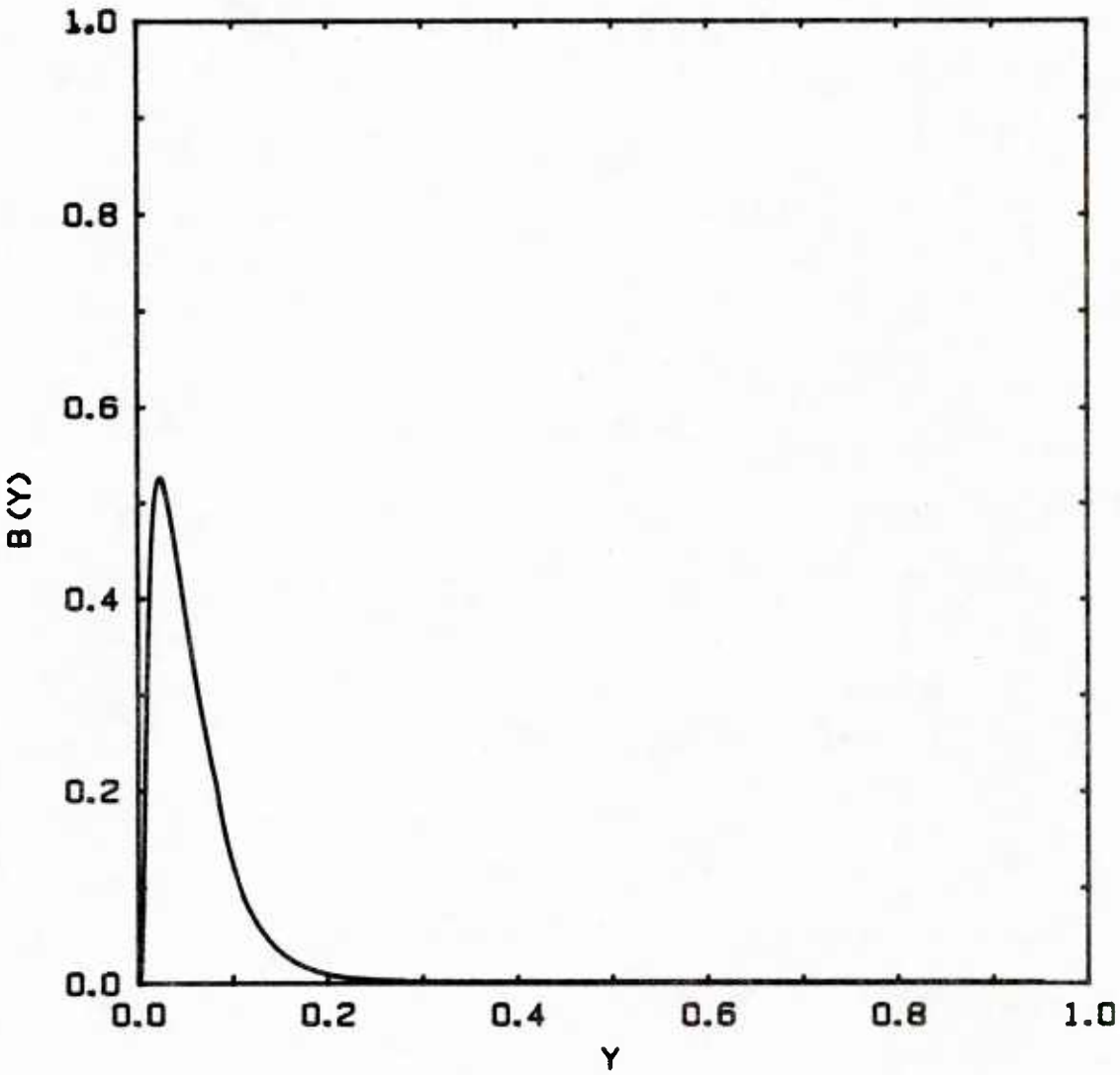


Figure 3.7 Profile of B(Y)

(Re = 30,000)

$$\frac{d\left(\frac{dp}{dx}\right)_{eff}}{d\ (xu^*/\nu)} = \frac{\left(\frac{dp}{dx}\right) - \left(\frac{dp}{dx}\right)_{eff}}{k_L} \quad , \tag{3.47}$$

where $k_L$ is a relaxation constant approximately equal to 3000.

Thorsness et al. (1978) and Abrams (1984) adopted this approach in accounting for the non-equilibrium effects in the viscous wall region for wavy surface flows. With $k_1 = -35$, $k_L = 1800$, Abrams obtained good agreement between the model and experimental measurements of the variation of wall shear stress along a wave surface.

The pressure gradient in a pulsating flow is varying with time rather than with space. A straightforward application of (3.47) to this case requires the definition of a convection velocity which characterizes the streamwise propagation of disturbances in viscous wall region to relate spatial variations to time variations. A convection velocity of $C_x^+ = 15$ has been chosen to take account of this effect. Therefore, the effective pressure gradient for a pulsating flow is defined as

$$\frac{d\left(\frac{d\tilde{p}}{dx}\right)_{eff}}{d\left(\frac{t\bar{u}^{*2}}{\nu}\right)} = \frac{\left(\frac{d\tilde{p}}{dx}\right) - \left(\frac{d\tilde{p}}{dx}\right)_{eff}}{k_L/15} \quad . \tag{3.48}$$

The oscillation induced eddy viscosity is then given as

$$\tilde{\nu}_t = \frac{\bar{\nu}_t + B(\nu + \bar{\nu}_t)}{(1 - B)\frac{\partial \bar{u}}{\partial y}} \frac{\partial \tilde{u}}{\partial y} - \frac{2B\ (1 - y/r_0)\ \bar{u}^{*2}}{(1 - B)\frac{\partial \bar{u}}{\partial y}} \frac{\tilde{A}}{\bar{A}} \tag{3.49}$$

with $\frac{\tilde{A}}{\bar{A}} = k_1 p^+_{eff}$. A comparison with (3.42) shows that the second term on the right side of (3.49) considers the influence of flow relaxation

for high frequencies. In general, this term is not in phase with the oscillation velocity gradient $\frac{\partial \tilde{u}}{\partial y}$. It is a strong contributor to $\tilde{\nu}_t$ in the wall region. The oscillation induced Reynolds stress is described as

$$\tilde{\tau}(t) = \rho \left[\phi_1(y) \frac{\partial \tilde{u}}{\partial y} - \phi_2(y) \frac{\tilde{A}}{\bar{A}}\right] \tag{3.50}$$

where

$$\phi_2(y) = \frac{2B\ (1 - y/r_0)\ \bar{u}^{*2}}{1 - B} \ . \tag{3.51}$$

These relations predict that the relaxation effect is confined in the wall region because B approaches zero at large y.

In the core region, $\tilde{\ell}$ is assumed to be zero, and $\tilde{\tau}(t) = 2\rho\bar{\nu}_t \frac{\partial \tilde{u}}{\partial y}$, where $\bar{\nu}_t$ is taken as a constant calculated from (3.23) at the pipe center. The match point $y_0$ is where the calculated $\phi_1(y_0)$ is equal to twice the value of the eddy viscosity evaluated at pipe center.

## 3.8 Numerical Scheme

The time variation of the wall shear stress caused by an imposed variation of pressure gradient defined by (3.29) is calculated by solving equation (3.17) numerically. The equation was made dimensionless in the following manner:

$$\frac{\partial U}{\partial T} = \cos T + \frac{1}{\Omega^2(1 - Y)} \frac{\partial}{\partial Y}\left[(1 - Y)\left(1 + \frac{\bar{\nu}_t}{\nu}\right)\frac{\partial U}{\partial Y}\right]$$

$$+ \frac{1}{\Omega^2(1 - Y)} \frac{\partial}{\partial Y}\left[(1 - Y)\frac{\tilde{\nu}_t}{\nu}\frac{\partial U'}{\partial Y}\right] \tag{3.52}$$

with

$$U = \frac{\tilde{u}\omega}{a} , \quad \Omega = \sqrt{\frac{\omega}{\nu}}\, r_0 ,$$

$$Y = 1 - \frac{r}{r_0} , \quad T = \omega t, \tag{3.53}$$

and

$$U' = \frac{\overline{u\omega}}{a} .$$

The boundary conditions are

$$U = 0 \qquad \text{at} \quad Y = 0$$

and

$$\frac{\partial U}{\partial y} = 0 \qquad \text{at} \quad Y = 1 \tag{3.54}$$

The equation was solved numerically by a Crank-Nicolson implicit scheme with variable spatial grid size. Since the oscillation velocity changes rapidly in the wall region and the final goal of the calculation is to find the velocity gradient at the wall, it is necessary to use a very small grid size close to the wall. Grid sizes which are increasing in a geometric series of Y were chosen:

$$Y_j = \frac{\Delta Y_1 (H^{j-1} - 1)}{(H - 1)} , \qquad 1 \le j \le J \tag{3.55}$$

where $\Delta Y_1$ is the first grid size near the wall, and factor H is the ratio of two consequent grid sizes. Ratio H is chosen as 1.05 for present

work. The total number of grid points in the radial direction is then given as

$$J = \log \left[ \frac{(H - 1)}{\Delta Y_1} + 1 \right] \; / \; \log H \; , \tag{3.56}$$

where J takes integer number.

The first grid size $\Delta Y_1$ was selected small enough so that the velocity gradient at the wall can be calculated by the assumption of linear variation of velocity in that region. After several tries, $\Delta Y_1$, was taken as 1/30 of the Stokes layer thickness. Figure 3.8 gives the schematic description of the grids.

The initial condition, time zero, was chosen as the quasi-laminar result. Equal time steps of $\Delta T = \frac{2\pi}{128}$ were used. At each new time level the velocities at all points in Y direction were calculated from previous time level results. After about five periods calculation, the velocities at each phase of the cycle are found to converge to constant values.

Because of the variable grid size in space, the finite difference expression for derivatives used with an equal grid size cannot be employed. Expressions for finite difference with variable grid size have been derived by approximating a function piecewise with a second order polynomial

$$U(Y) = a_j + b_j Y + C_j Y^2, \quad \text{at } Y_{j-1} \leq Y \leq Y_{j+1} \tag{3.57}$$

where U(Y) is the approximated value; $a_j$, $b_j$ and $c_j$, the coefficients in the polynomial. Then, the finite difference forms of derivatives are derived as

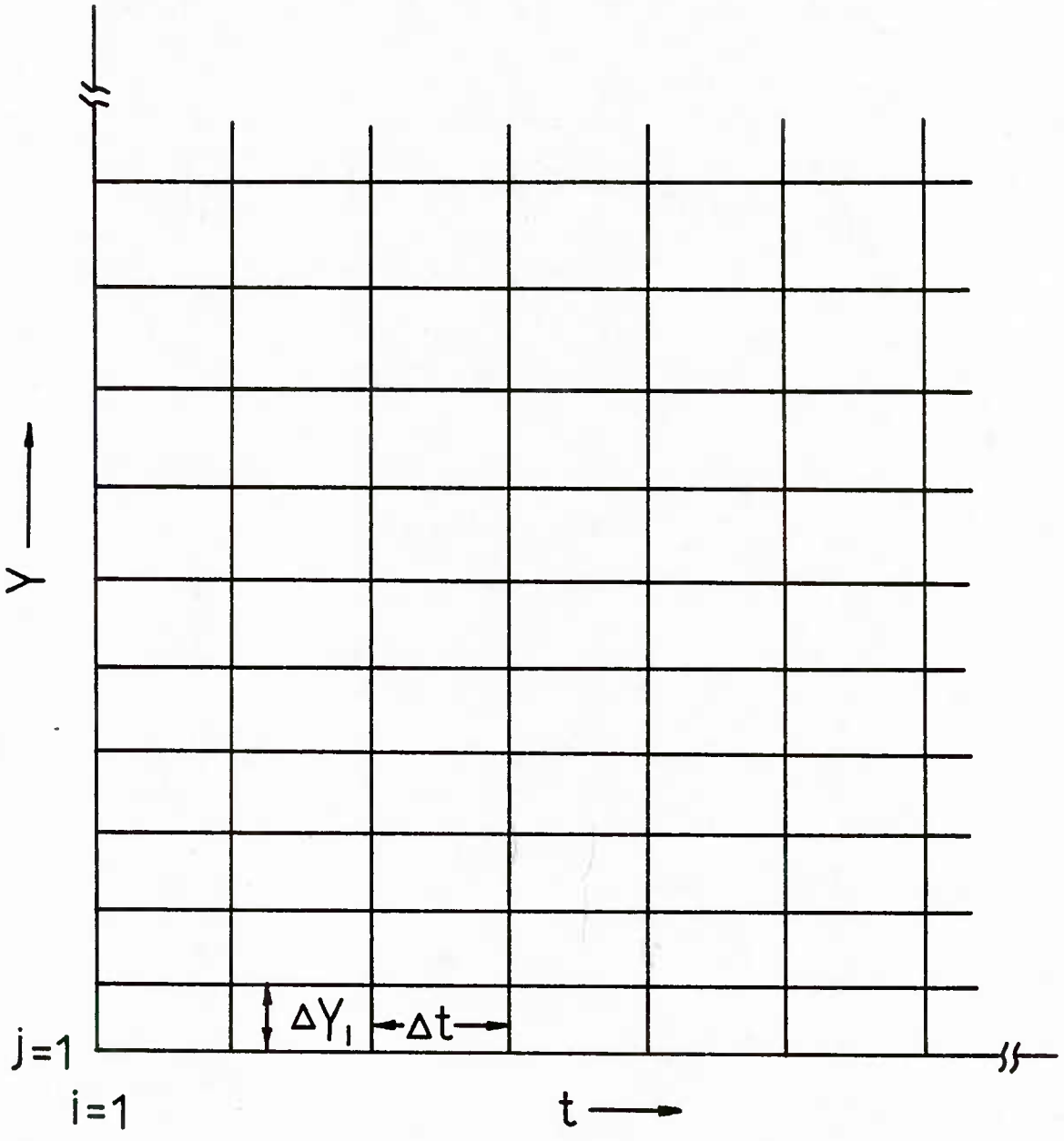


Figure 3.8 Grids used for finite difference

$$\left.\frac{\partial U}{\partial Y}\right|_j = \left[\frac{U_{j+1}}{H(H+1)} + \frac{(H-1)\,U_j}{H} - \frac{H\,U_{j-1}}{H+1}\right] \Big/ (\Delta Y_1\, H^{j-2}) + O(\Delta Y_1^2)\,, \quad (3.58)$$

and

$$\left.\frac{\partial^2 U}{\partial Y^2}\right|_j = \left[\frac{2\,U_{j+1}}{H(H+1)} + \frac{2\,U_j}{H} + \frac{2\,U_{j-1}}{H+1}\right] \Big/ (\Delta Y_1\, H^{j-2})^2 + O(\Delta Y_1^2)\,, \quad (3.59)$$

where $2 \le j \le J-1$. Details of the derivation are given in Appendix II. It is clear that the above forms reduce to the standard central finite difference expressions for equal grid sizes, i.e., $H = 1$.

# CHAPTER 4. DESCRIPTION OF EXPERIMENTS

## 4.1 Experimental Flow Loop

A schematic drawing of the loop in which the experiments were performed is shown in Figure 4.1. The loop was originally built by Sirkar. Details regarding its design may be found in a thesis by Sirkar (1969) and in a paper by Sirkar and Hnaratty (1970). In this work, a reciprocating piston was connected to the loop.

The mean flow was generated by a centrifugal pump while the imposed oscillation was introduced by a piston with a diameter of 6.35 cm and an adjustable stroke length from 0 to 15.2 cm. The mean flow rate was measured by a vortex shedding flow transmitter (Eastech, Model 2420) with an accuracy of 0.5%. The frequency of oscillation in the experiment was fixed at 0.325 Hz or 0.625 Hz by adjusting the circular frequency of the motor driving the piston. The oscillating flow component was introduced into the system between diaphragm valve 3 and calming section 4. The uniform flow that emerges from the calming section is tripped by a 1.26 cm long ring consisting of a series of 0.95 cm equilateral triangles around the circumference of the entrance of the 19.4 cm pipe line. In the experiment, diaphragm valve 3 and bypass valve 17 were adjusted to impose a large pressure drop across them. This minimized the distortions of the sinusoidal oscillation in the 19.4 cm pipe, caused by the time response of the whole system.

Rectangular electrode made of platinum were mounted flush with the wall of a test section located 67.5 pipe diameters downstream from the pipe entrance. The fluid was an aqueous solution, 0.1 M in potassium iodide and 0.0038 M in iodine, maintained at a temperature of 25 ± 0.1°C. The kinematic viscosity of the solution was 0.00866 $cm^2/sec$.

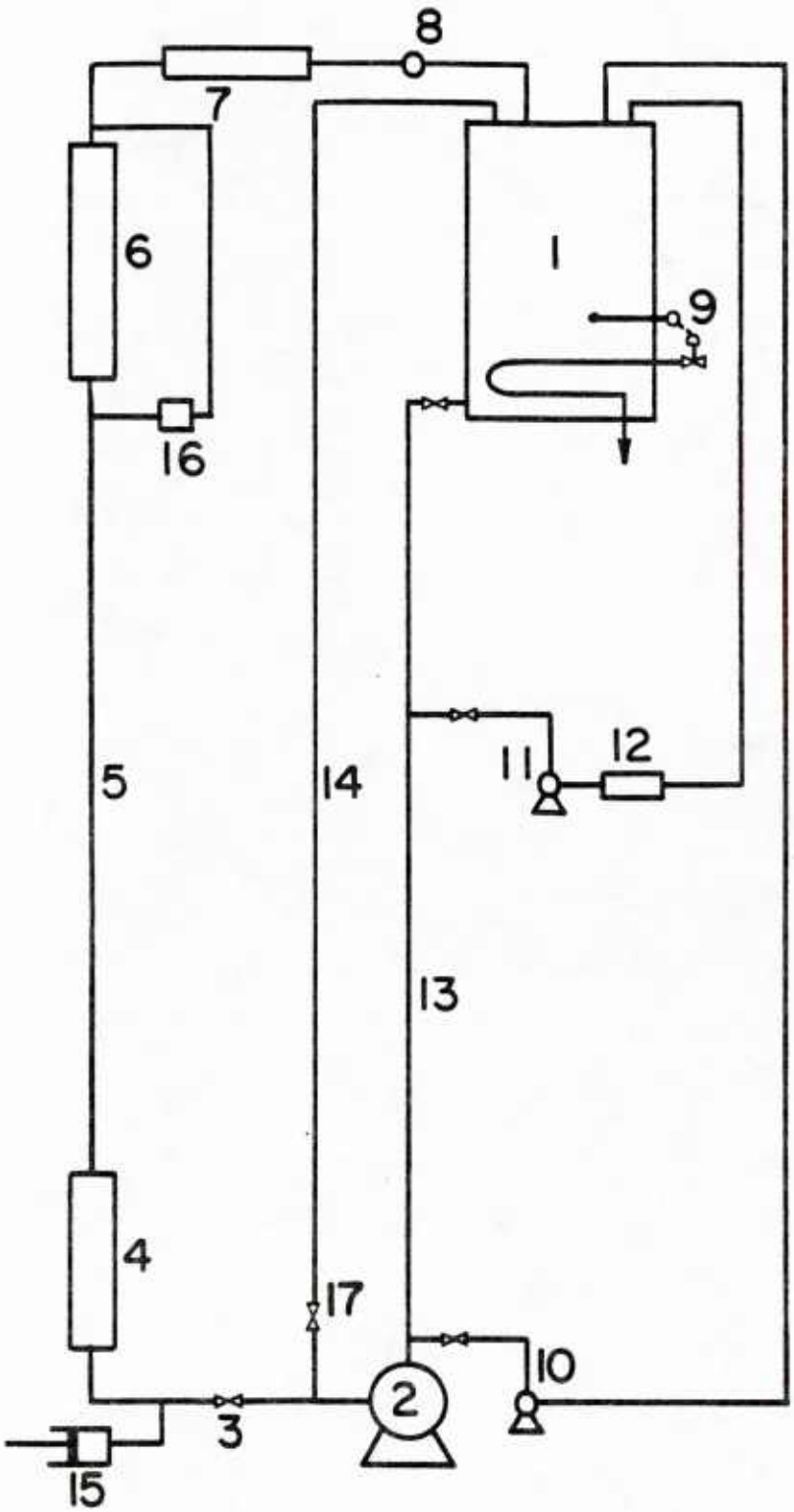


1. Storage tank
2. Worthington pump
3. Diaphragm valve
4. Calming section
5. 19.4 cm pipe upflow
6. Test section
7. Anode
8. Vortex flow meter
9. Temperature control unit
10. Recycling pump
11. Filter pump
12. Filter
13. 10.2 cm pipe downflow
14. 10.2 cm bypass pipe
15. Pulsating generator
16. Pressure transducer
17. Bypass valve

Figure 4.1 Schematic of 19.4 cm flow loop

## 4.2 Electrochemical Technique

Electrochemical techniques were used to measure flow in the immediate vicinity of the solid wall. These were developed by Reiss and Hanratty (1963) in this laboratory. The principle behind them is as follows: When a voltage is applied to an electrochemical cell in an aqueous solution of potassium iodide and iodine, the following reactions are carried out on the surfaces of the electrodes:

$$\text{Cathode} \qquad I_3^- + 2e \rightarrow 3I^-$$

$$\text{Anode} \qquad 3I^- \rightarrow I_3^- + 2e.$$

When the electrochemical process is controlled by the rate of mass transfer at the surface of the cathode (the test electrode), the current flowing in the cell, I, is related to the rate of mass transfer, N, by the equation

$$N = \frac{I}{A_e n_e F}, \tag{4.1}$$

Where $A_e$ is the area of the test electrode, $n_e$, the number of the electrons involved in the reaction and F, Faraday's constant.

Consider a rectangular probe embedded in the wall with its long side perpendicular to the direction of mean flow. If the dimensions of the element are selected correctly (Hanratty & Campbell, 1983), diffusion in both the transverse and streamwise directions may be neglected. Furthermore, the thickness of the concentration boundary-layer will be small enough that the effect of velocities normal to the

surface can be neglected and the velocity in the streamwise direction is given by

$$u = Sy \ . \tag{4.2}$$

The mass balance equation in the concentration boundary layer can be described as

$$\frac{\partial C}{\partial t} + Sy \frac{\partial C}{\partial x} = \alpha \frac{\partial^2 C}{\partial y^2} \ , \tag{4.3}$$

where $\alpha$ is the diffusivity. Equation (4.3) is to be solved using the boundary conditions

$$C\ (x,\ o,\ t) = 0 \qquad 0 \leq x \leq L$$

$$C\ (x,\ \infty,\ t) = C\ (0,\ y,\ t) = C_b \tag{4.4}$$

For steady flow or if the flow is unsteady and changing slowly with time, the first term in (4.3) can be neglected. The solution of this equation is the pseudosteady state approximation given by Reiss (1963):

$$\frac{C}{C_b} = \frac{1}{\Gamma(4/3)} \int_0^{\eta} e^{-z^3} dz \ , \tag{4.5}$$

where

$$\eta = y \left(\frac{S}{9\alpha x}\right)^{1/3} = y^+ Sc^{1/3} \left(\frac{1}{9x^+}\right)^{1/3} \ , \tag{4.6}$$

and Sc, the Schmidt number. The terms $y^+$ and $x^+$ are the coordinate distances made dimensionless with respect to friction velocity $u^*$

and kinematic viscosity $\nu$. The transfer coefficient, $K = N/C_b$, is then given as

$$K = \frac{\alpha}{C_b L} \int_0^L \left(\frac{\partial C}{\partial y}\right)_{y=0} dx = 0.807 \left(\frac{\alpha^2 S}{L}\right)^{1/3} . \qquad (4.7)$$

Equation (4.7) is normally used to obtain the velocity gradient at the wall, or wall shear stress, from the measured values of K. Details regarding the measurement of the current and the electrochemical technique are given in a review article by Hanratty and Campbell (1983).

When this technique is applied to unsteady flows, especially at high frequencies of oscillation, the pseudosteady approximation might not hold. Fortuna and Hanratty (1971) considered the effect of the frequency response of concentration boundary layer on the measured amplitude of the fluctuating flow by solving a linearized form of the time varying conservation equation. In the present work, particular attention was given to the phase lag errors that arise in using (4.7) to calculate time variation of $\tau_w(t)$. Numerical and experimental studies of this problem, summarized in a recent paper by Mao and Hanratty (1984), are described in the following section.

## 4.3 Use of Electrochemical Wall Probes to Pulsating Flow

Let C and S be the sum of average and time dependent terms.

$$C = \overline{C} + c$$

$$S = \overline{S} + s \qquad (4.8)$$

Equation (4.3) can then be decomposed into equations for $\overline{C}$ and for c. The solution for $\overline{C}$ is the same as (4.5). The equation for c is solved by using a harmonic variation for s,

$$s = \hat{s}\, e^{i\omega t} , \tag{4.9}$$

where $\hat{s}$ and $\omega$ are real numbers. Since the differential equation for c is linear,

$$c = \hat{c}\, e^{i\omega t} = c_1 \frac{\hat{s}}{\bar{s}} e^{i\omega t} , \tag{4.10}$$

where $\hat{c}$ and $c_1$ can be complex numbers.

The differential equation defining $c_1$ is

$$i\omega^* L^{+2/3} c_1 + y^* \frac{\partial c_1}{\partial X} + y^* \frac{\partial \overline{C}}{\partial X} = \frac{\partial^2 c_1}{\partial y^{*2}} , \tag{4.11}$$

with

$$X = x^+/L^+ = x/L , \tag{4.12}$$

$$y^* = y^+ \, Sc^{1/3}/L^{+1/3} \tag{4.13}$$

$$\omega^* = \frac{\omega \nu}{u^{*2}} Sc^{1/3} . \tag{4.14}$$

The boundary conditions are

$$c_1 (X, 0) = 0 \qquad 0 \le X \le 1$$

$$c_1 (X, \infty) = 0$$

$$c_1 (0, y^*) = 0 . \tag{4.15}$$

The transfer coefficient can also be represented as the sum of an average and time dependent term

$$K = \overline{K} + k \tag{4.16}$$

Again, because of the linear assumption,

$$k = \hat{k}\, e^{i\omega t} , \tag{4.17}$$

where $\hat{k}$ is a complex amplitude. For the case where a pseudosteady state assumption can be made, one obtains from (4.7)

$$\hat{k}_s = \frac{0.807}{3} \frac{\alpha^{2/3}}{L^{1/3}} \frac{\hat{s}}{\overline{s}^{2/3}} \tag{4.18}$$

Since

$$\hat{k} = \frac{\hat{s}}{\overline{s}} \frac{\alpha}{C_b} \int_0^1 \left.\frac{\partial c_1}{\partial y}\right|_{y=0} dX , \tag{4.19}$$

it follows from (4.11), (4.15) and (4.18) that

$$\frac{\hat{k}}{\hat{k}_s} = f\,(\omega^* L^{+2/3}) , \tag{4.20}$$

where $\hat{k} = \hat{k}_R + i\,\hat{k}_I$ is complex and $\hat{k}_s$ is real.

The periodic variation of k, defined by (4.17), is characterized by an amplitude,

$$|\hat{k}| = \left[(\hat{k}_R)^2 + (\hat{k}_I)^2\right]^{1/2} \tag{4.21}$$

and by a phase angle

$$\theta = - \tan^{-1} \left[ \frac{\hat{k}_I}{\hat{k}_R} \right] , \tag{4.22}$$

where positive $\theta$ means k lags s in phase. The term (4.22) represents the phase correction and

$$A = \frac{\hat{k}_s}{|\hat{k}|} , \tag{4.23}$$

the amplitude correction that must be applied to the signal coming from the probe, if the pseudosteady state relation (4.7) is used to calculate S(t) from the time varying signal.

Values of A and $\theta$ were obtained by numerically solving (4.11) with a scheme similar to that used by Fortuna & Hanratty (1971).

Plots of $1/A^2$ and phase lag, $\theta$, are plotted versus $\omega^* L^{+2/3}$ in Figures 4.2 and 4.3. The much stronger effect of the frequency response of the scalar boundary-layer on the phase lage, $\theta$, is immediately evident. At $\omega^* L^{+2/3} = 1$ the amplitude correction $1/A^2$ is only about 1.07; however, at this same condition the phase lag correction will be close to 16°.

The principal unconfirmed assumption in the above analysis is that the fluctuating scalar field is described by a linearized form of the conservation equation. In order to verify the numerical results obtained in Figures 4.2 and 4.3, experimental tests were carried out for four different sizes of mass transfer probes.

Table 4.1 gives the dimensions of the electrodes and compares the estimated thickness of the concentration boundary-layer with the thickness

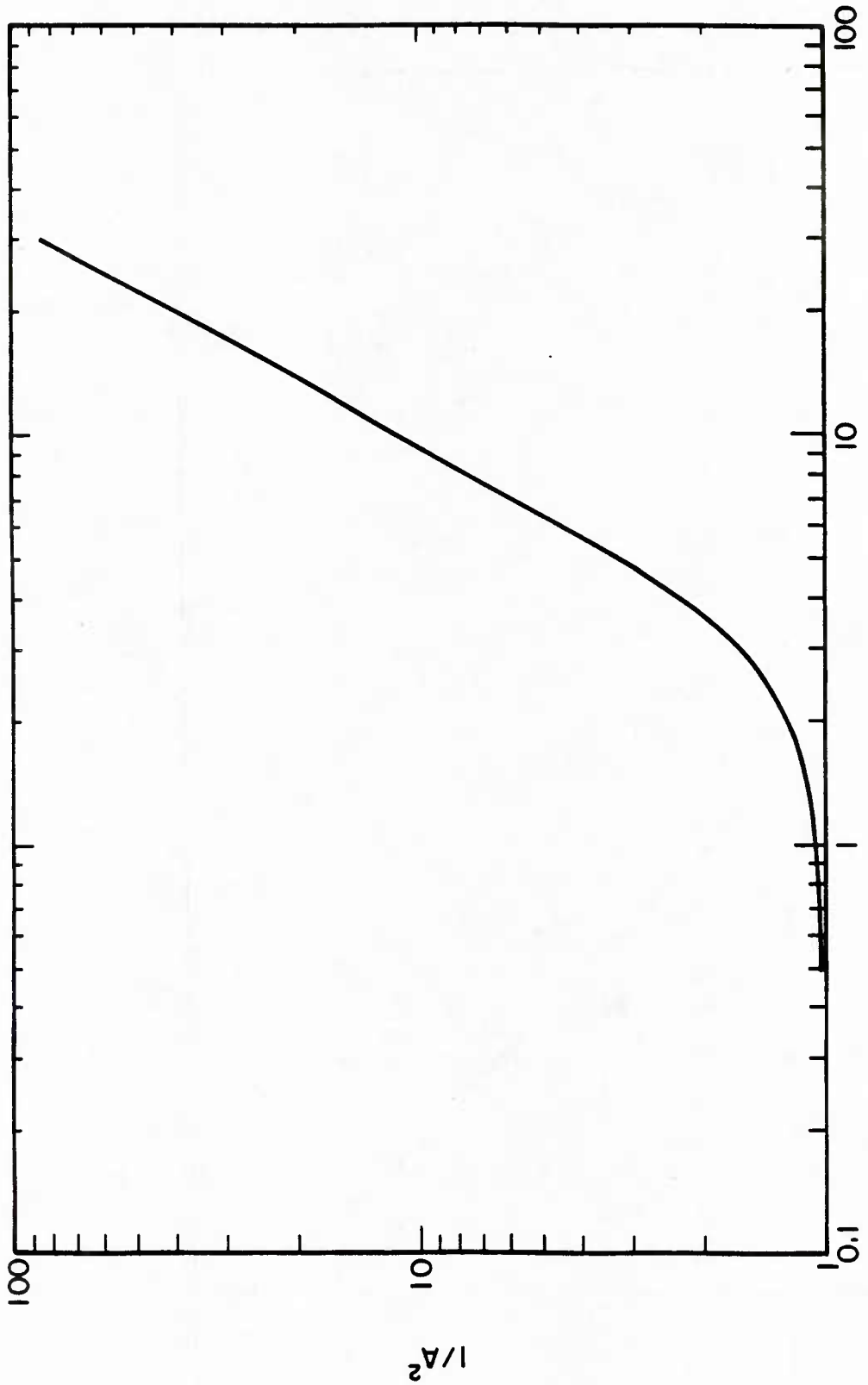


Figure 4.2 Correction factor of amplitude for frequency response

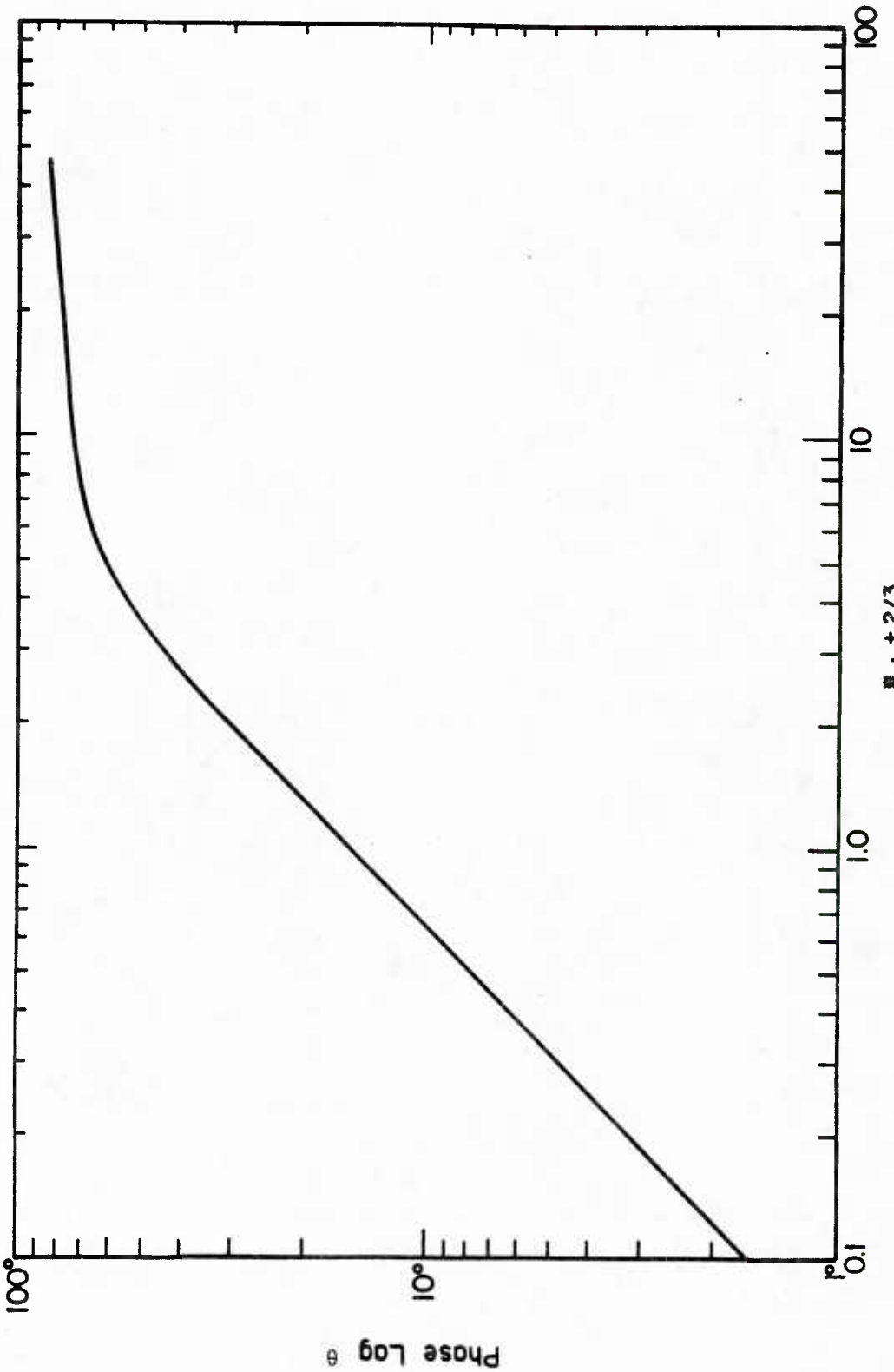


Figure 4.3 Phase lag due to frequency response

Table 4.1

Dimensions of the electrodes and experimental range for the test of frequency response

| Electrode | L(cm) | $L^+$ | $\delta^+_c$ | $\delta^+_s$ | $\omega^* L^{+2/3}$ |
|---|---|---|---|---|---|
| 1 | .00762 | .352-.634 | .22-.27 | 2.5-7.6 | .23-1.4 |
| 2 | .0127 | .587-1.06 | .27-.32 | 2.5-7.6 | .32-1.9 |
| 3 | .0254 | 1.17-2.11 | .33-.41 | 2.5-7.6 | .51-3.1 |
| 4 | .0406 | 1.88-3.38 | .39-.48 | 2.5-7.6 | .69-4.2 |

Re = 15,000 - 29,400

f = .325 - .900 1/sec

W = .102 cm

of the Stokes layer in the range of variables covered by the experiments. Here L is the length of the electrode in the direction of mean flow and W, the width of the electrode.

The thickness of the concentration boundary-layer is defined as

$$\delta_c\big|_{X=L} = 2.92 \frac{L^{+1/3}}{Sc^{1/3}} \cdot \frac{\nu}{u^*} \quad , \tag{4.24}$$

and the Stokes layer thickness is described in (3.32).

As shown in Table 1, $\delta_c^+$ is one order of magnitude less than $\delta_s^+$ and the viscous sublayer thickness of $\delta_v^+ = 5$. Consequently the assumption of a linear variation of the velocity within the concentration boundary layer is valid.

The analog signals from the four probes were sampled simultaneously and were processed in a manner described in section (4.5). Figures 4.4 and 4.6 show the uncorrected amplitudes and phases characterizing the variation of the wall shear stress measured with the different probes. Here the amplitude $|\hat{\tau}_w|$ is plotted as

$$\hat{\tau}(o) = \frac{|\hat{\tau}_w|}{\bar{\tau}_w} \Big/ \frac{|\hat{u}_c|}{u^*} \tag{4.25}$$

so as to normalize effects of changes in the amplitude of the induced flow oscillations. At low values of the dimensionless frequencies, there is reasonably close agreement among the uncorrected measurements from the different probes, indicating the validity of the pseudosteady state assumption. However, at high $\omega^+$ large differences are noted.

Figures 4.5 and 4.7 show the results obtained by correcting the measurements in Figures 4.4 and 4.6, using the factors in Figures 4.2 and 4.3. The good agreement now shown among the measurements from all

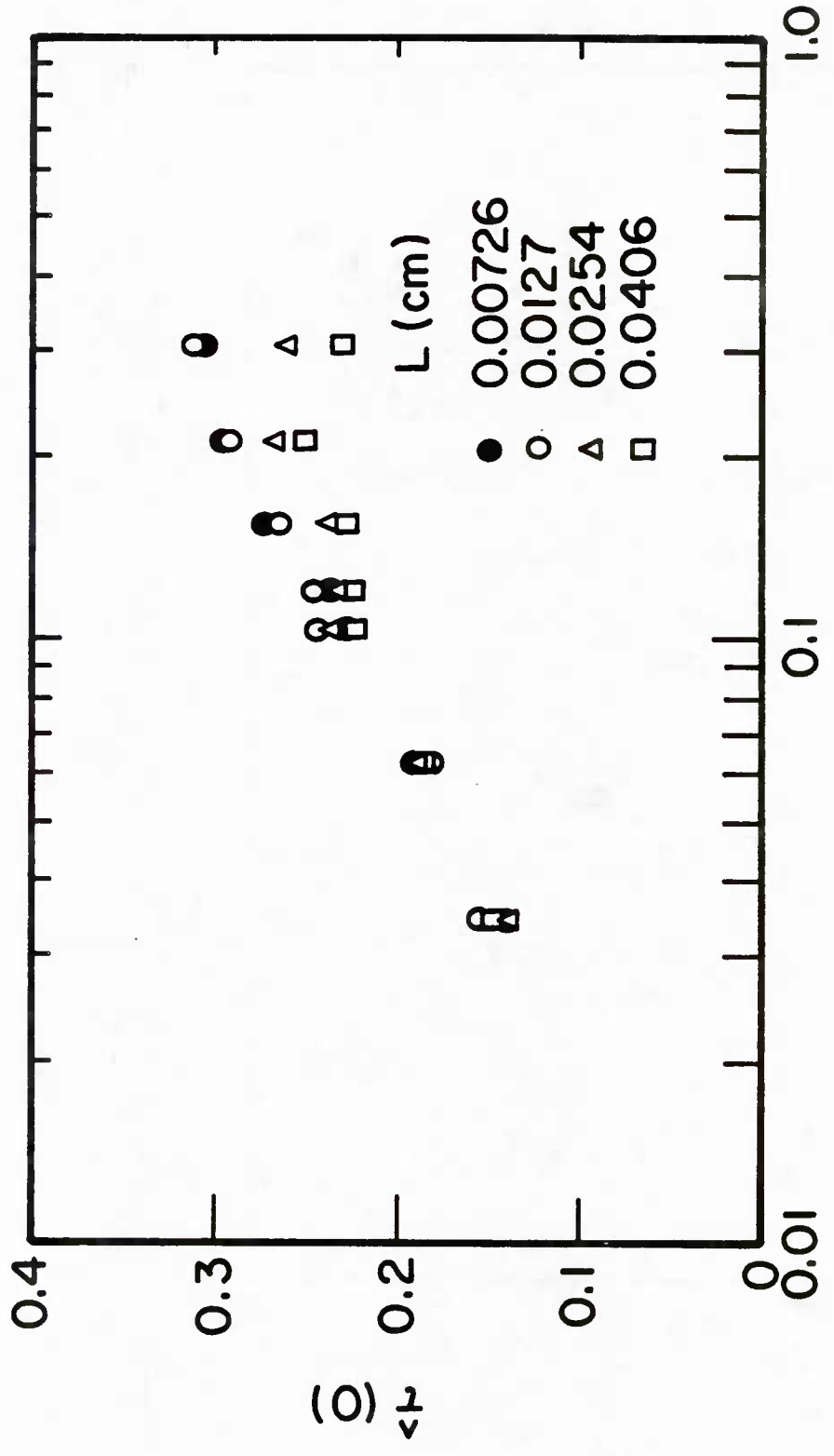


Figure 4.4 Amplitude of wall shear stress measured by different probes without a correction for frequency response

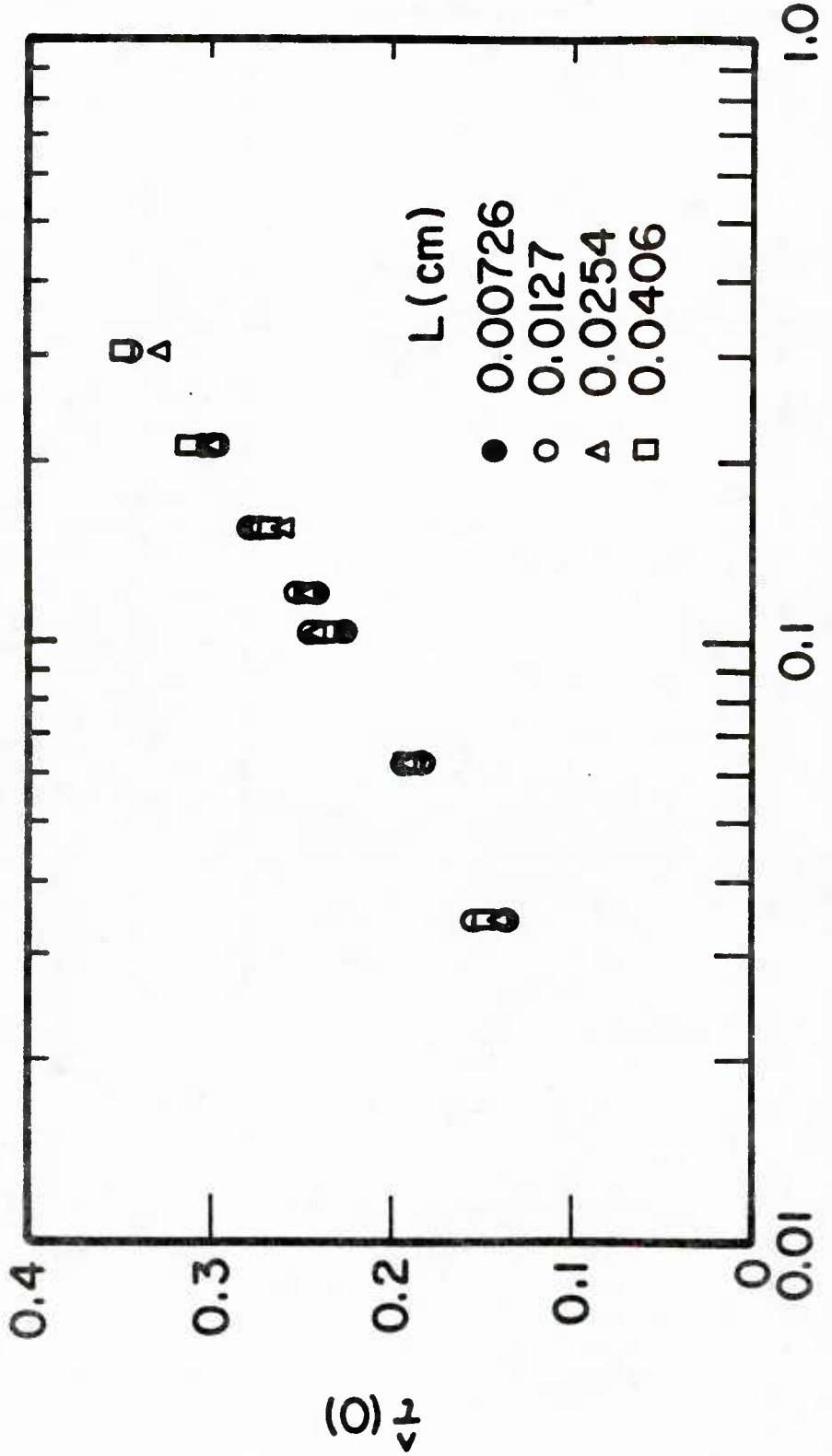


Figure 4.5 Amplitude of wall shear stress measured by different probes with a correction for frequency response

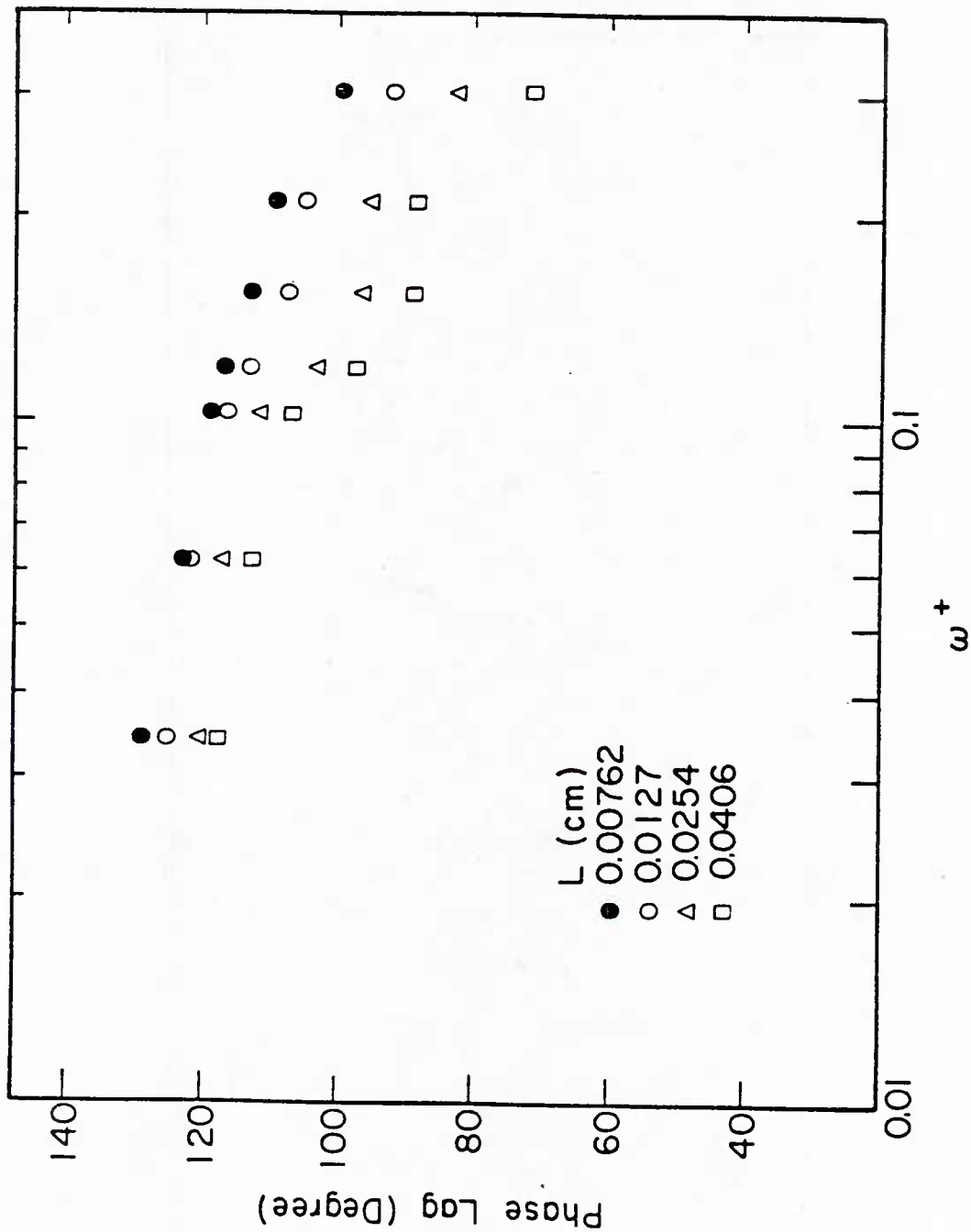


Figure 4.6 Phase lag of wall shear stress (relative to the trigger pulse) measured by different probes without a correction for frequency response

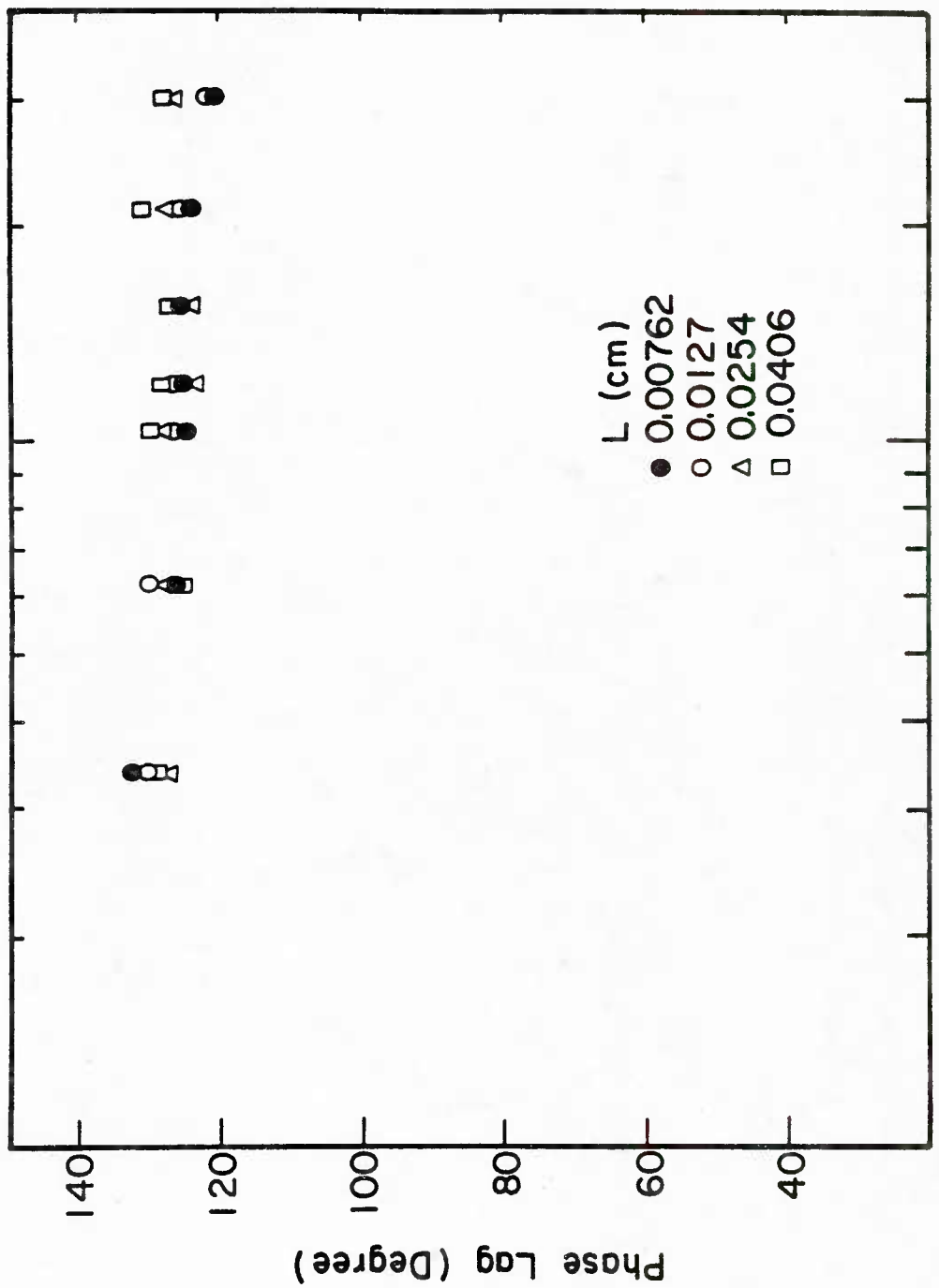


Figure 4.7 Phase lag of wall shear stress (relative to the trigger pulse) measured by different probes with a correction for frequency response

four probes provides support for the method of correcting for frequency response presented in the numerical analysis.

The effects of the amplitudes of flow oscillation on the amplitude of shear stress at the wall are shown in Figure 4.8. Here a is the ratio of the amplitude of velocity variation to the mean velocity at the pipe center. The amplitude of shear stress at the wall is found to increase linearly with the increase of the amplitude of the imposed flow oscillation. If the amplitude $|\hat{\tau}_w| \; / \; \overline{\tau}_w$ is plotted as $\hat{\tau}$ (0), the same results are obtained for different amplitudes of the imposed oscillations. This supports the linearization assumption used in deriving (4.11).

A number of restrictions must be met if wall transfer probes are to be used properly in a turbulent flow with imposed oscillations. These are summarized below.

The concentration boundary-layer should be thinner than the viscous sublayer if (4.2) is to be satisfied. This requires that

$$\delta_c^+|_{x^+=L^+} = 2.92 \frac{L^{+1/3}}{Sc^{1/3}} < 5$$

or that

$$L^+ < 5 \; Sc \quad . \tag{4.26}$$

The presence of imposed oscillations adds the additional restriction that $\delta_c^+$ be less than the thickness of the Stokes layer:

$$\delta_c^+|_{x^+=L^+} < \delta_s^+ = \sqrt{\frac{2}{\omega^+}} \quad ,$$

or

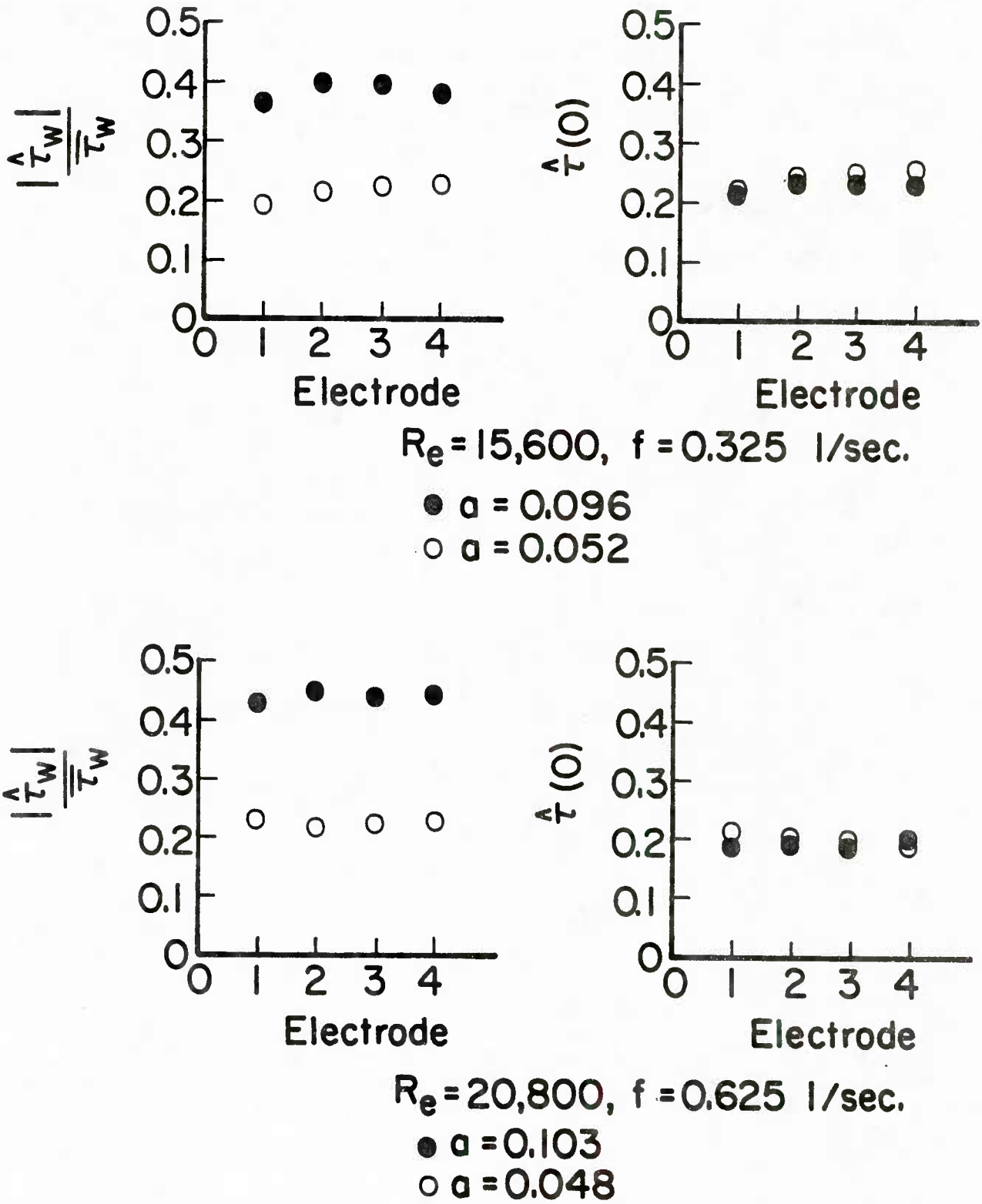


Figure 4.8 Effect of the amplitude of flow oscillation on the amplitude of wall shear stress

$$L^+ < 0.11\ (\omega^+)^{-3/2}\ Sc. \tag{4.27}$$

The neglect of the effects of diffusion in the flow direction (Hanratty & Campbell, 1983) requires that

$$L^+ > 14\ Sc^{-1/2} \tag{4.28}$$

if errors are to be less than 5 percent.

Restrictions (4.26), (4.27) and (4.28) must be satisfied if the analysis of the time response of the scalar boundary-layer presented in this work is to be used. The restriction imposed by the linearization assumption made in the analysis is not as well defined. The experiments described in this study had ratios of the amplitude of oscillation in the wall shear stress to the time averaged wall shear stress, $|\hat{\tau}_w| \ / \ \overline{\tau}_w$, as high as 0.6. The successful experience in correcting these measurements suggests that (4.28) might be more restrictive than the linearization assumption, regarding the size of oscillations that can be measured. If the oscillations become so large that during portions of the cycle convection is no longer completely dominant over streamwise diffusion errors can arise. From (4.28)

$$L^+ \left( 1 - \frac{|\hat{\tau}_w|}{\overline{\tau}_w} \right)^{1/2} > 14\ Sc^{-1/2}$$

or

$$\left( 1 - \frac{|\hat{\tau}_w|}{\overline{\tau}_w} \right) > \left( \frac{14}{Sc^{1/2} L^+} \right)^2 \tag{4.29}$$

If restrictions (4.26-4.29) are met, Figures 4.2 and 4.3 can be used to correct for the frequency response of the concentration boundary-layer.

The numerical analysis suggests that

$$\omega^{+} Sc^{1/3} L^{+2/3} \leq 1 \tag{4.30}$$

if it is desired that the correction on the amplitude is less than 5%. This implies that it might be necessary to correct measurements of turbulent spectra in the high frequency range. Fortuna & Hanratty (1971) did this and found that the intensity of turbulent shear stress fluctuations at the wall is 0.349 rather than the value of 0.302 obtained by using pseudo-steady state relation (4.7). The criterion for avoiding corrections of the phase angle is more restrictive:

$$\omega^{+} Sc^{1/3} L^{+2/3} \leq 0.3 \tag{4.31}$$

for an error of less than 5°.

The strong effect of Schmidt numbers is evident. Consider for example Sc = 1000, which might be realized with an electrochemical probe. Restrictions (4.26) and (4.28) indicate $0.44 < L^{+} < 5000$.

If $L^{+} = 0.44$ is used in (4.27) it is found that the thinness of the Stokes layer is not a limitation in that frequenceis as high at $\omega^{+} = 40$ can be studied without violating (4.27). From (4.31) it is found, with $L^{+} = 0.44$, that frequencies as high as $\omega^{+} = 0.052$ can be used without correcting for the frequency response of the scalar boundary-layer. For reference, this is approximately equal to the median frequency of the turbulent velocity fluctuations close to a wall or to the bursting frequency. This means that the phase corrections for the frequency

response of the scalar boundary-layer will have to be taken into account in experiments with imposed oscillations, unless the oscillation has a much lower frequency than the turbulent velocity fluctuations.

## 4.4 Fabrication of Rectangular Electrode

A rectangular electrode was built in a plexiglass block which was then inserted into the wall of the test section. The procedure of manufacture is shown in Figure 4.9. A block of plexiglass is machined to the configuration as shown in Figure 4.9(a). The depth of the groove at one end is the thickness of the platinum sheet, which is the desired length of the electrode. At the other end the depth of the groove is greater, so that it can accommodate the junction of the platinum sheet and a copper wire. The platinum sheet is glued in the groove with epoxy (Techkits A-12). Another piece of plexiglass is glued on the top of the sheet as shown in Figure 4.9(b). After curing of the epoxy, the block is machined to the configuration shown in Figure 4.9(c) and inserted into a slit which is cut parallel to the pipe axis in the wall of the test section. The block is glued with epoxy in the slit and allowed to protrude a little to ensure the electrode is fully exposed and yet not leave an inordinate amount of the electrode to be abraded off. The surface of the electrode is sanded and polished progressively with wetted 400A, 600A and 4/0 emery paper. Finally polishing is done with Mirror Glaze Plastic Cleaner and Polish. In this manner, the rectangular electrode can be orientated with its longer side perpendicular to the axial flow direction and mounted flush with the wall.

## 4.5 Differential Pressure Measurement

Since there was a slight difference between the phase and the amplitude of the flow oscillation in the test section and the motion

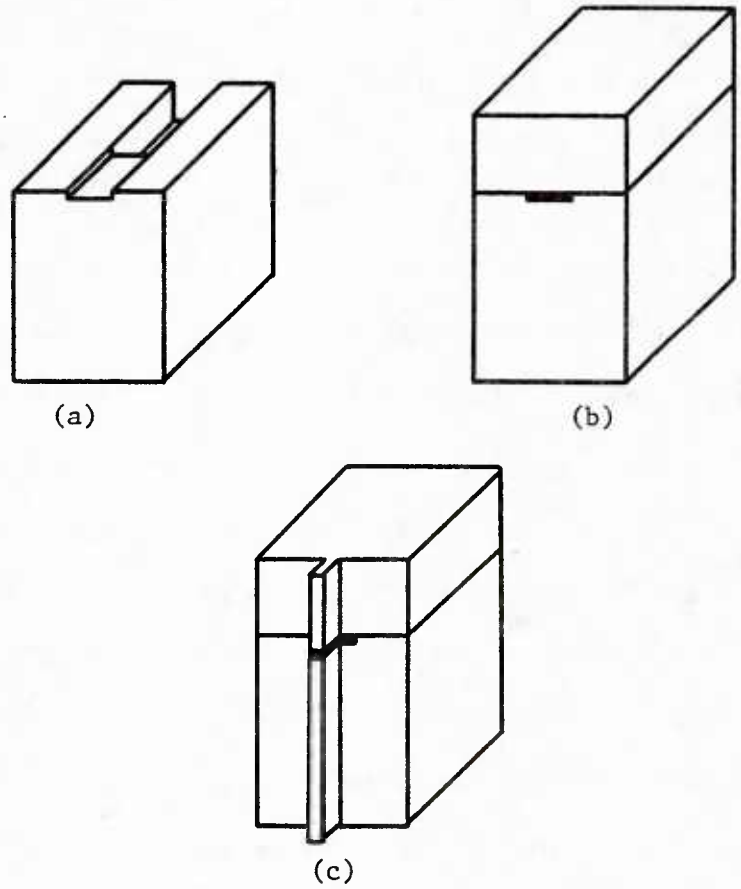


Figure 4.9 Fabrication of rectangular electrode

of the pulse generator, it was necessary to measure directly the flow oscillation in the test section. This was done with a differential pressure transmitter (Viatran, Model 704-115) having a full scale ± 2.54 cm water column corresponding to ± 5 volts output. Two pressure taps, 437.4 cm apart, were located on the two ends of the test section.

For a fully developed pipe flow, $p$ is dependent of $x$ and $t$, so the pressure gradient $\frac{\partial p}{\partial x}$ is only a function of time. That is,

$$\frac{\partial p}{\partial x} = \frac{\Delta p}{\Delta x}\,(t) \tag{4.32}$$

This measured time variation of the pressure gradient was used, along with equation (1.4), to calculate the time variation of the velocity at the center of the pipe.

The dynamic response of the pressure transmitter was determined in the following way: The flow loop was first filled with the solution. Then, the flow in the 19.4 cm pipe was oscillated by the motion of the piston with diaphragm valve 3 completely closed. Because of the incompressibility of the fluid, the motion in the test section was in phase with the piston and the amplitude of the pressure gradient variation could be calculated from the piston stroke length and frequency. The instanteous differential pressure signals were sampled and processed as described in the next section. Several frequencies and stroke lengths were tested. It was found that the phase lags of the pressure transmitter was dependent on frequency as shown in Figure 4.10. It was 9° for a frequency of 0.325 Hz and 25° for 0.625 Hz. The amplitude correction was dependent on $L_s f^2$, where $L_s$ is the stroke length of the pump. Figure 4.11 compares the measured amplitude with that calculated

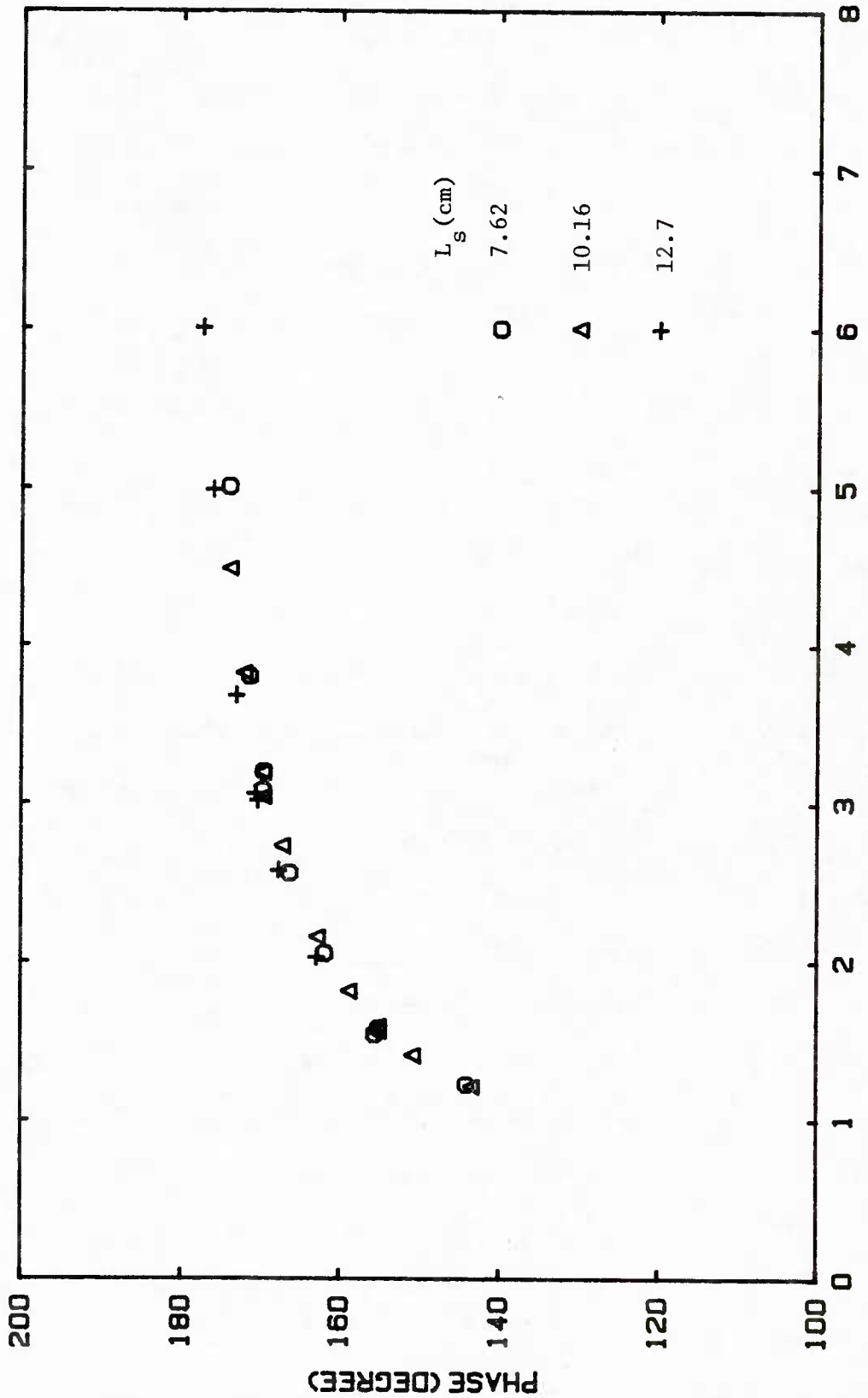


Figure 4.10 Phase correction for pressure transmitter

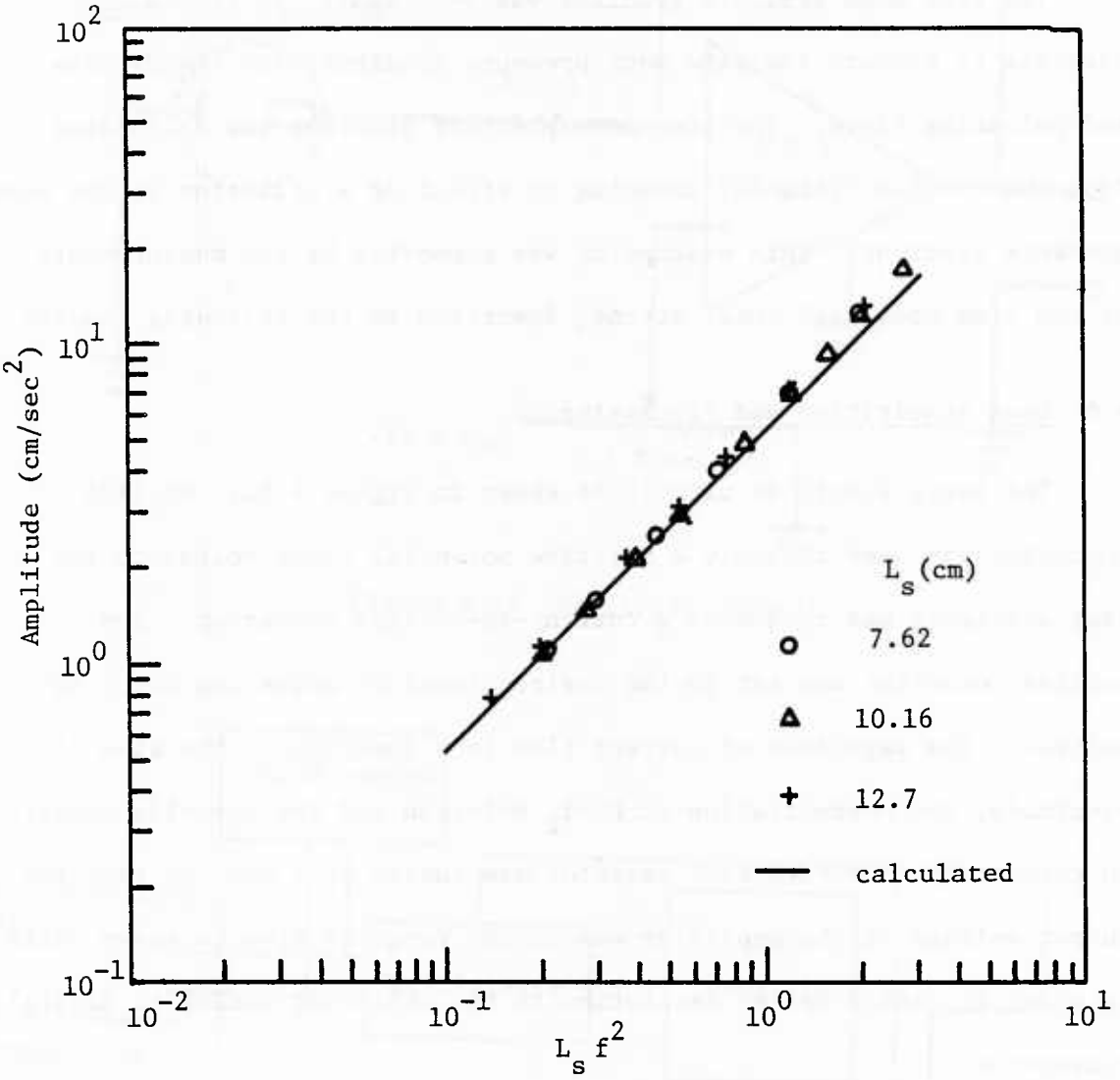


Figure 4.11 Amplitude calibration of pressure transmitter

were taken for each run. A sampling program was written for this purpose and is given in Appendix III.

In the measurement of pulsating flow, an optointerruptor on the pulse generator was used to provide a pulse of 4 volts when the piston reached a certain position in each cycle. This pulse served as a phase reference. The time between the two consecutive pulses is the period of the oscillation. It was measured with a programmable timer (Berkeley, 6401) and sampled through a real time clock board in the computer. Drift of the period of different cycles was found to be less than 0.1%. For each cycle of oscillation, this pulse initiated data sampling. Thirty two or sixty four samples per cycle were taken in equal time intervals and a total of 500 periods of data were collected on the disc of the computer in each experiment. At each sampling point the probes and the pressure transmitter were sampled at a high enough speed so that the measurements for all practical purposes, could be considered simultaneous. A program which controls this sampling process is given in Appendix III.

The digitized data were recorded on the disc in a binary format in order to save storage space. During data processing, the binary data were first converted to voltages in decimal format. These voltage data correspond to the output voltages of the electrode circuit and the pressure transmitter at each sampling instant. The output voltage of the electrode circuit is related to the velocity gradient at the wall:

$$S_x = \beta(V_{out} - V_{app})^3 , \tag{4.33}$$

according to (4.1) and (4.7), where $V_{out}$ is the output voltage and $V_{app}$, the applied voltage in the electrode circuit. Parameter $\beta$ is a constant

for each run. Therefore, the periodic variation of wall shear stress normalized by the time averaged value was obtained as

$$\frac{\langle S_x \rangle}{\overline{S}_x} = \frac{\langle (V_{out} - V_{app})^3 \rangle}{\overline{(V_{out} - V_{app})^3}} \quad . \tag{4.34}$$

The intensity of the turbulent velocity gradient fluctuations at the wall was given as

$$\frac{\overline{(s_x^2)}^{1/2}}{\overline{S}_x} = \frac{\left[\overline{(S_x - \langle S_x \rangle)^2}\right]}{\overline{S}_x} \quad , \tag{4.35}$$

and the intensity of the phase averaged turbulent fluctuations, as

$$\frac{(\langle s_x^2 \rangle)^{1/2}}{\overline{S}_x} = \frac{\left[\langle (S_x - \langle S_x \rangle)^2 \rangle\right]^{1/2}}{\overline{S}_x} \tag{4.36}$$

The output voltage of the pressure transmitter is proportional to the instantaneous pressure drop (2.54 cm water column per volt). The time averaged pressure drop was calculated by the Blasius formula rather than from the measured values, because serious errors were caused by the large zero drift of the transmitter and the small value of time mean pressure drop.

Phase averages and time averages were calculated on the computer in the following manner:

$$\langle E \rangle = E_i = \frac{1}{n} \sum_{j=1}^{n} E_{ij} \quad , \tag{4.37}$$

where $< E >$ are phase averaged data in one period and n, the number of periods to be averaged. Time averaging was done by averaging the phase averaged data over one period:

$$\overline{E} = \frac{1}{m} \sum_{i=1}^{m} E_i = \frac{1}{mn} \sum_{i=1}^{m} \sum_{j=1}^{n} E_{ij} , \tag{4.38}$$

where m is the number of samples in one period. The oscillating component was then obtained as

$$\check{E} = < E > - \overline{E} . \tag{4.39}$$

Only the first harmonic of the oscillation was considered, so the amplitude and the phase of the velocity gradient at the wall were obtained by a least-square fit of the phase averaged data with a cosine function.

The spectrum of the turbulent fluctuations of the velocity gradient at the wall was obtained by a Fast Fourier Transformation (Bendat and Piersol 1971). The analog singals from the wall probe were filtered by an analog low pass filter with a cut-off frequency 20 Hz before they were sampled by the computer at a rate of 40 Hz. The cut-off frequency was much higher than the medium frequency, $f^+ = .01$. Therefore, turbulent fluctuations with frequencies higher than the cut-off frequency make a negligible contribution to the total energy (Hanratty, et al., 1977). The actual sample size for each of FFT was 512. A total number of 20,480 of data points were used, i.e., 40 realizations were averaged to give an estimated spectrum. The spectrum was normalized so that the area under the curve is unity.

## 4.7 Experimental Procedure and Range

Before doing an experiment the solution was circulated between the filter and the lower storage tank for eight hours in order to remove small particles or dirt. Then the solution was pumped into the upper storage tank and the loop was filled through the downflow pipe line. However the piping above the solution level in the tank couldn't be filled with the solution. When the centrifugal pump started, the air inside this portion of the piping was pushed into the tank and part of it was entrained into the flow loop. Another origin of the air bubbles in the fluid was the decrease of solubility of the air with the increase of solution temperature when the solution was circulated through the loop. These bubbles, sometimes, stuck on the wall of the test section and made measurement impossible. It took a long time to get rid of the bubbles. The flow was turned on at a high flow rate and then turned off to settle for an hour. This process was repeated several times. Sometimes, it was necessary to run the flow for a long time to increase the temperature of the solution above the experimental temperature. Then the flow was allowed to settle for an hour. Afterwards, the loop was run again and the flow temperature was cooled down to the experimental temperature 25 ± 0.1 °C by adjusting the cooling water through the cooling coil. This was a very tedious process, but it was very important for obtaining satisfactory data.

Mean flow rate was adjusted by diaphragm valve 3 and was measured by the vortex shedding flow transmitter. For steady flow measurements, at least thirty minutes for stabilizing the flow was necessary before taking data. For the measurements of the pulsating flow, the frequency

of the oscillation was adjusted to the desired value and was kept constant for at least 500 periods before sampling the data in order to reach stationary oscillation.

The polarization curves of the electrode in the experimental range of Reynolds numbers were measured, as shown in Figure 4.14. These suggested the choice of -0.4 volts as the applied voltage to the test electrode.

The wave form of the oscillation was monitored by the differential pressure signal on the oscilloscope. If the pressure signal was distorted from a sinusoidal variation, it was likely to that air was in some portion of the system. Data were not taken until the pressure signal showed a sinusoidal variation. The period of each cycle was indicated by the programmable timer. If the drift of the period was greater than 0.1% of its value in the experiment, the data were disregarded.

The experiments were designed to cover a range of oscillation frequencies around the medium frequency of the turbulent velocity fluctuations in the vicinity of the wall, i.e., $\omega^+ = 2\pi \times 0.01$. This was realized by fixing the frequency of the imposed oscillation at 0.625 Hz or 0.325 Hz and varying the Reynolds number of the mean flow from 15,000 to 70,000. The amplitude of the central velocity variation was 10% of the mean velocity for most of the experiments. However, for high Reynolds numbers, an amplitude of less than 10% had to be used because of the limited capacity of the pulse generator. An oscillation amplitude of 5% was also used at Reynolds numbers of 15,000 and 20,000 with a frequency 0.625 Hz in order to examine the assumption of a linear response of the wall shear stress to the imposed oscillation.

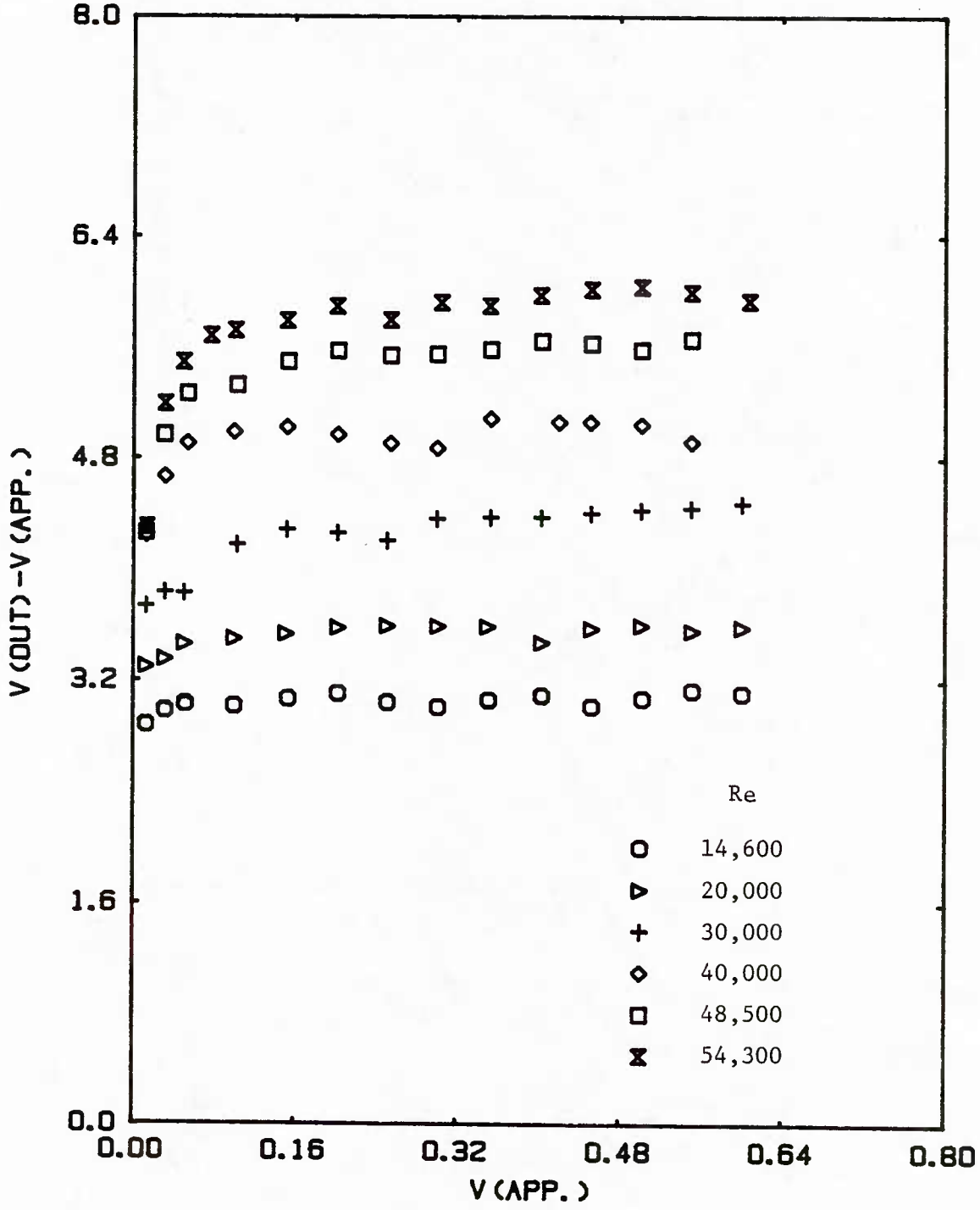


Figure 4.14 Polarization of electrode (L = 0.00762 cm)

The reason for using a small amplitude was to eliminate nonlinear effects and, therefore, to make the analysis of the results easier. The experimental conditions are listed in Table 4.2. Several dimensionless groups of frequency are also calculated for comparison with studies of other researchers.

Table 4.2

Experimental Range

| Re | f(1/sec) | $L_s$(cm) | $\lvert\hat{u}_c\rvert / \bar{u}_b$ | $\Omega = \frac{\omega}{\nu} R$ | $\frac{\omega D}{\bar{u}^*}$ | $\frac{\omega D}{\bar{u}_b}$ | $\frac{\omega^*}{15}$ |
|---|---|---|---|---|---|---|---|
| 15,000 | 0.325 | 8.7 | 0.1 | 149 | 99 | 5.9 | 0.0074 |
| 20,000 | 0.325 | 8.2 | 0.1 | 149 | 77 | 4.4 | 0.0045 |
| 30,000 | 0.325 | 11.9 | 0.1 | 149 | 54 | 3.0 | 0.0023 |
| 40,000 | 0.325 | 12.7 | 0.077 | 149 | 40 | 2.2 | 0.0013 |
| 50,000 | 0.325 | 12.7 | 0.062 | 149 | 35 | 1.8 | 0.0009 |
| 60,000 | 0.325 | 12.7 | 0.052 | 149 | 29 | 1.5 | 0.00065 |
| 70,000 | 0.325 | 12.7 | 0.044 | 149 | 26 | 1.3 | 0.00050 |
| 15,000 | 0.625 | 3.2 | 0.1 | 207 | 190 | 11.4 | 0.014 |
| 20,000 | 0.625 | 4.3 | 0.1 | 207 | 148 | 8.53 | 0.0086 |
| 30,000 | 0.625 | 6.4 | 0.1 | 207 | 104 | 5.69 | 0.0042 |
| 40,000 | 0.625 | 8.5 | 0.1 | 207 | 77 | 4.27 | 0.0026 |
| 50,000 | 0.625 | 10.7 | 0.1 | 207 | 66 | 3.41 | 0.0017 |
| 60,000 | 0.625 | 12.8 | 0.1 | 207 | 57 | 2.84 | 0.0013 |
| 70,000 | 0.625 | 12.7 | 0.086 | 207 | 49 | 2.44 | 0.00095 |

# CHAPTER 5. RESULTS

## 5.1 Numerical Results

The numerical scheme was first tested by comparing the numerical result for the quasilaminar model A with the asymptotic solution for laminar pulsating flow at high frequency. Figure 5.1 shows velocity profiles of the oscillating component, normalized by the amplitude of velocity at the pipe center, at eight phases of a cycle at $\Omega = 206$. Figures 5.2 and 5.3 give the amplitude profiles and the phase profiles of the oscillating velocity component for the two frequencies used in the present study. The solid lines represent the numerical results of Model A while the symbols are the asymptotic results obtained from the analytical solution for high frequencies. Agreement between the two is very good. This indicates that the numerical scheme used in this study is suitable for further studies of the four models described in Chapter 3.

Figures 5.4 and 5.5 give the amplitude profiles and the phase profiles of oscillation velocity calculated from four different models at Re = 15,000 and f = 0.625 Hz. This corresponds to the high $\omega^+$ extreme covered in the experiments. It is seen that the variation of the oscillating velocity is confined to a thin layer close to the wall about 0.01 of the pipe radius, which corresponds to $y^+ = 5$, i.e., the thickness of viscous sublayer. The four models behave very similarly because of the negligible effects of turbulence in the viscous sublayer. In the range of $0.01 < Y < 0.04$ the four models have slight differences because they use amounts of oscillation induced eddy viscosity in this

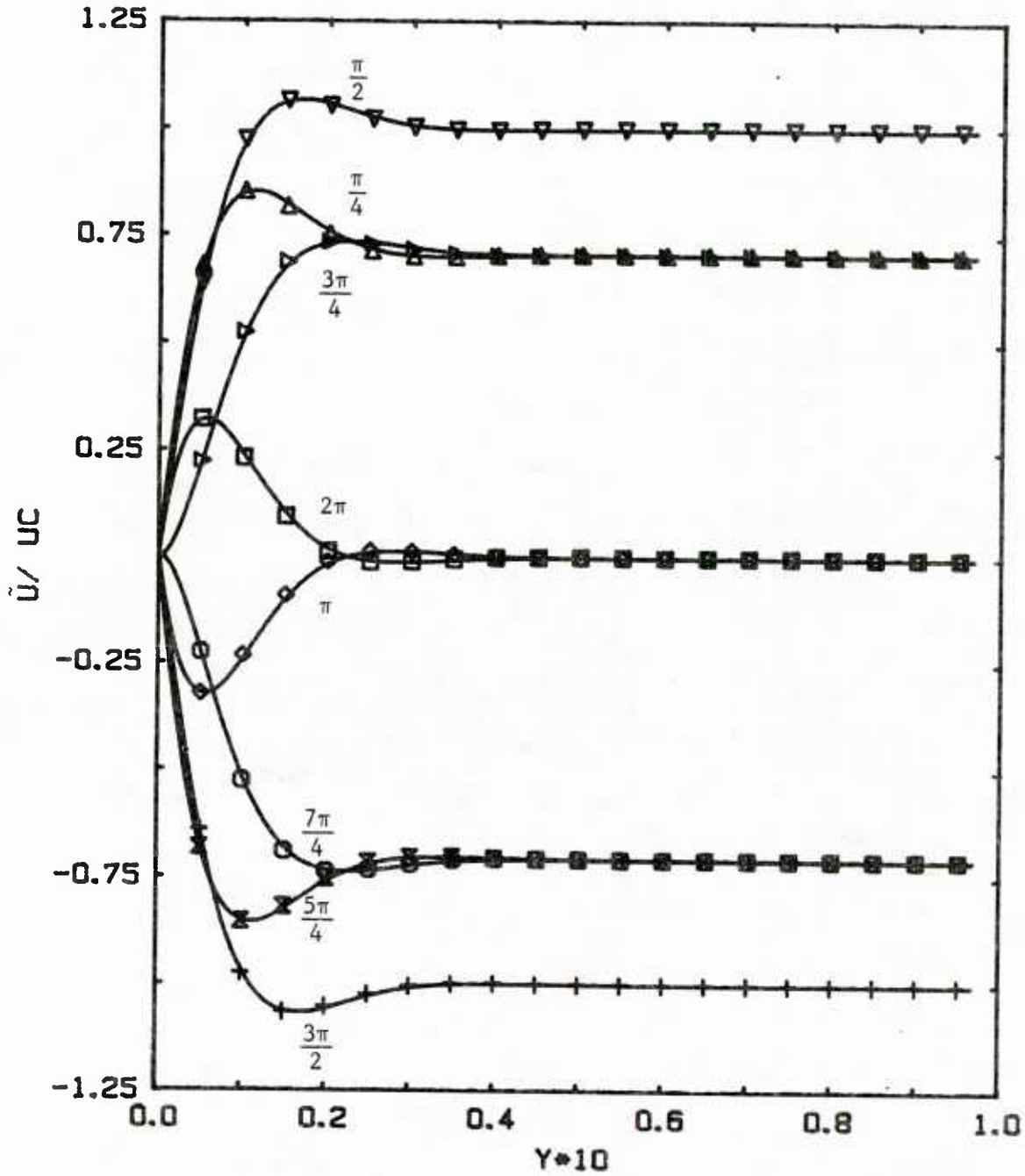


Figure 5.1 Oscillation velocity profiles at $\Omega$ = 206
(— numerical solution of Model A
symbol: asymptotic solution of laminar
pulsating flow at high frequency)

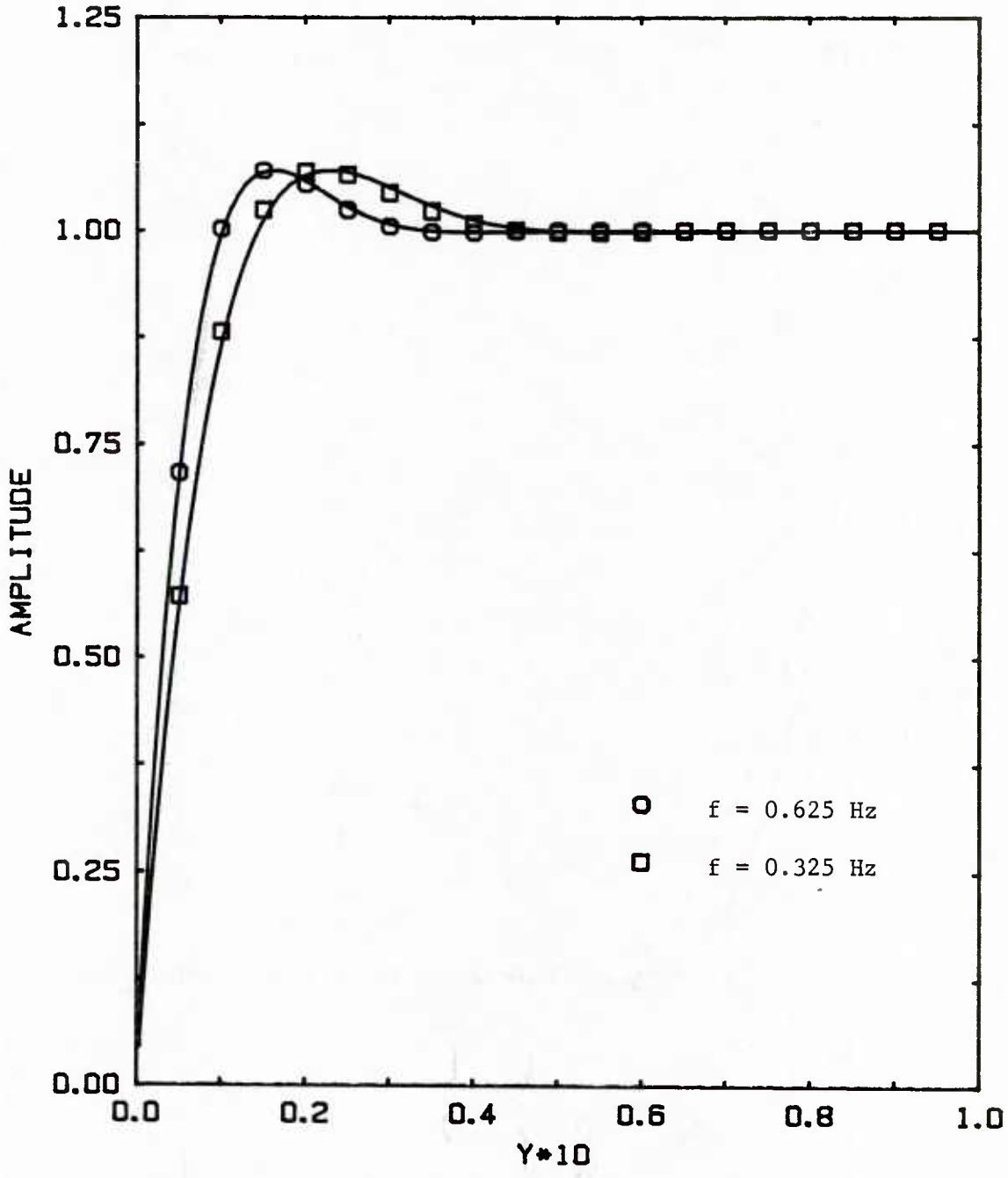


Figure 5.2 Amplitude profiles of oscillation velocity
(— numerical solution of Model A
symbol: asymptotic solution of laminar
pulsating flow)

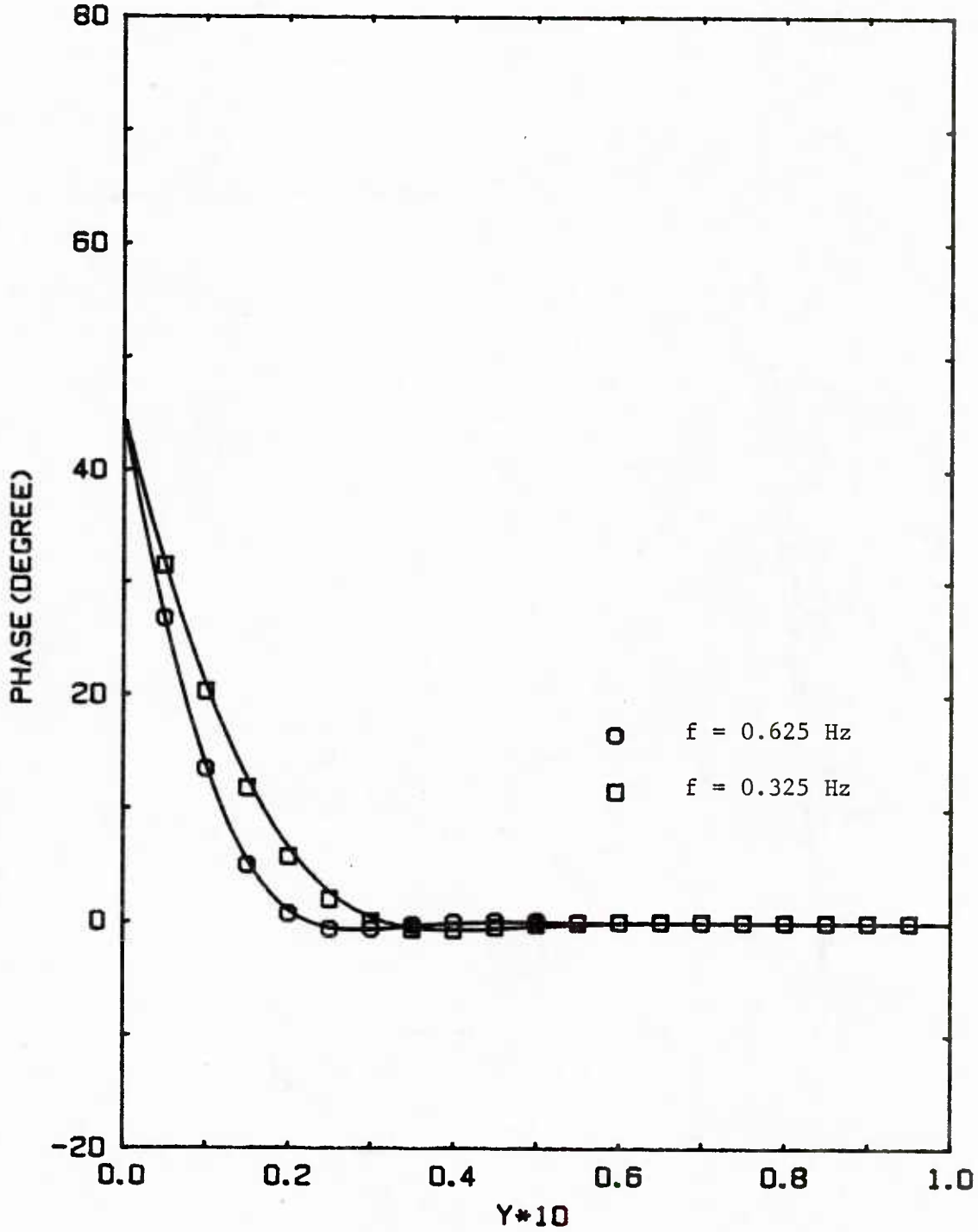


Figure 5.3 Phase profiles of oscillation velocity
(— numerical solution of Model A
symbol: asymptotic solution of laminar
pulsating flow)

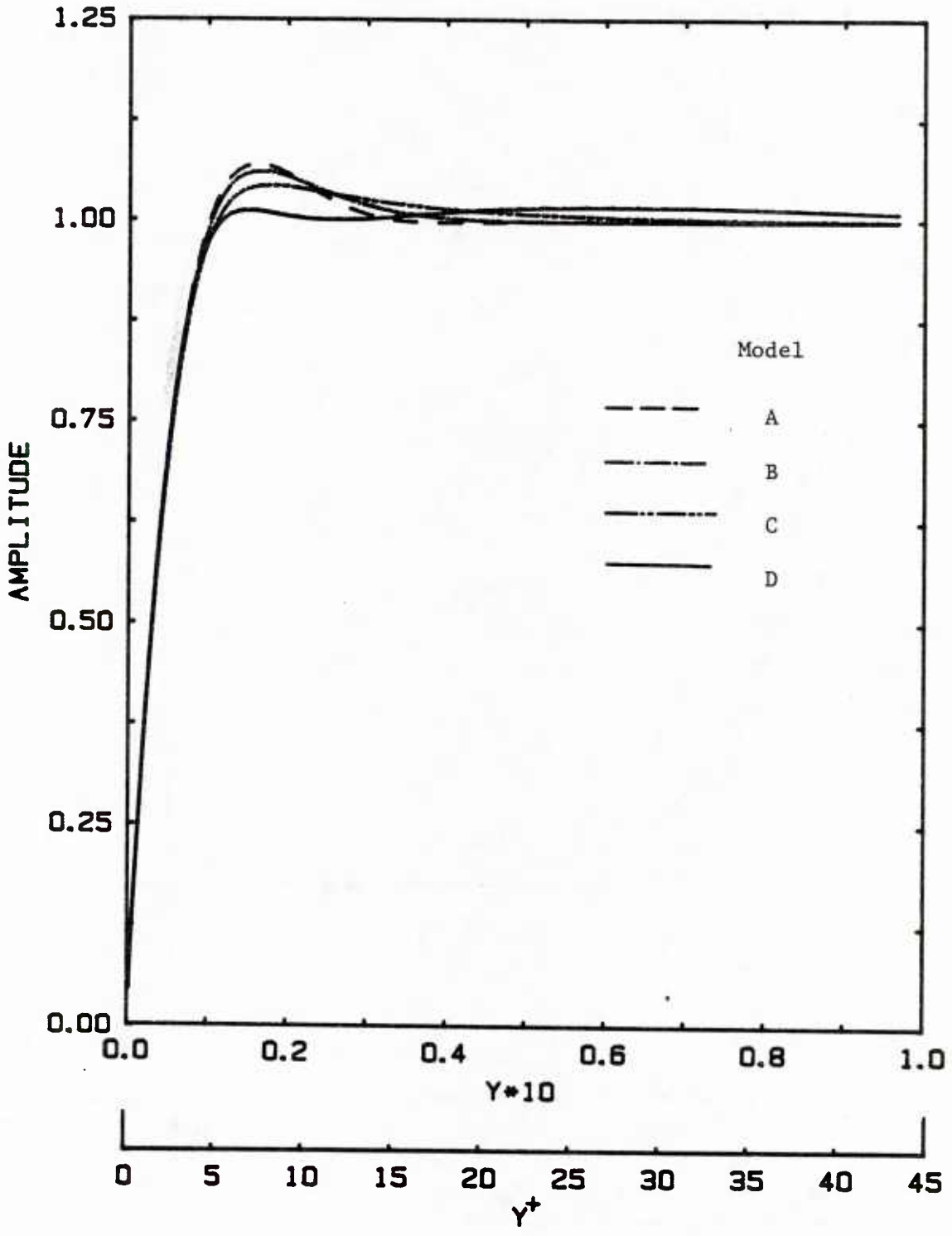


Figure 5.4 Amplitude profiles of oscillation velocity for different models at Re = 15,000 and f = 0.625 Hz ($\omega^+/15 = 0.014$)

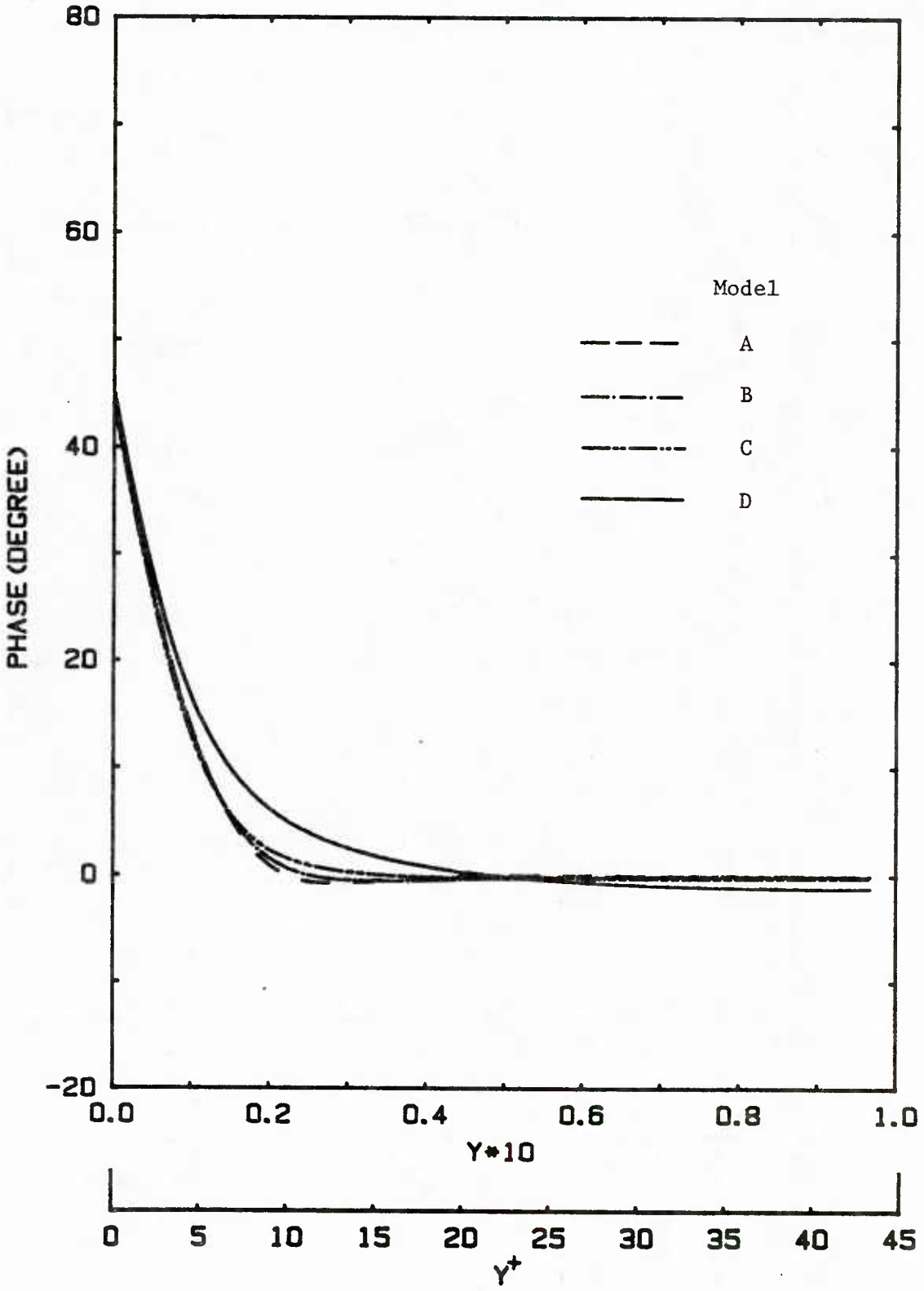


Figure 5.5 Phase profiles of oscillation velocity for different models at Re = 15,000, f = 0.625 Hz ($\omega^+/15 = 0.014$)

range. The models C and D give larger oscillation induced eddy viscosities than models A and B, so that the over shoots of amplitude for models C and D are less then models A and B. The difference between model C and model D is caused by the pressure gradient effect considered in model D. In the range of $Y > 0.04$ the results of the four models become closer again. This is because inertial effects are so large in this region that differences in eddy viscosities predicted by the four models have negligible influence on the solution.

Figures 5.6 and 5.7 show the amplitude profiles and the phase profiles calculated from the four models at Re = 60,000 and f = .325 Hz. The profiles of model A are very similar to that shown in Figures 5.4 and 5.5, except that the hump in the amplitude profile moves slightly away from the wall due to the lower frequency in this case. However, the results from models B, C and D are quite different. At a Reynolds number 60,000 the viscous sublayer is much thinner than at Re = 15,000. Although the spatial variation of oscillation velocity is in a thin layer of $Y = 0.02$, the turbulent effects on the flow oscillation are no longer negligible because this layer corresponds to $y^+ \approx 25$. It is seen in Figure 5.7 that the phase of velocity gradient at the wall is very sensitive to the different turbulent models. In the range of $Y > 0.08$ the inertial force controls the flow oscillation and the different models show similar results.

From the comparison of different turbulent models, it is clearly seen that the modeling of turbulence in the region of $y^+ < 40$ is the key to understanding turbulent pulsating flow at high oscillation frequencies and that the relative thickness of the stokes layer and the viscous sublayer is a measure of the importance of turbulent effects on

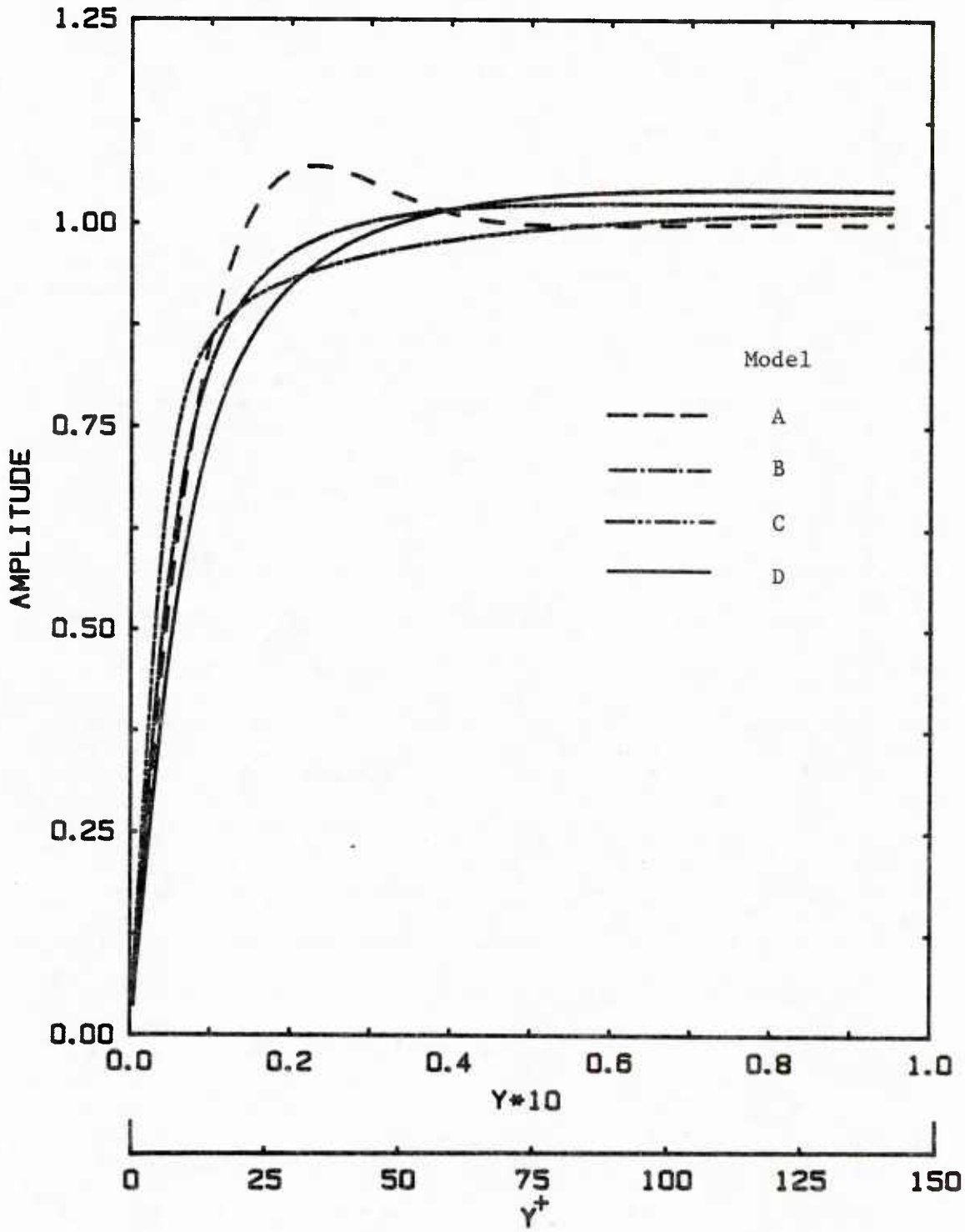


Figure 5.6 Amplitude profiles of oscillation velocity for different models at Re = 60,000, f = 0.325 Hz ($\omega^+/15 = 0.00065$)

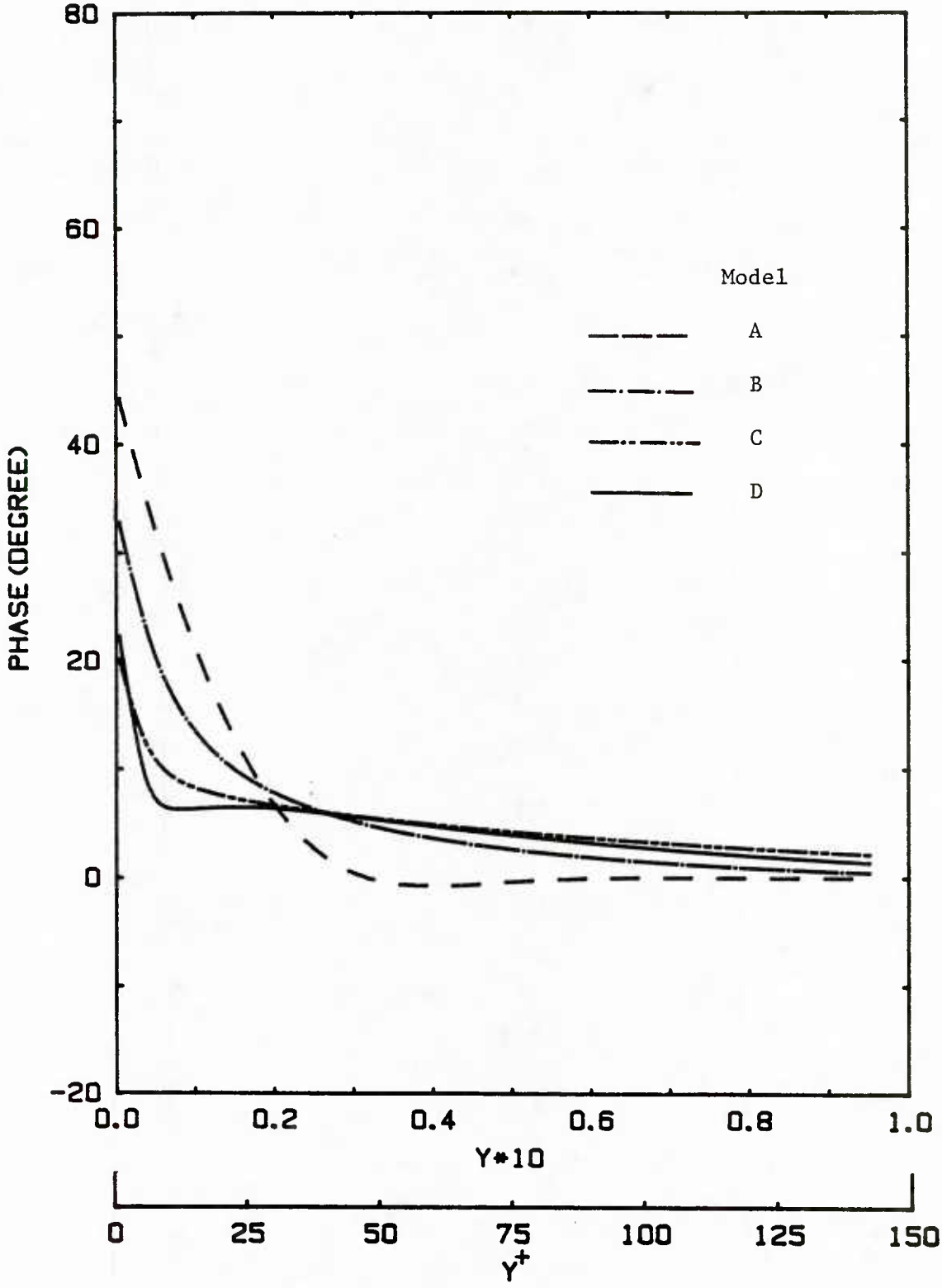


Figure 5.7 Phase profiles of oscillation velocity for different models at Re = 60,000, f = 0.325 Hz ($\omega^+/15 = 0.00065$)

the flow oscillation. It is also found that the wall shear stress is very sensitive to the turbulent modeling. These types of numerical results will be compared with experimental data in section 5.3.

## 5.2 Experimental Results

### (a) Instantaneous velocity gradient at the wall

Figure 5.8 shows typical measurements of the streamwise components of the instantaneous velocity gradient at the wall for a Reynolds number 30,000. In Figure 5.8(a), the time averaged value is subtracted from the instantaneous value, so the signal represents a summation of the oscillation component and turbulent fluctuations. Since turbulent fluctuations at the wall are large, the organized part of velocity gradient is buried in random fluctuations. However, the periodic variation can still be distinguished when the signal is compared to the ticks, representing the time period of the flow oscillation, in Figure 5.8(a). It is observed that the period of the organized variation in 5.8(a) is of the same order as the period of the characteristic turbulent fluctuations in a steady flow at the same Reynolds number 30,000, shown in Figure 5.8(c). This is expected since the imposed oscillation frequency, 0.625 Hz, was chosen to match the characteristic frequency of the turbulent fluctuations in the vicinity of the wall at Reynolds number 30,000.

In Figure 5.8(b), phase averaged values are subtracted from the instantaneous signals, i.e., the oscillation component is removed from 5.8(a). The signal in Figure 5.8(b) represents the turbulent fluctuations of the velocity gradient at the wall in the pulsating flow. A comparison 5.8(b) with 5.8(c) shows no major differences. This indicates that for imposed oscillations of small amplitude, the interaction between the

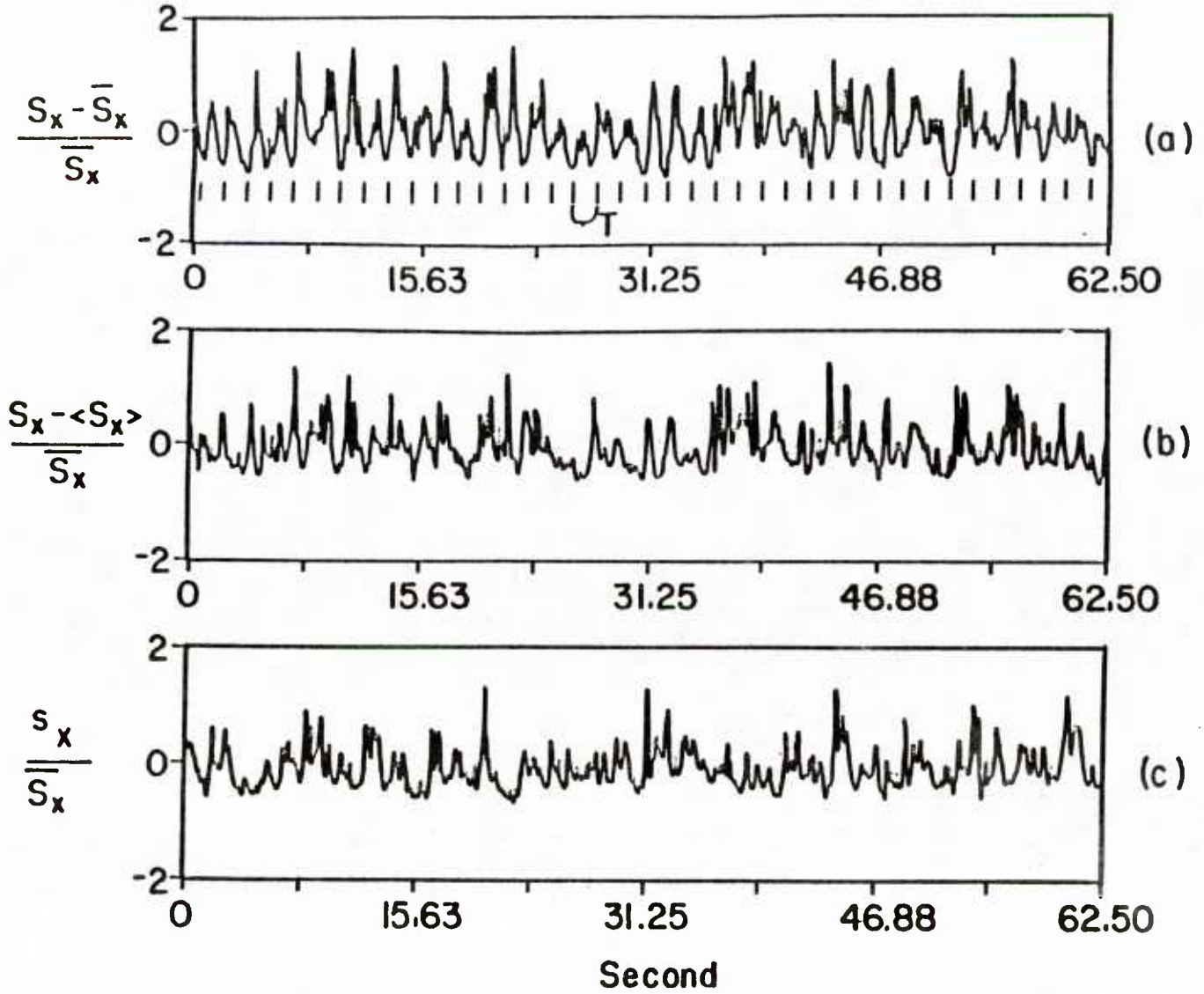


Figure 5.8 Instantaneous signals from wall probe at Re = 30,000

(a) with oscillation, f = 0.625 Hz ($\omega^+/15 = 0.042$)

(b) with oscillation, f = 0.625 Hz, but subtracting oscillation component from (a)

(c) steady flow

turbulence and the imposed oscillation is not clearly seen, even though their frequencies are similar.

Power spectra of the instantaneous signals are shown in Figure 5.9. The sharp peak at a frequency 0.63 Hz in Figure 5.9(a) represents the contribution of the imposed oscillation to the total energy. Figure 5.9(b) shows the spectrum of turbulent fluctuations of velocity gradient at the wall after removing the phase averaged values from the instantaneous signals. Figures 5.9(c) is the spectrum of turbulent fluctuations of the velocity gradient at the wall in steady flow at a Reynolds number 30,000. No major difference is observed between Figures 5.9(b) and 4.9(c). This would seem to suggest that the turbulent properties are not affected by the imposed oscillation.

The peaks at frequencies 13 Hz and 3 Hz are considered to be caused by some unknown disturbance in the flow system, because the peaks appear at the same frequencies in the steady flow at different Reynolds numbers.

(b) Time averaged values of the velocity gradient at the wall

Figure 5.10 shows the measured time averaged values of the velocity gradient at the wall at different flow conditions. It is observed that the imposed oscillation has no effect on the time mean velocity gradient at the wall.

Intensities of turbulent fluctuations of the velcotiy gradient at the wall are shown in Figure 5.11. The intensities are the results of long time averaging, and are noticed to be independent of Reynolds number and of imposed flow oscillation. The value, 0.35, agrees with previous measurements by other researchers (Sirkar 1969, Fortuna and Hanratty 1971, Eckelman 1971).

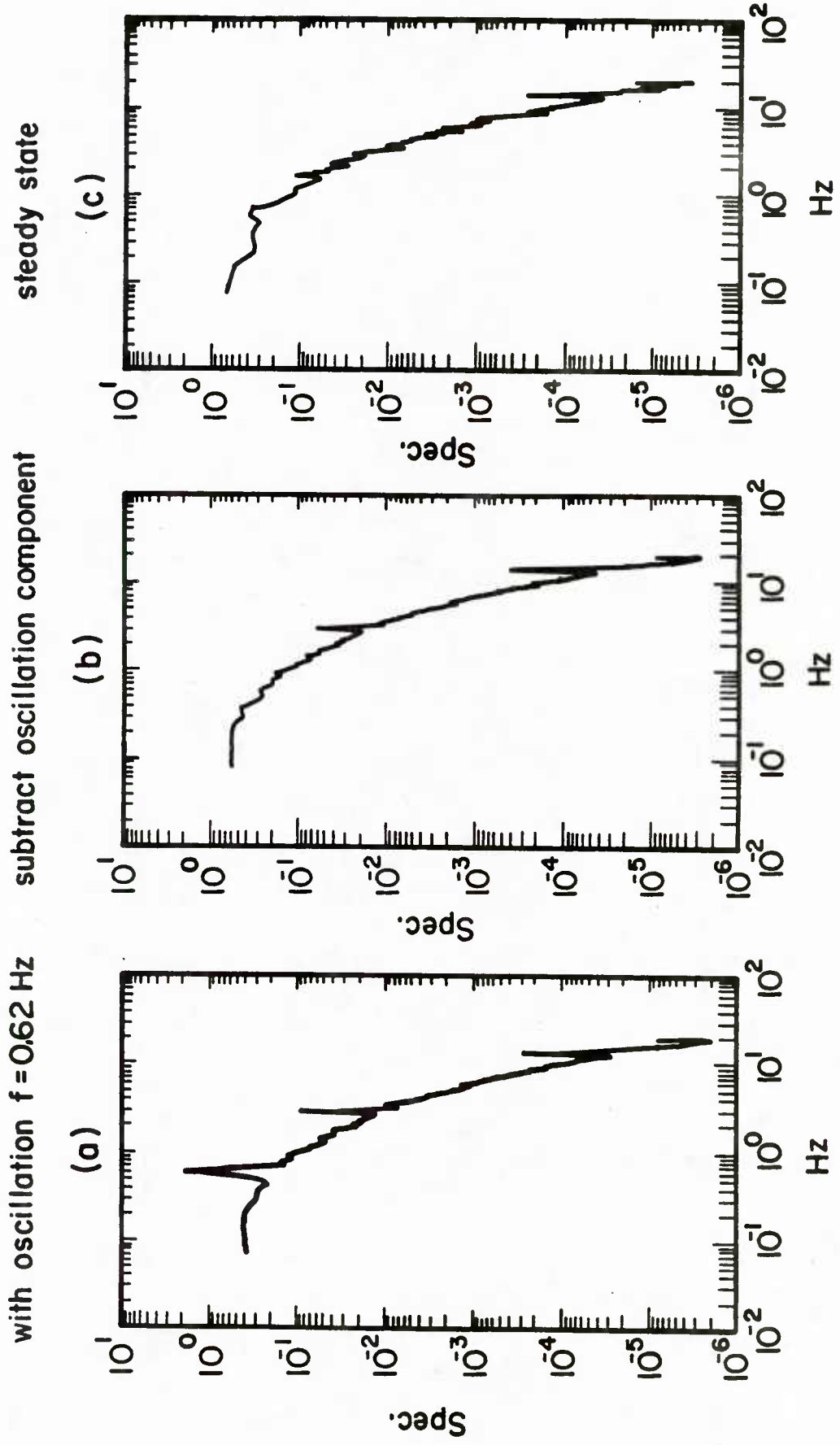


Figure 5.9 Spectrum of fluctuations of velocity gradient at the wall (Re = 30,000)

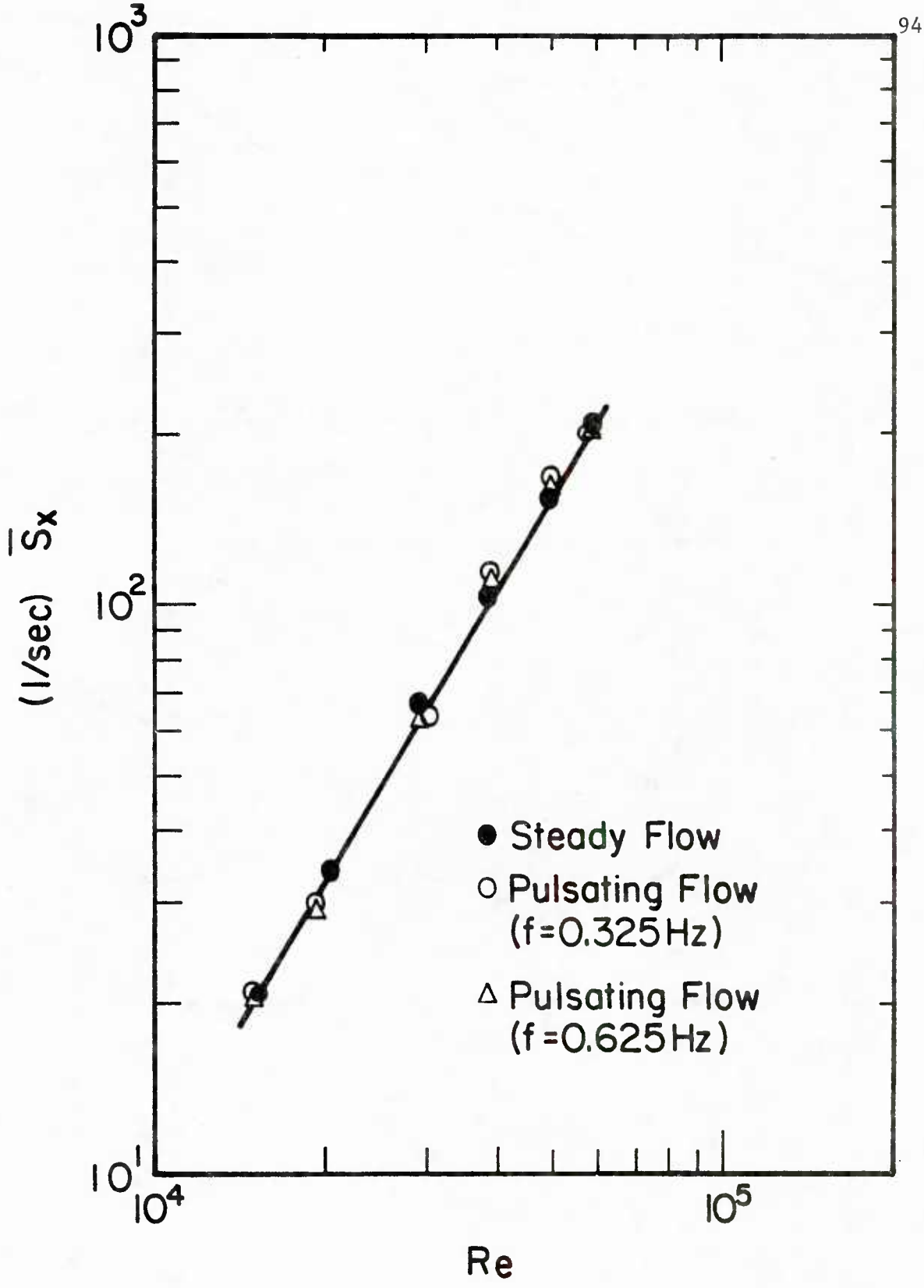


Figure 5.10 Time average velocity gradient at the wall in different flow conditions

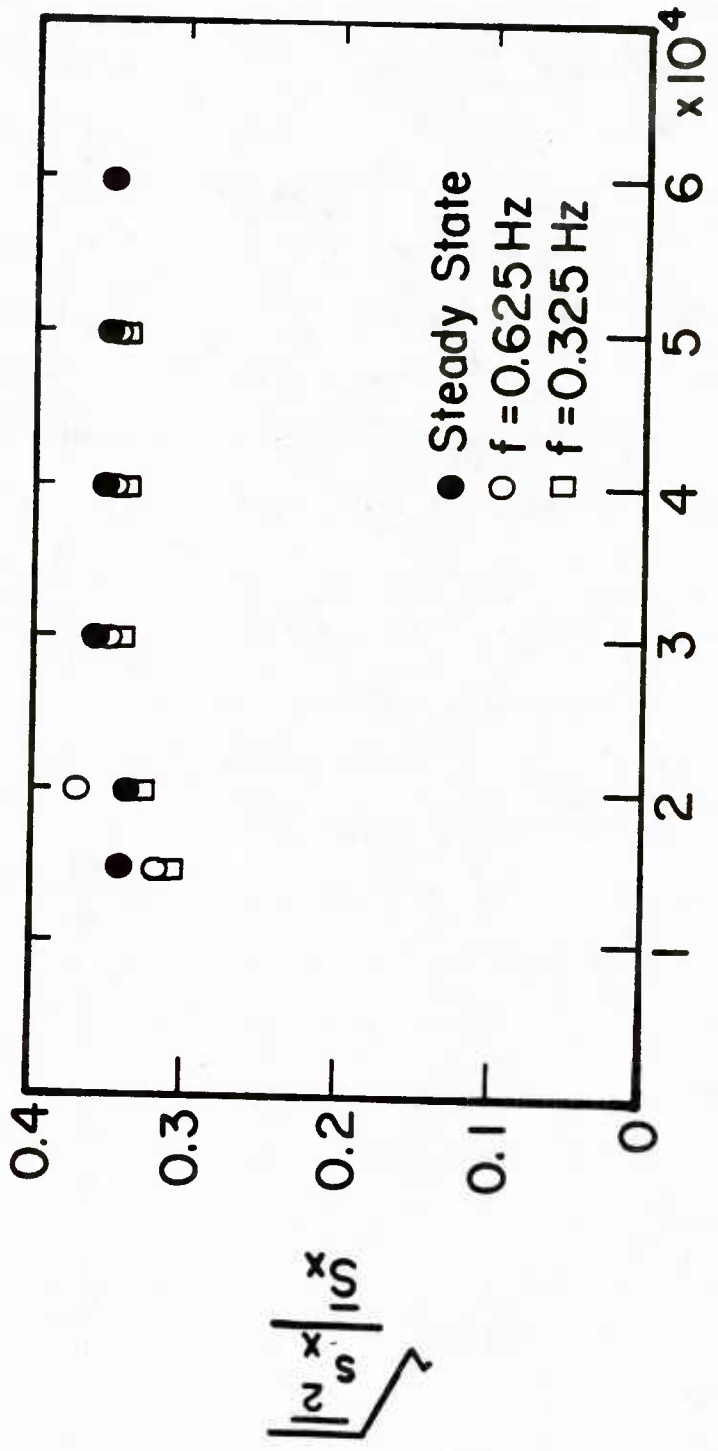


Figure 5.11 Time averaged intensities of turbulent fluctuations of velocity gradient at the wall in different flow conditions

The results that have been presented here indicate that time averaged properties in a pulsating flow are not different from those observed in a flow without pulsations. These agree with the findings by most of previous investigators and serve as a base to separate the oscillation flow field by simply subtracting the mean flow field, which is the same as the steady flow, from the phase averaged flow field.

(c) Phase averaged values of the velocity gradient at the wall in a pulsating flow

Figures 5.12 to 5.26 give a set of phase averaged data measured at different flow conditions in the experimental range. In each figure, the phase averaged favorable pressure gradient normalized by its time mean value is given in (a), the phase averaged vleocity gradient at the wall or wall shear stress normalized by its time mean value is shown in (b) and the phase averaged intensity of turbulent fluctuations of velocity gradient at the wall is plotted in (c). The abscissa is the phase in a cycle, referred to the trigger signal from the piston as described in Chapter 4. The data, which are the phase averaged results for the instantaneous signal over 500 periods, have been corrected for errors caused by the frequency response of the sensors. In the following, two extremes in the experimental range will be discussed in detail.

Figure 5.12(a) shows the phase averaged pressure gradient measured at a Reynolds number of 15,400 using an imposed 0.625 Hz oscillation which has an amplitude 10% of the central mean velocity. It is seen that the amplitude of the pressure gradient oscillation is very large in this case, about eighty times its mean value. This is caused by the relatively high frequency of the oscillation and the low time mean velocity. This case represents one extreme in the experimental range,

i.e., a low Reynolds number and a high frequency oscillation. The solid line is the least square fit of the data with a cosine curve. It is seen that most of the energy of the flow oscillation is contained in a single harmonic.

Figure 5.12(b) shows the phase averaged vleocity gradient at the wall, normalized with its mean value. The 50% variation of velocity gradient at the wall, compared with the 10% variation of the central velocity, arises because the spatial variation of the oscillation velocity is confined to a thin layer close to the wall for this high frequency case. The data are fit quite well with a cosine curve which is shifted about 54° relative to the curve describing the pressure gradient. This indicates a linear response of the phase averaged flow field to the imposed pressure variation. A linear response is also indicated from experimental results shown in Figure 5.13, which were obtained with a 5% variation of the central velocity. The amplitude of pressure gradient is about fourty times that of the mean and the amplitude of velocity gradient is one half of that indicated in Figure 5.12(b). The phase shifts of the velocity gradients are the same for both cases.

It is interesting that phase averaged intensities of turbulent fluctuations are highly nonlinear, as shown in Figure 5.12(c), even though their time average is the same as in steady flow. This nonlinear effect seems to be related to the amplitude of the imposed oscillation. For example, the nonlinear effect is not as obvious in Figure 5.13(c) as it is in Figure 5.12(c). It is of interest to note that the maximum value of intensity occurs close to when the pressure gradient has its maximum favorable value, and the minimum, close to when the maximum of

unfavorable pressure gradient occurs. This contrasts with the finding for boundary layer flows that turbulence near the wall is suppressed by a favorable pressure gradient and enhanced by an unfavorable pressure gradient. These results indicate that the turbulence does not respond immediately to a high frequency oscillation of the pressure gradient.

Figure 5.25 shows another set of data at a Reynolds number 60,000 and a frequency 0.325 Hz. The amplitude of the central velocity oscillation is about 5%. This case represents another extreme in the experimental range; that is, a high Reynolds number and a low frequency. In Figure 5.25(a), the amplitude of the pressure gradient is seven times its time mean value and there is some scatter of the data. However, the data still clearly show a sinusoidal variation if only the first harmonic is considered. Phase averaged data of the velocity gradient at the wall are shown in Figure 5.25(b). For the same 5% amplitude of central velocity variation, the responses at the wall for the two extremes of the experiments are quite different, as can be seen by comparing Figure 5.13(b) and 5.25(b). For example, the amplitude of the velocity gradient is about 6% and the phase shift is 67° in this case rather than about 25% and 54° in the case of low Reynolds number and high frequency. The intensity data shown in 5.25(c) are more scattered. However, a sinusoidal variation can still be distinguished. It is interesting to note that in this case the minimum value of the intensity occurs close to the maximum favorable pressure gradient and the maximum occurs near the maximum of unfavorable pressure gradient. This indicates that high frequency turbulence that occurs at large Reynolds number can adjust to a slow oscillation of the pressure gradient.

Some general trends can be seen from this set of figures. For a fixed oscillation frequncy and amplitude of the central velocity, the normalized amplitude of pressure gradient decreases as the Reynolds number increases; so does the amplitude of wall shear stress. This is very different from the results of laminar pulsating flow, which depends only on the dimensionless frequency $\Omega$. This difference can be attributed to the strong effects of turbulence on the flow oscillation. For the same Reynolds number and amplitude of flow oscillation, a higher oscillation frequency gives higher an amplitude of the variation of the wall shear stress. The amplitude effect is linear when it is small, as shown in Figures 5.12, 5.13 and 4.8.

At large Reynolds number the imposed oscillation is found not to be perfectly sinusoidal. This is attributed to the use of a large stroke length, which is necessary to maintain the same amplitude, as shown in Appendix IV.

It is difficult to draw any quantitative conclusion from the scattered intensity data. However, it seems that certain qualitative trends can be recognized. For both imposed frequencies studied, the nonlinear response of the phase averaged turbulent intensity of the wall shear stress exists at low Reynolds number or high $\omega^+$. This nonlinearity becomes smaller as Reynolds number increases and as the amplitude of imposed oscillation decreases. At high $\omega^+$ the variation of the phase averaged intensity is roughly in phase with the favorable pressure gradient. At about $\omega^+/15 \cong 0.002$, the periodic variation of the intensity is hardly seen, and a further decrease of $\omega^+$ the variation of the intensity in a cycle become clear again but its phase is roughly 180° out of phase with the favorable pressure gradient.

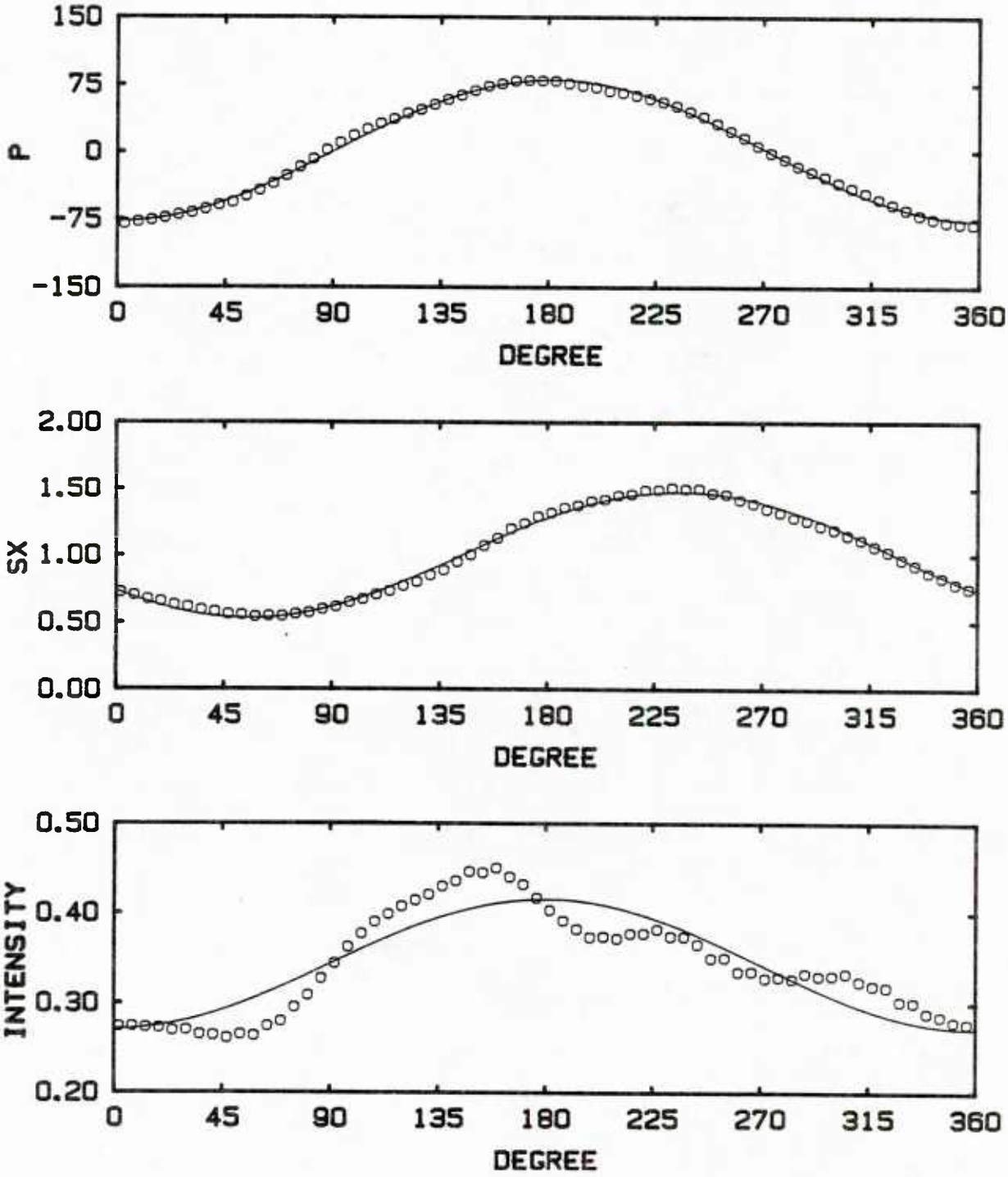


Figure 5.12 Phase averaged values at Re = 15,400, f = 0.625 Hz and a = 0.1 ($\omega^+/15 = 0.014$)

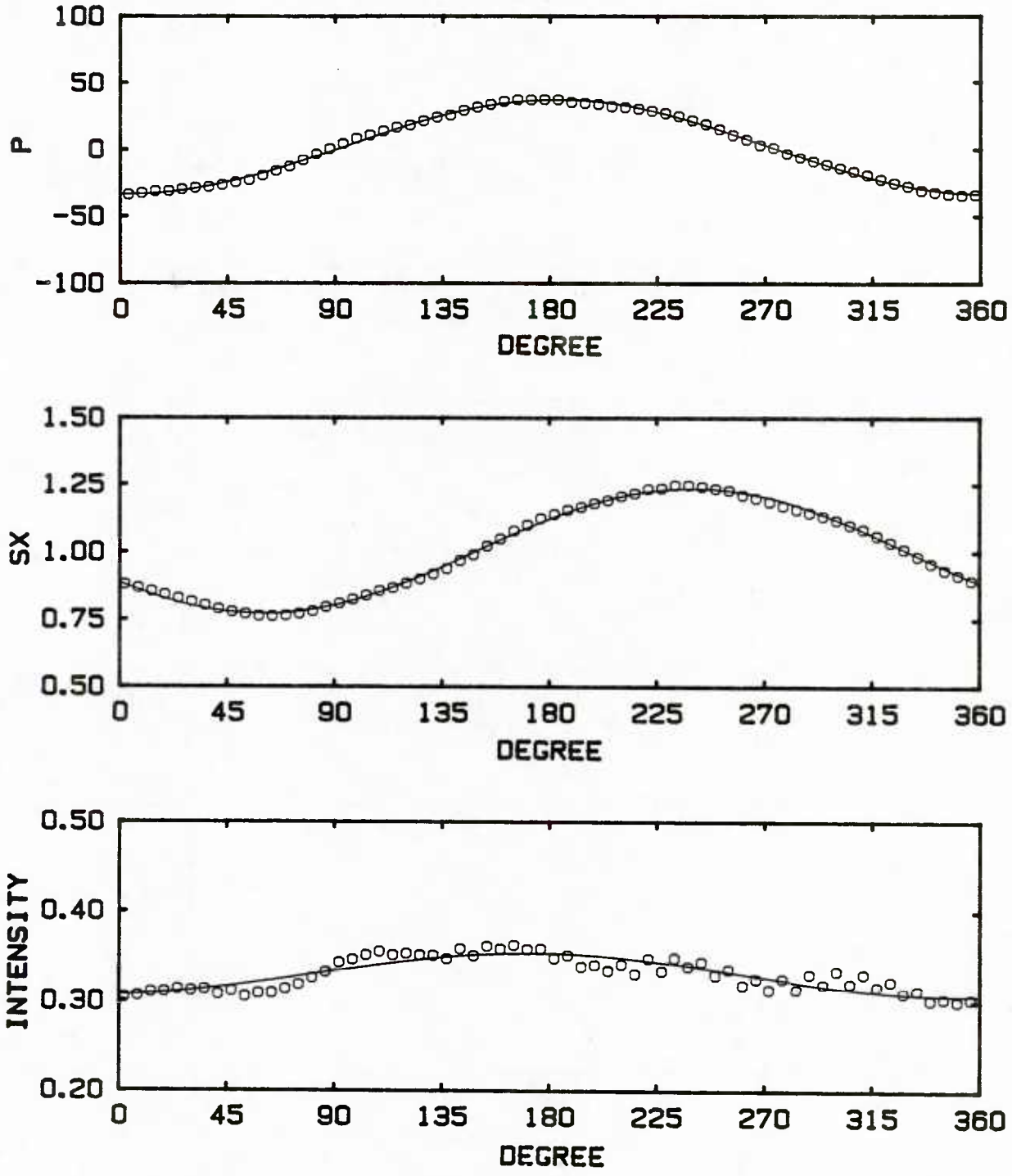


Figure 5.13 Phase averaged values at $Re = 15,400$, $f = 0.625$ Hz and $a = 0.05$ ($\omega^+/15 = 0.014$)

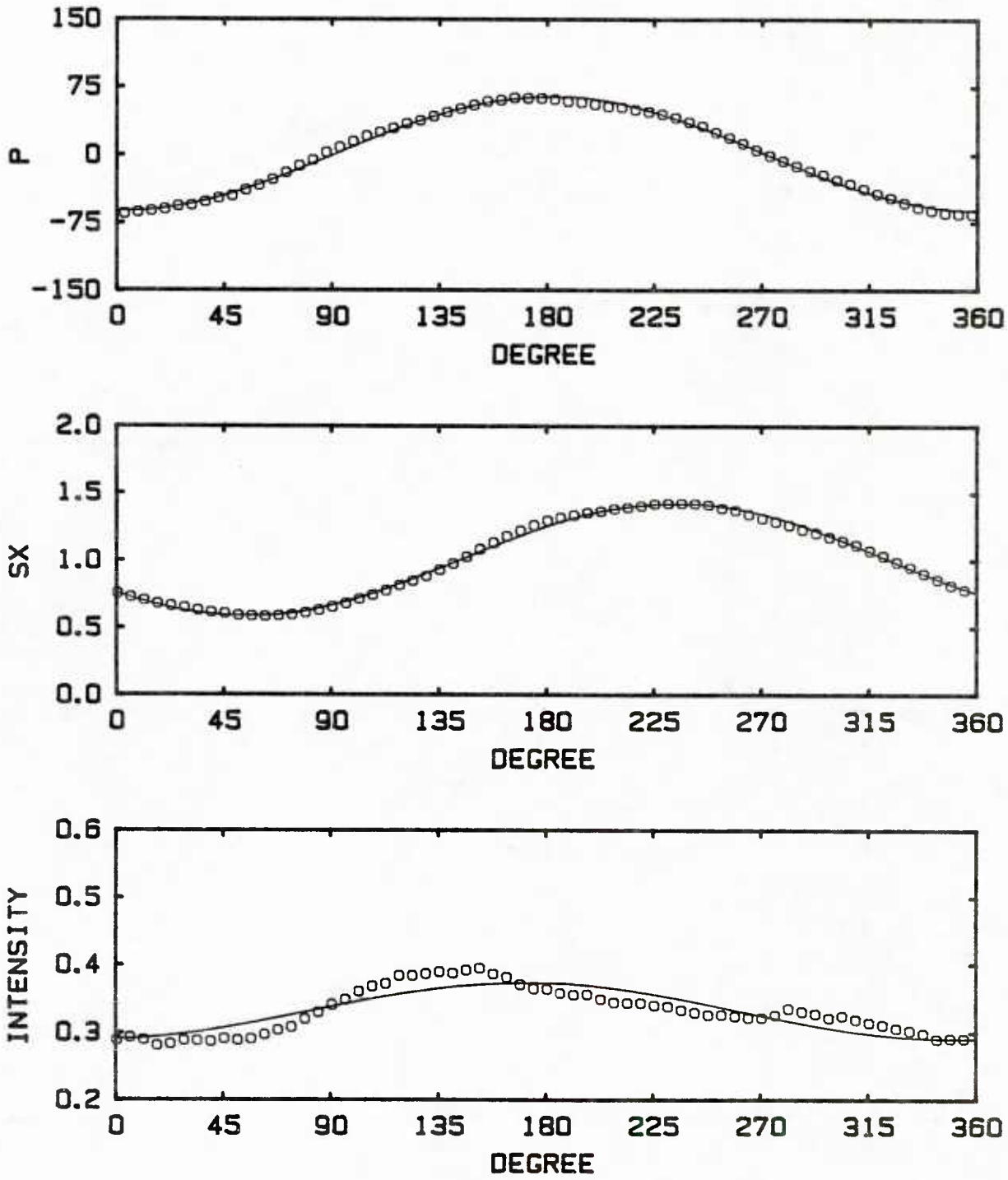


Figure 5.14 Phase averaged values at Re = 19,900, f = 0.625 Hz and a = 0.1 ($\omega^+/15$ = 0.0086)

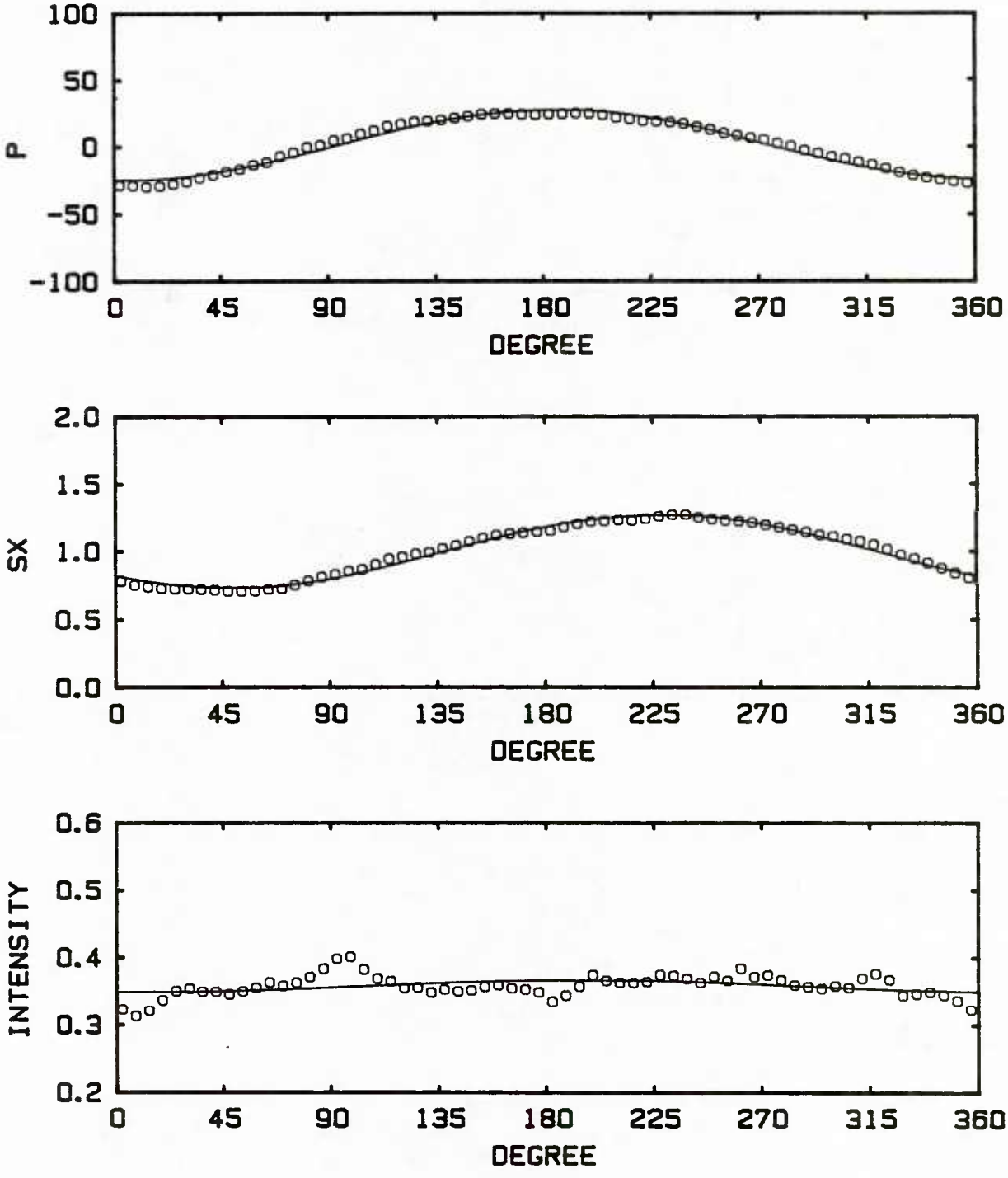


Figure 5.15 Phase averaged values at $R_e$ = 30,400, f = 0.625 Hz and a = 0.1 ($\omega^+$ = 0.0042)

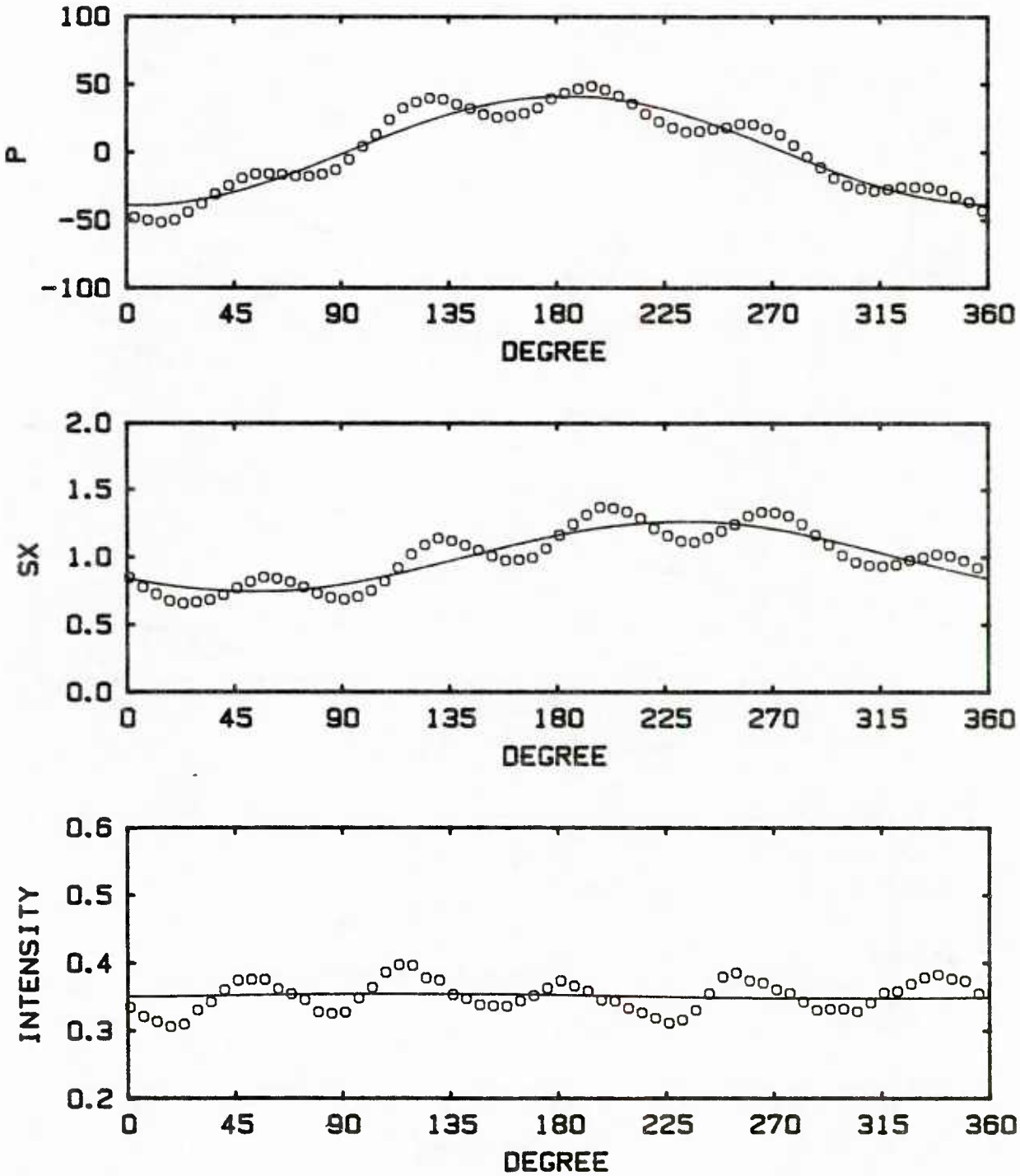


Figure 5.16 Phase averaged values at Re = 40,000 and f = 0.625 Hz and a = 0.1 ($\omega^+/15 = 0.0025$)

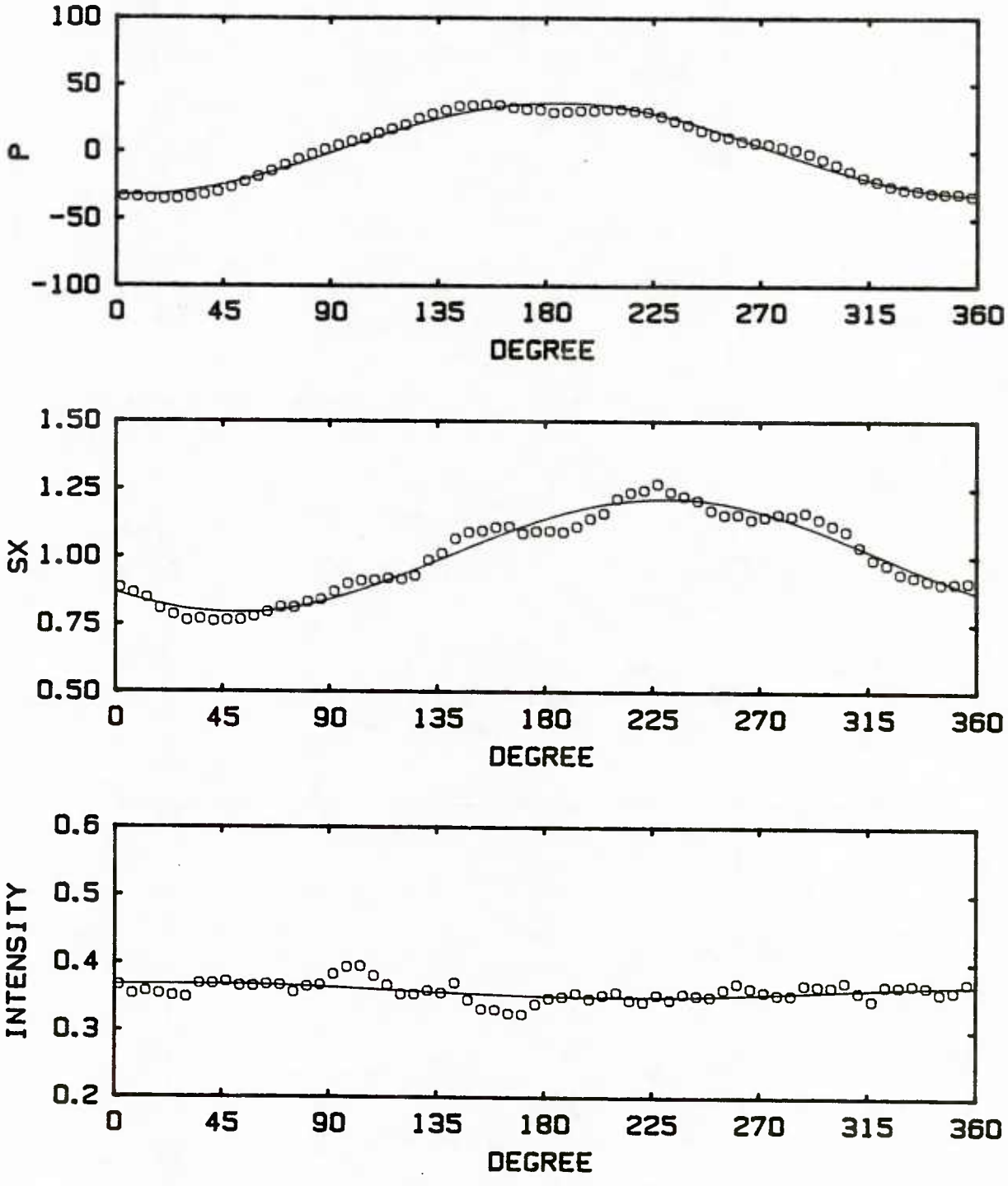


Figure 5.17 Phase averaged values at Re = 49,800, f = 0.625 Hz and a = 0.1 ($\omega^+/15$ = 0.00174)

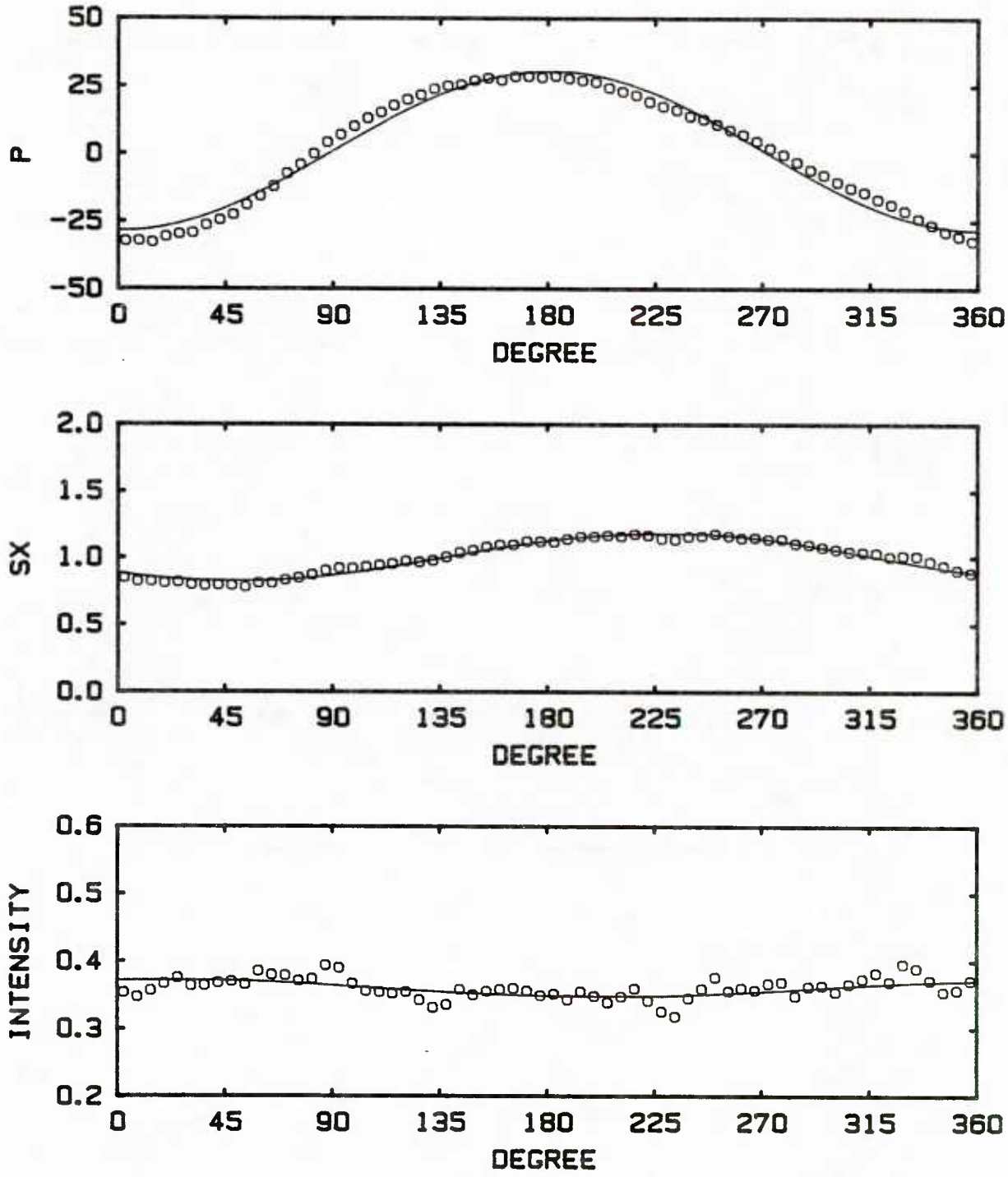


Figure 5.18 Phase averaged values at Re = 57,500, f = 0.625 Hz and a = 0.1 ($\omega^+/15$ = 0.00135)

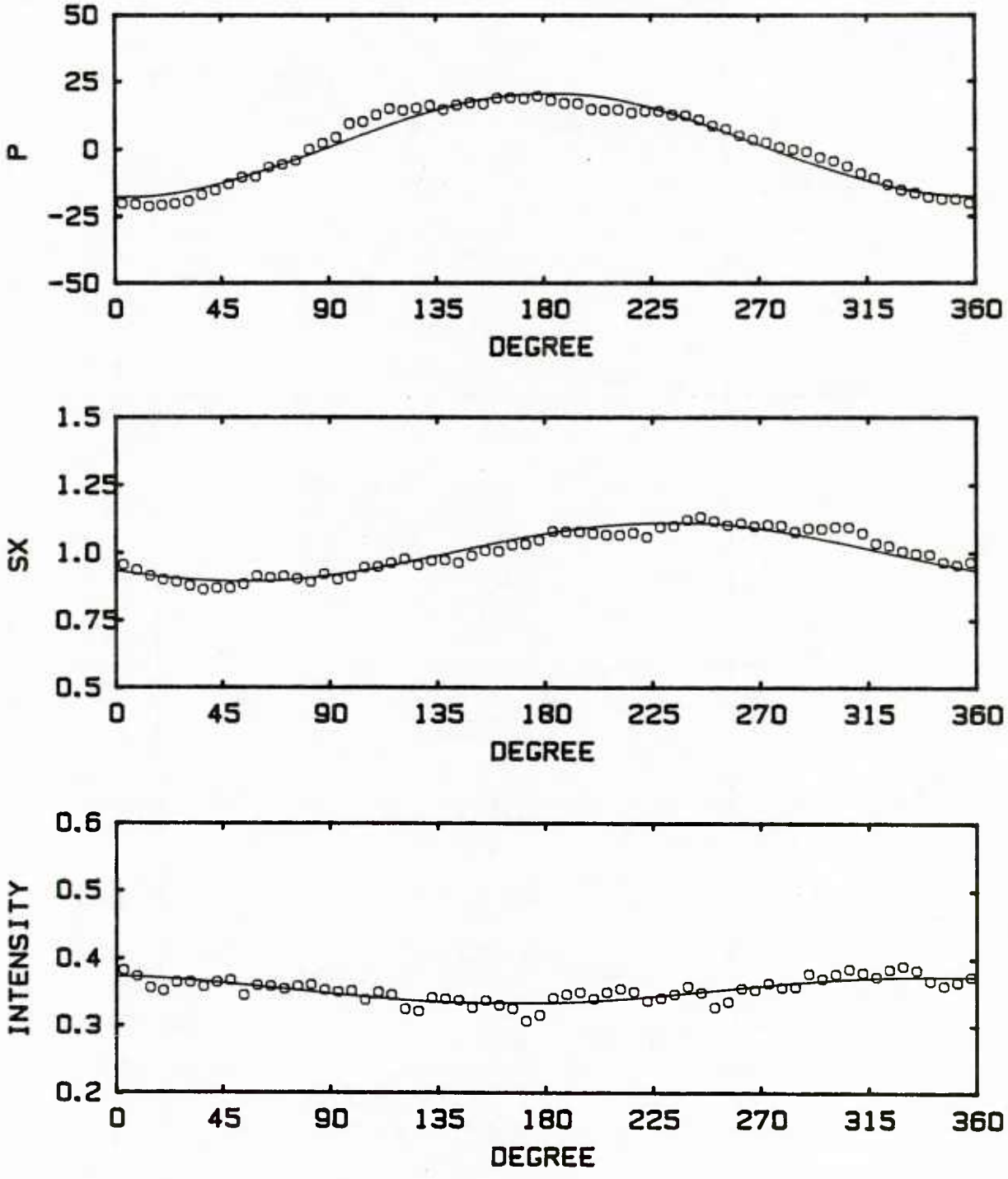


Figure 5.19 Phase averaged values at Re = 70,000, f = 0.625 Hz and a = 0.086 ($\omega^+/15$ = 0.00095)

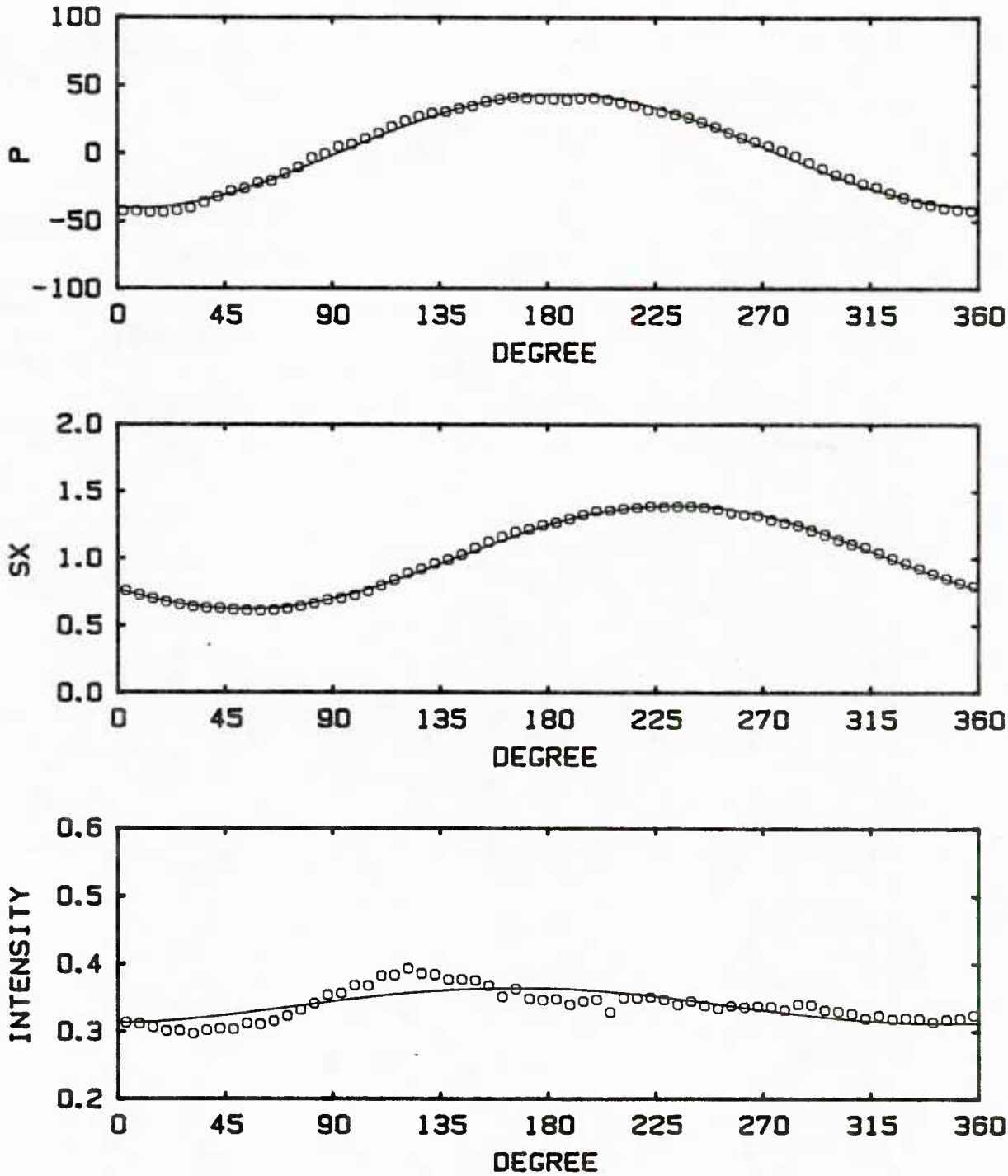


Figure 5.20 Phase averaged values at Re = 15,200, f = 0.325 Hz and a = 0.1 ($\omega^+/15 = 0.0074$)

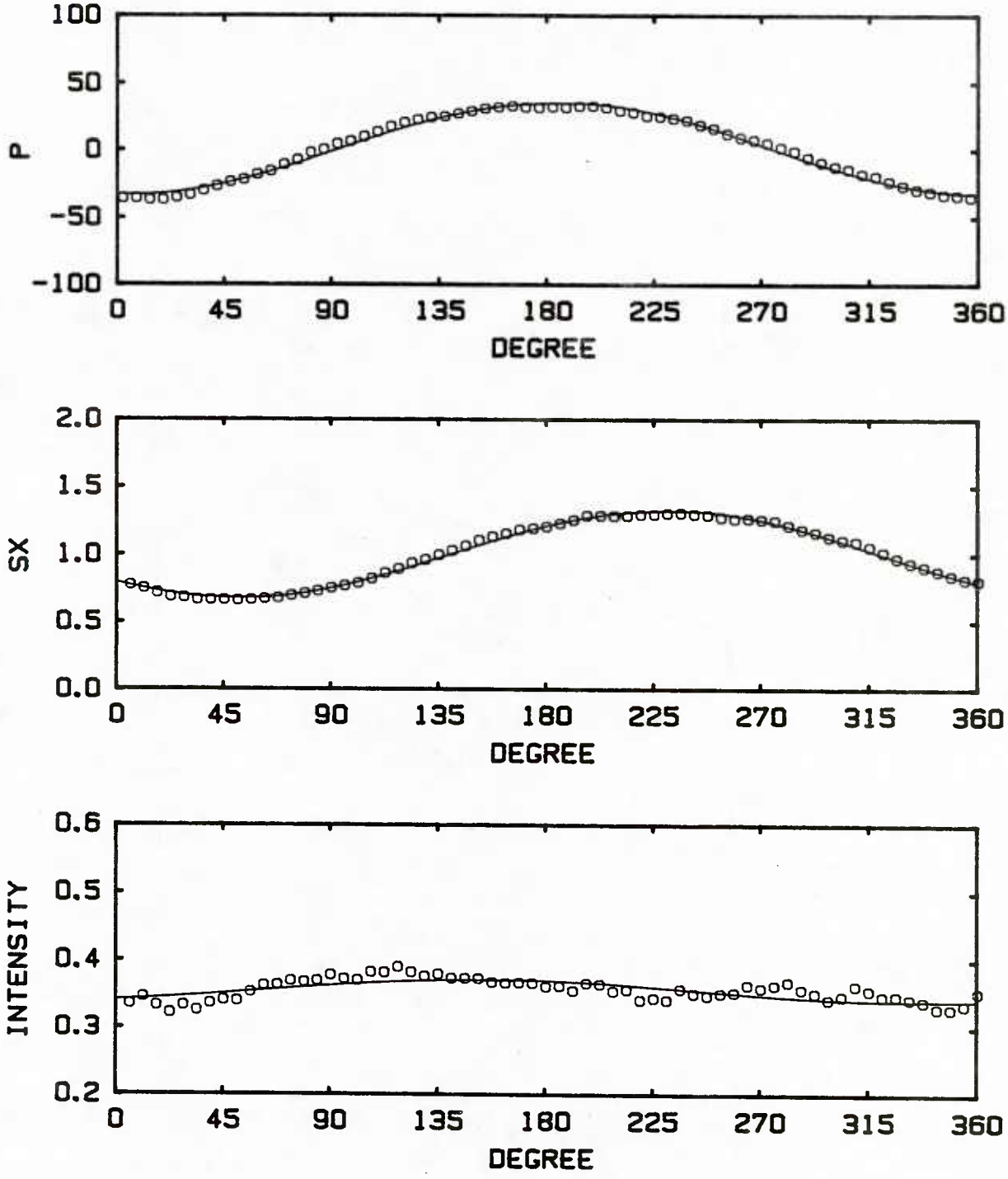


Figure 5.21 Phase averaged values at Re = 20,000, f = 0.325 Hz and a = 0.1 ($\omega^+/15 = 0.0045$)

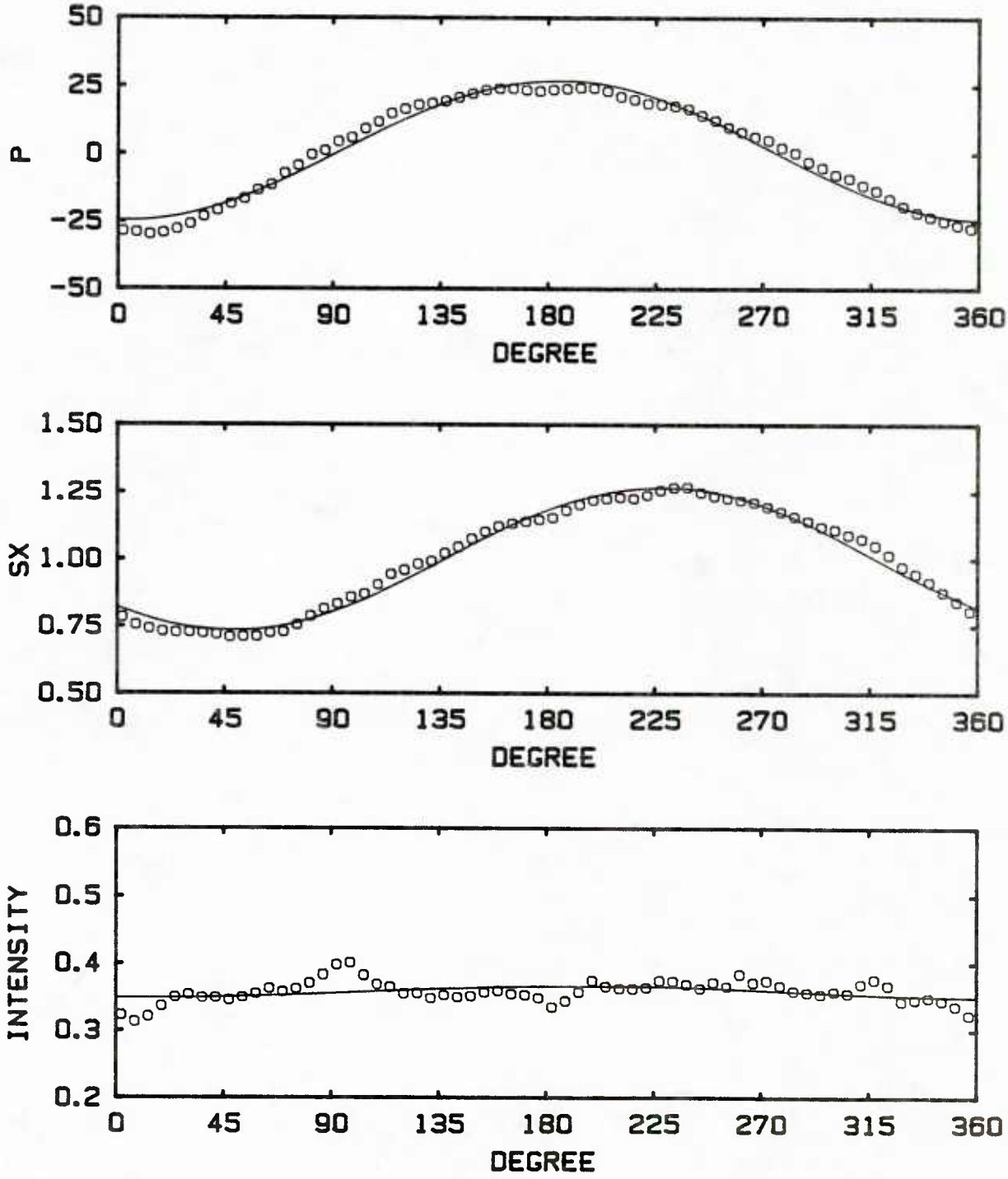


Figure 5.22 Phase averaged values at Re = 30,200, f = 0.325 Hz and a = 0.1 ($\omega^+/15 = 0.0022$)

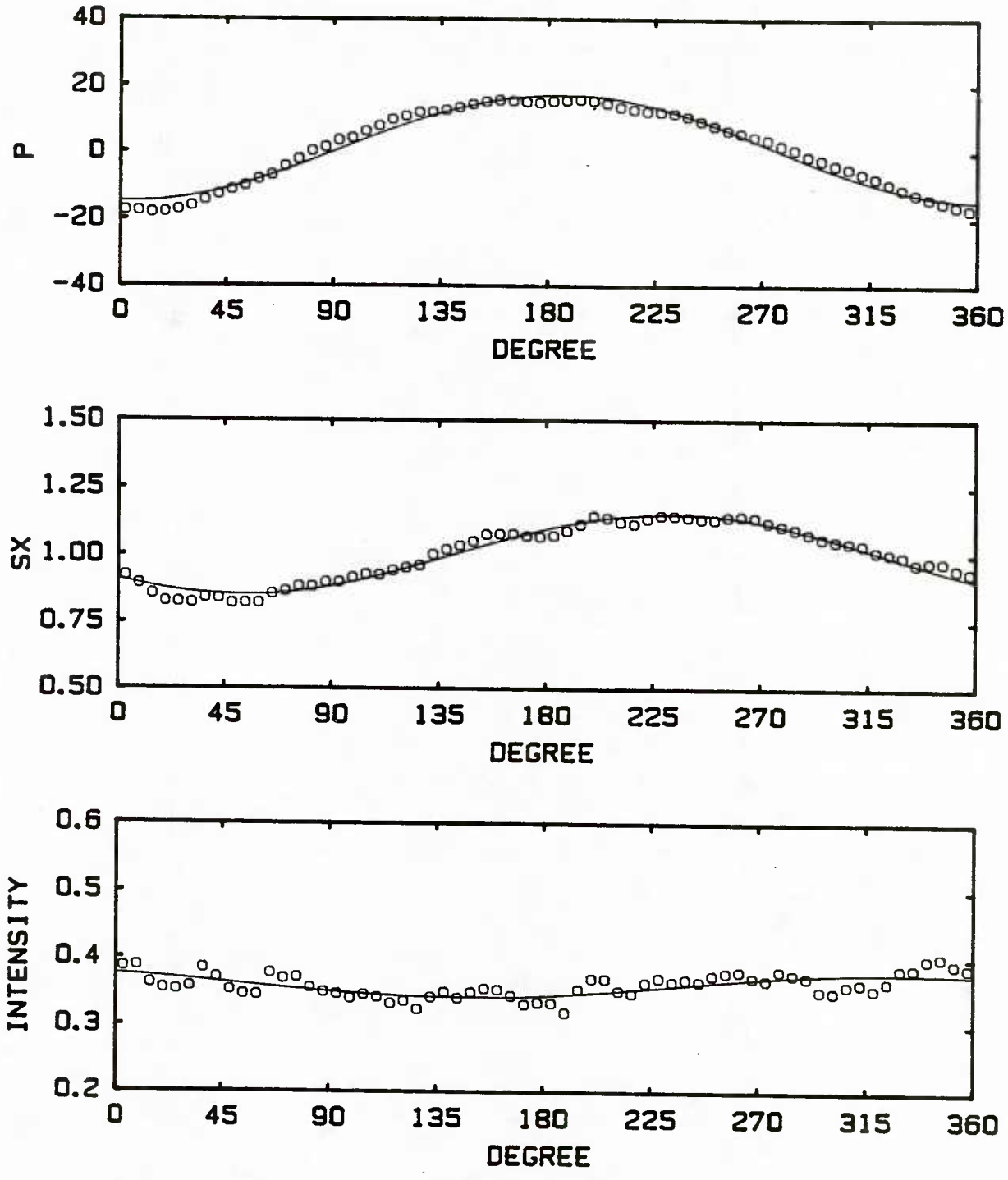


Figure 5.23 Phase averaged values at Re = 40,400, f = 0.325 Hz and a = 0.077 ($\omega^+/15$ = 0.0013)

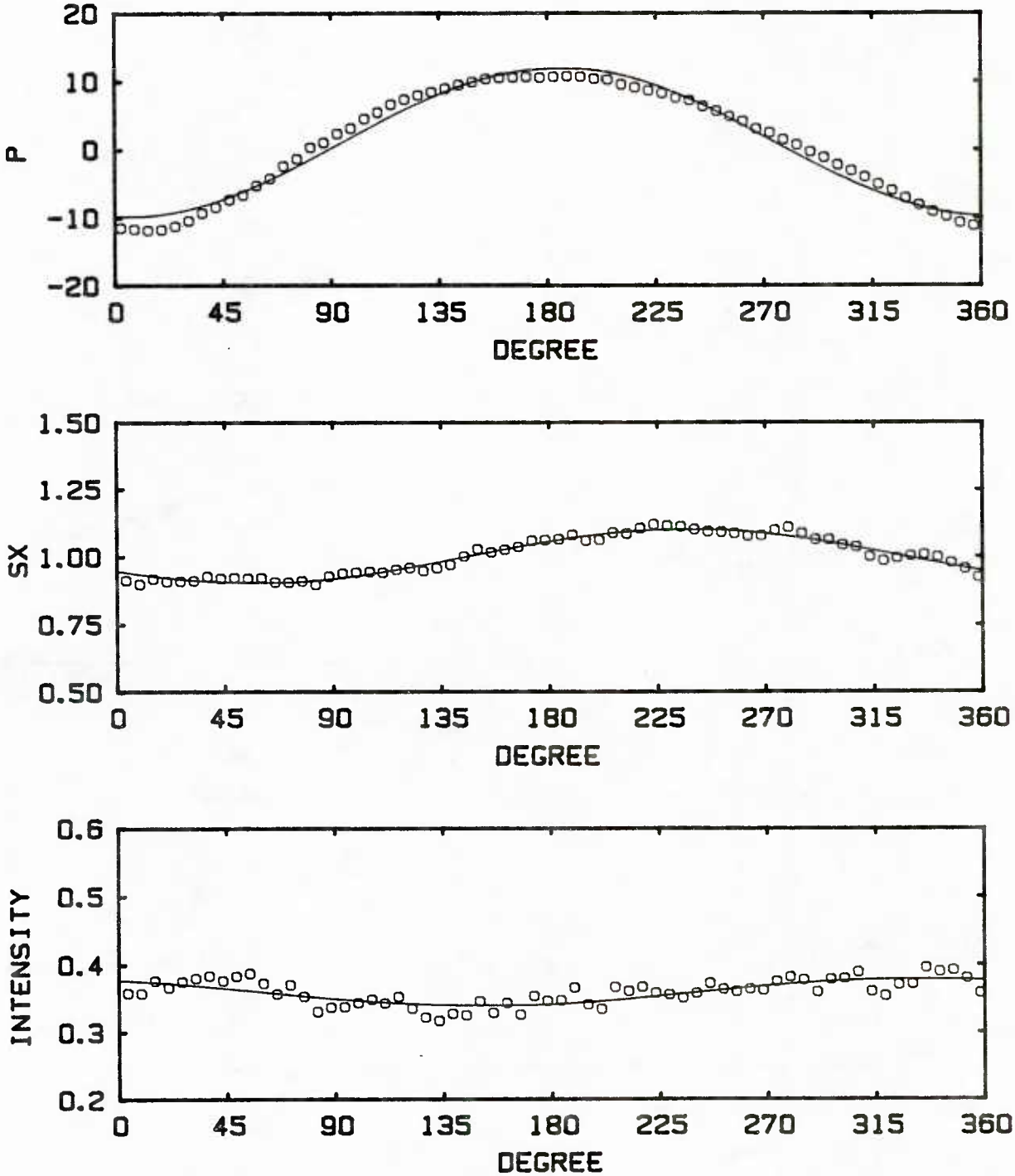


Figure 5.24 Phase averaged values at Re = 49,800, f = 0.325 Hz and a = 0.062 ($\omega^+/15 = 0.00091$)

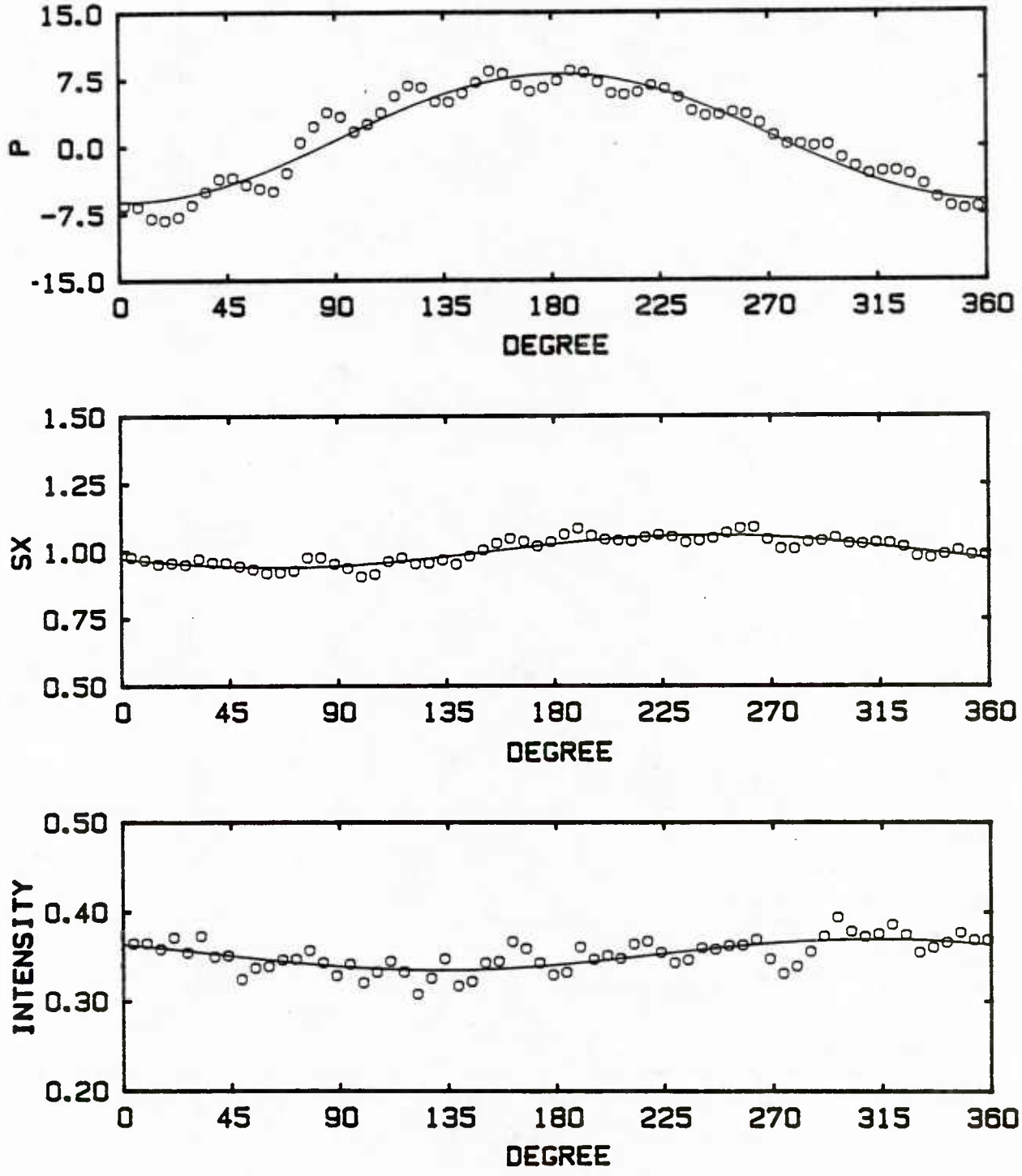


Figure 5.25 Phase averaged values at Re = 60,000, f = 0.325 Hz and a = 0.05 ($\omega^+/15 = 0.00065$)

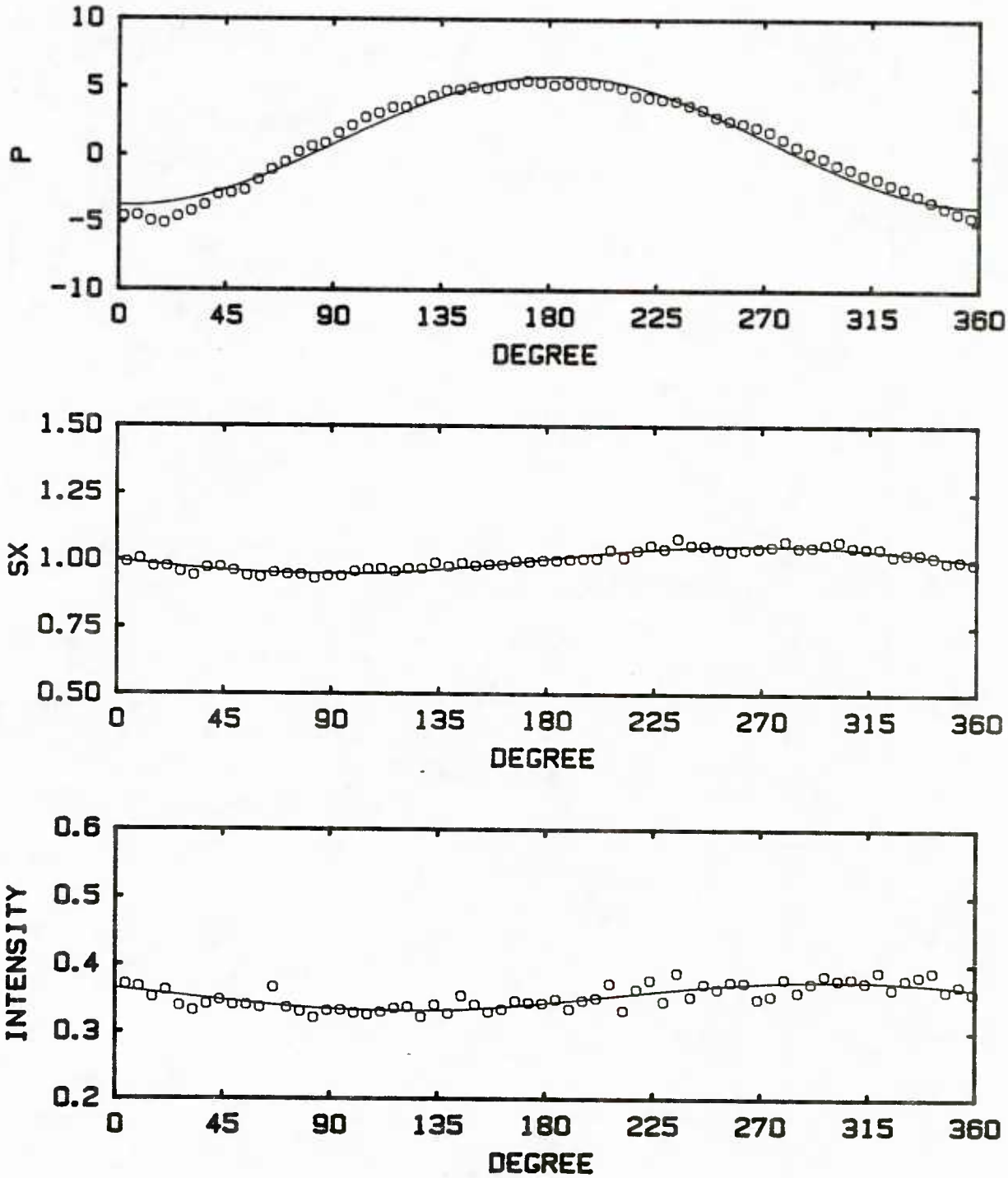


Figure 5.26 Phase averaged values at Re = 69,800, f = 0.325 Hz and a = 0.044 ($\omega^+/15$ = 0.00050)

In summary, the phase averaged data indicate that the velocity gradient at the wall responds to the imposed flow oscillations differently at different flow conditions.

## 5.3 Comparison of the Experimental Data and the Numerical Results

The velocity gradient at the wall shows a linear response to sinusoidal imposed oscillations of small amplitude. Its variation can be characterized by an amplitude and a phase shift relative to the imposed oscillation. Figures 5.27 and 5.28 summarize the experimental results obtained under different flow conditions. The phase shifts are plotted relative to the variation of the central velocity, which lags the pressure gradient by 90°, as described in equation (1.6). The amplitude $|\tilde{S}_x| / \bar{S}_x$ is normalized by $|\tilde{u}_c| / \bar{u}^*$ to take account of the effect of using different amplitudes of oscillation. The correlation is similar to what was used by Abrams and Hanratty (1984) to characterize the spatial variation of shear stress along a wavy surface. The abscissa $\omega^+/15$ corresponds to the $\alpha^+ = 2\pi\nu/\lambda u^*$ used by Abrams and Hanratty (1984). The 15 is the dimensionless turbulence convection velocity in the viscous wall region. For fixed frequencies, an increase of $\frac{\omega^+}{15}$ corresponds to a decrease of Reynolds number. Consequently, the data show that the phases and amplitudes for fixed frequencies are changing with Reynolds number. It is noted that the results obtained for the two frequencies studied fall on the same curves when plotted in the manner shown in Figures 5.27 and 5.28. For reference, the data obtained by Ramaprian (1983) are also plotted in Figures 5.27 and 5.28. The experimental data for all runs are tabulated in Appendix I.

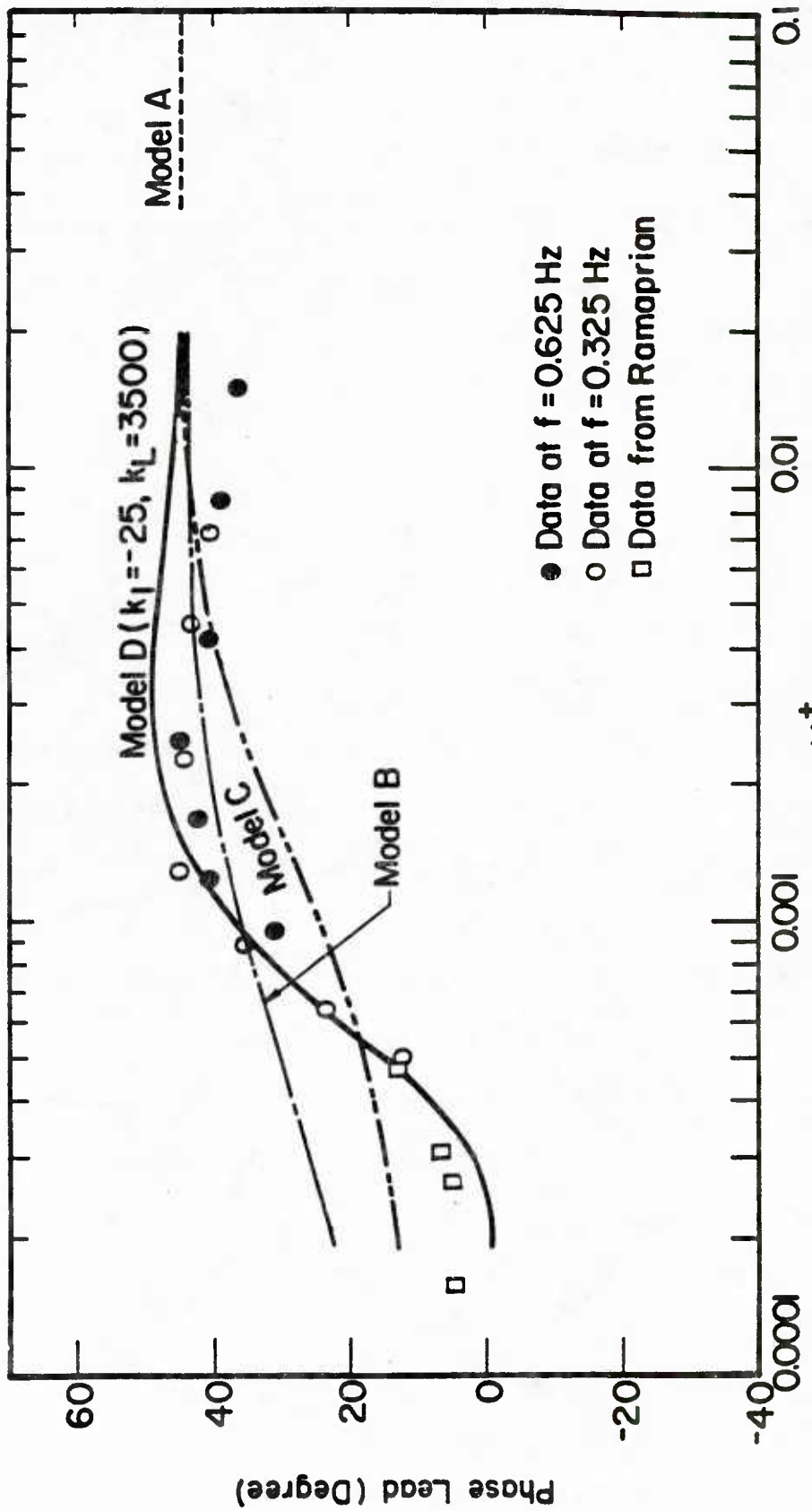


Figure 5.27 Phase lead (relative to the central velocity) of velocity gradient at the wall

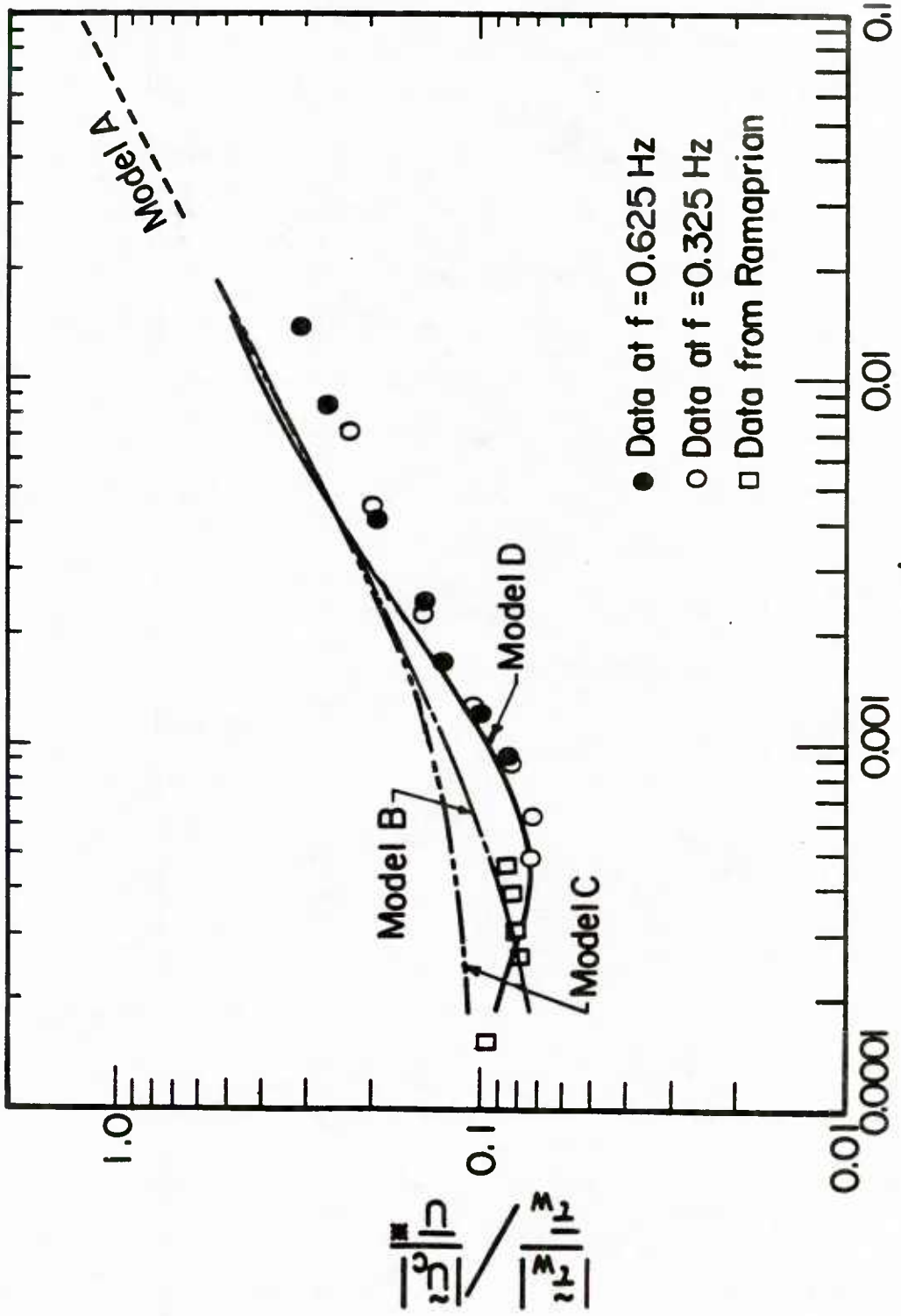


Figure 5.28 Amplitude of velocity gradient at the wall

In Figures 5.27 and 5.28 numerical results obtained with the different models described in Chapter 3 are compared with the data. When $\frac{\omega^+}{15} > 0.01$, the results of all models approach that predicted by a quasi-laminar model. Only Model D with $k_1 = -25$, $k_L = 3500$ predicts the rapid change of phases and amplitudes in the range $\frac{\omega^+}{15} = 0.0005 - 0.002$. It is interesting to note that this range of $\frac{\omega^+}{15}$ is the same range of $\alpha^+$ in which the phase angle characterizing the wall shear stress variation along a wavy surface undergoes a rapid change. These results suggest that the change of phase in this range for the two different types of flows can be attributed to the same relaxation phenomenon.

However, none of the models are able to predict the experimental data in the range of $\frac{\omega^+}{15} > 0.02$. This suggests that the models fail to predict the experimental results if the imposed oscillation frequency is close to or greater than the median frequency of the turbulence in the vicinity of the wall, $\frac{\omega^+}{15} \cong 0.042$. The experimental results indicate that at these high frequencies turbulence is still affecting the imposed oscillations.

No reliable measurements of the oscilation velocity profile were obtained in this study. Attempts were made to use a mass transfer probe to measure the velocity in the fluid. Unfortunately, contamination of the surface of the sensor wire made reliable measurement impossible. Moreover, the interaction between the wall and the sensor wire might cause large errors in the measurement close to the wall. Therefore, the ability to predict the oscillation velocity profile for the four models is checked by comparing the numerical results with the measured LDV data by Ramaprian and Tu. The data were taken at Re = 50,000 and f = 3.6 Hz in a water pipe flow with a pipe diameter of 5 cm. This flow condition

corresponds to the lowest $\omega^+$ in the present experimental range. Figures 5.29 and 5.30 show these comparisons for the amplitude and the phase of the oscillation velocity in the wall region. It is seen that Model D does the best job and agrees with the data very well.

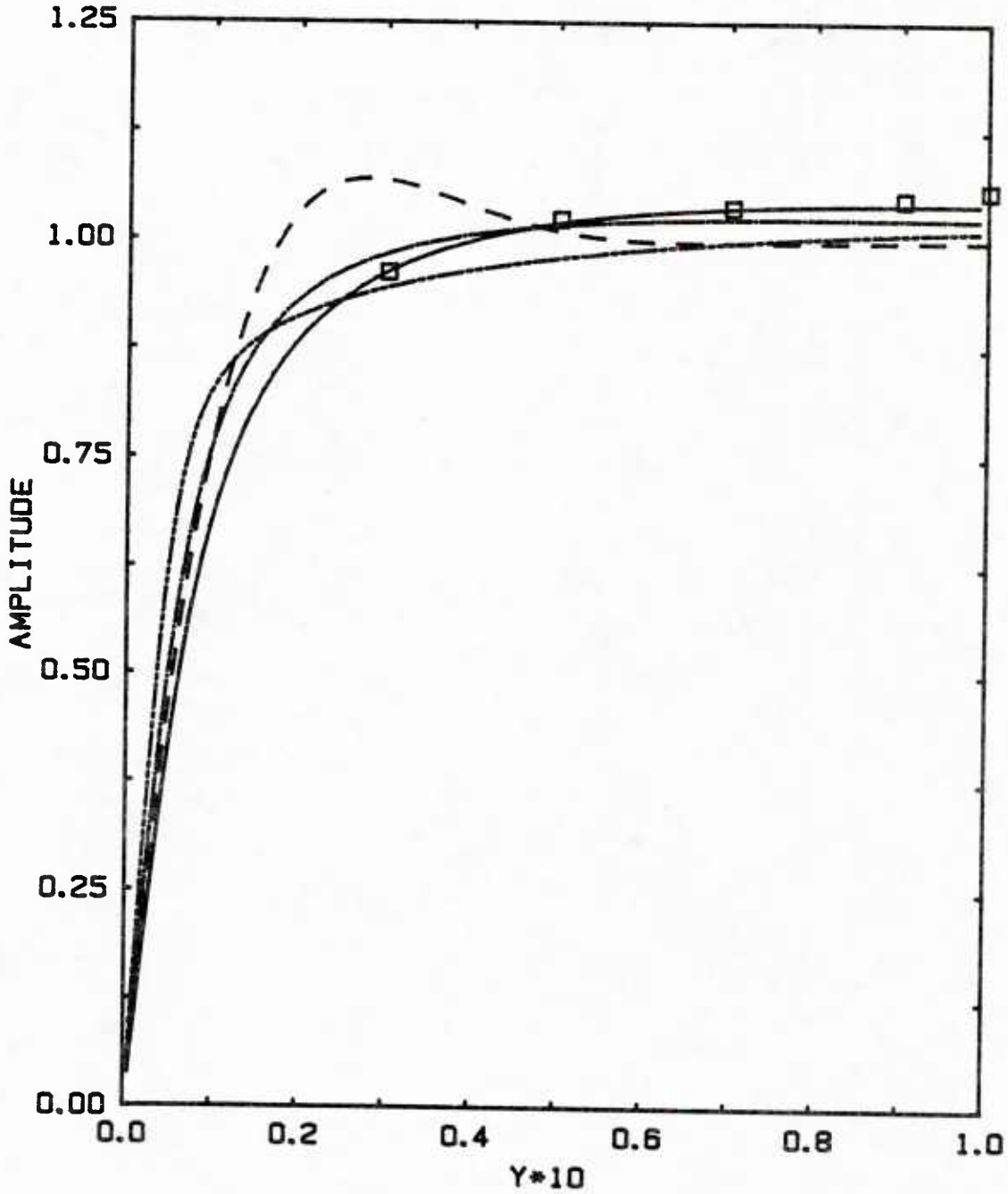


Figure 5.29 Comparison of amplitude profile among numerical results and Ramaprian's data (Re = 50,000, f = 3.6 Hz, d = 5 cm)

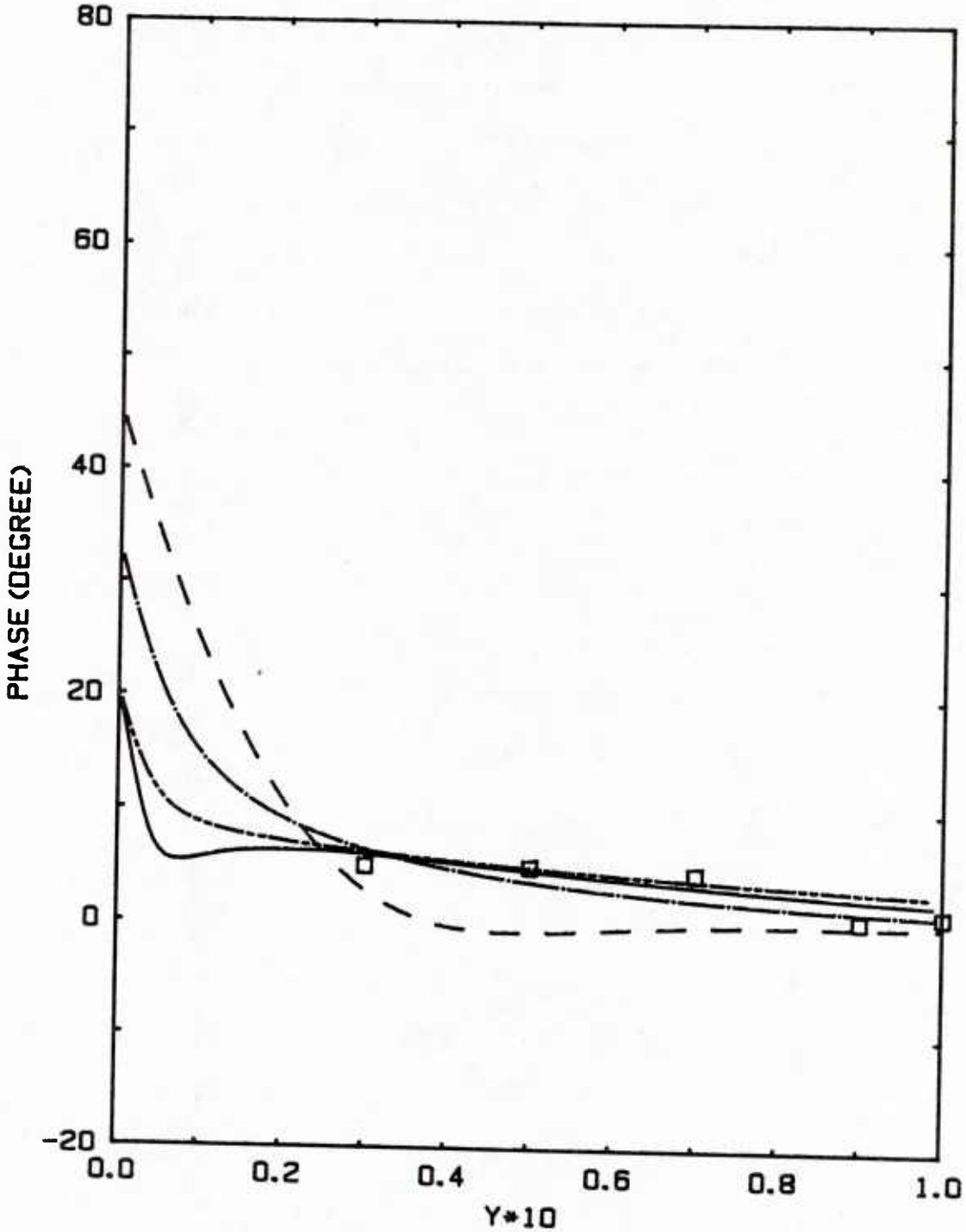


Figure 5.30 Comparison of phase profile among the numerical results and Ramaprian's data (Re = 50,000, f = 3.6 Hz, d = 5 cm)

# CHAPTER 6. DISCUSSION

This thesis reports on measurements of the time variation of the phase averaged wall shear stress caused by the imposition of controlled sinusoidal oscillations on the flow of a turbulent fluid through a pipe. Results are presented for a range of dimensionless frequencies, $\omega^+$, higher than had been presented by previous investigators. By using a small amplitude of imposed oscillation a linear response is obtained whereby the wall shear stress variation is described by a single harmonic with the same frequency as the imposed oscillation and with an amplitude which varies linearly with the amplitude of the imposed oscillation. The measurements can therefore be characterized by a relative amplitude and a relative phase.

It is found that these measurements, with two different frequencies and a range of flow rates, are correlated with $\omega^+$. This contrasts to the characterization of turbulent oscillating flow by $\omega D / \bar{u}_b$, suggested by Jayaraman, et al. (1982), and by $\omega D / u^*$, by Ramaprian and Tu (1983). The influence of frequency at high frequencies can, therefore, be studied either by changing the flow rate or by changing the frequency.

The dimensionless frequency is defined as $\omega^+ = \frac{\nu^2}{u^{*2}} / \frac{\nu}{\omega}$ or as $\omega^+ = 2(\delta_v/\delta_s)^2$, where $\delta_v = \nu/u^*$ is the length scale of the viscous sublayer and $\delta_s = \sqrt{2\nu/\omega}$ is the thickness of the Stokes layer. Consequently, for $\omega^+ > 0.08$ (or $\omega^+/15 > 0.0053$) the Stokes layer is thinner than the viscous sublayer, and it might be expected that turbulence will have a small effect on the imposed oscillations. However, it is to be noted that measured amplitudes are much lower for $\omega^+ > 0.08$ than what is predicted for a quasi-laminar behavior. This result was unexpected and is not yet understood.

Considerable work was done (Mao and Hanratty, 1984) to examine the frequency response of the wall probes. The consequence of this work is that the possible errors involved in correcting for frequency response are far less than the difference from the quasi-laminar solution shown in Figure 5.28. The measurements of the oscillation induced variation in the wall shear stress would suggest the possibility that the result could be due to some nonlinear effect. This explanation is ruled out since the same results have been obtained with two different oscillation amplitudes, as shown in Figures 5.12 and 5.13. Furthermore, measurements of the velocity field very close to the wall by Jayaraman, et al. (1982) and by Binder, et al. (1982) also seem to suggest lower oscillation amplitudes at high frequencies that would be calculated by the quasi-laminar model. Consequently, we conclude that oscillation induced variations of the turbulence in the viscous wall layer, not taken into account by present theories of turbulence, occur in the viscous sublayer at high $\omega^+$. However, these variations appear to have no measurable effect on the time-average velocity (Figure 5.10) or on the time-averaged turbulence properties.

It is to be noted that the medium frequency of the turbulence is $\omega^+/15 \simeq 0.004$. Thus, the effect discussed above appears to occur when the imposed oscillation is equal to or greater than the dominant frequency of the turbulence. This result seems consistent with the suggestion by Mizushina, et al. (1973) that significant changes in the turbulence structure occur when the frequency of the imposed oscillation is the same as the bursting frequency of turbulence.

For $\frac{\omega^+}{15} < 0.0021$ the dimensionless Stokes layer thickness is greater than eight wall units, $\delta_s^+ \geq 8$. One would not expect a quasi-laminar model to be applicable. The strightforward application of a turbulence model developed for flow over a flat surface (Model C) is not capable of describing the experimental resutls, and, in particular, the sharp change of the phase angle over a rather narrow range of $\omega^+$. However, the use of a model (Model D) which argues that flow-induced oscillations in the pressure-gradient can enhance (unfavorable pressure gradient) or dampen (favorable pressure gradient) turbulence in the viscous wall region ($y^+ < 40$) does appear to describe the results. In fact, the parameters, $k_1 = -25$ and $k_L = 3500$, chosen to fit the experimental results are very close to those used by Loyd, Moffat and Kays (1970) to describing boundary-layer flows and by Abrams and Hanratty (1984) to describe flow over a wavy surface.

According to Model D the sharp change in phase angle is associated with a relaxation phenomenon, whereby the turbulence does not respond immediately to the oscillation induced variation of the pressure gradient. Some support for this interpretation is obtained from the measurements of the oscillation induced variation of the mean-square values of the turbulence fluctuations in the wall shear stress. At low $\omega^+$ it is about in phase with an unfavorable pressure gradient while at high $\omega^+$ it is about in phase with a favorable pressure gradient (see Figures 5.12, and 5.25).

Of particular interest, from the viewpoint of the initial objective of these experiments, is the observation of a change of phase angle over

a range of $\omega^+/15$ approximately equal to the range of dimensionless wave number, $\alpha^+$, for which similar change was observed in the measured spatial variations of the wall shear stress along a solid wavy surface. This suggests that the same mechanism is operative and that the two experiments can be compared by using the convection velocity of the turbulence fluctuations in the viscous wall region.

# CHAPTER 7. CONCLUSIONS AND RECOMMENDATIONS

This thesis reports experimental and numerical results on how the wall shear stress responds to an imposed flow oscillation with small amplitude in a frequency around the median frequency of turbulent fluctuations at the wall. The results are summarized as follows:

a. There exists a linear response of the wall shear stress to the imposition of a small amplitude flow oscillation. The time averaged values of the wall shear stress are not affected by the imposed oscillation.

b. The amplitude and the phase of the wall shear stress, which characterizes the wall response, are found to be correlated by a single parameter $\omega^+$, which combines the effects of frequency and Reynolds number in the range of variables studied.

c. Relaxation of turbulence to the variation of pressure gradient in the wall region is found similar to what has been observed for flow over a wavy surface, whereby the phase angle which characterizes the temporal variation of the wall shear stress undergoes a rapid change over a rather narrow range of $\omega^+$. Model D which takes account of this effect with two parameters $k_1 = -25$, $k_L = 3500$ fits the data very well in this range.

d. When $\omega^+$ is close to or greater than the median frequency of the wall turbulence, the measured amplitude of wall shear stress is definitely lower than predicted by all the models. There appears to be an interaction between the imposed flow oscillation and turbulent fluctuations in the viscous sublayer, which is not described by present theories of turbulence.

The present work is a preliminary step toward the understanding of the interaction between a turbulent flow and an imposition of flow oscillation. Several interesting problmes emerge from this work for further studies:

a. In order to get a physical understanding of the relaxation phenomenon it is necessary to model the flow in a more fundamental way such as suggested by Nikolaides and Hanratty (1983).

b. The mechanism leading to the lower amplitude of wall shear stress at large $\omega^+$ needs to be explored both experimentally and theoretically.

c. At high $\omega^+$ and at larger amplitudes than used in this work, the determination of the effect of increasing amplitude on the flow is of great interest, since there might exist nonlinear interaction between turbulence and flow oscillation.

d. The determination of how the flow field can be affected by an imposed disturbance is of practical importance. Nonsinusoidal flow oscillations could be a means of achieving this without going to unduly large flow oscillations.

APPENDIX I. Amplitudes and Phases of Phase Averaged Data of Wall Shear Stress

| No. of Run | $R_e$ | f(1/sec) | $\frac{\omega^+}{15}$ | $\theta_p$ | $\theta_{u_c}$ | $\theta_{\tau_w}$ | $(\theta_{\tau_w} - \theta_{u_c})$ | $\frac{a\lvert\frac{\partial\tilde{P}}{\partial x}\rvert}{\lvert\frac{d\bar{P}}{dx}\rvert}$ | $\frac{\lvert\tilde{\tau}_w\rvert}{\bar{\tau}_w}$ | $\hat{\tau}(0)$ |
|---|---|---|---|---|---|---|---|---|---|---|
| 1-29-83 | 15,000 | .325 | .0074 | 175 | 85 | 128 | 43 | 42.4 | .402 | .234 |
| 2-10-83 | 15,000 | .324 | .0073 | 176 | 86 | 127 | 41 | 40.5 | .373 | .227 |
| 8-3-83 | 15,200 | .326 | .0072 | 177 | 87 | 129 | 42 | 42.0 | .397 | .231 |
| 8-10-83 | 15,400 | .325 | .0070 | 176 | 86 | 128 | 42 | 40.6 | .380 | .226 |
| 8-17-83 | 15,600 | .325 | .0069 | 177 | 87 | 127 | 40 | 38.1 | .360 | .226 |
| | | | .0072 | | | | 42 | | | .229 |
| 2-10-83 | 19,400 | .326 | .0047 | 177 | 87 | 132 | 45 | 31.9 | .330 | .205 |
| 8-2-83 | 20,400 | .326 | .0043 | 177 | 87 | 131 | 44 | 33.1 | .330 | .190 |
| 8-17-83 | 19,600 | .325 | .0046 | 177 | 87 | 127 | 40 | 32.2 | .323 | .196 |
| | | | .0045 | | | | 43 | | | .197 |
| 1-25-83 | 30,200 | .325 | .0022 | 176 | 86 | 131 | 45 | 23.1 | .245 | .142 |
| 2-9-83 | 29,400 | .326 | .0023 | 176 | 86 | 130 | 44 | 25.4 | .270 | .146 |
| 8-2-83 | 30,200 | .325 | .0022 | 177 | 87 | 132 | 45 | 24.2 | .257 | .142 |
| 8-10-83 | 29,900 | .325 | .0022 | 177 | 87 | 130 | 43 | 24.3 | .256 | .142 |
| 8-17-83 | 29,900 | .326 | .0022 | 177 | 87 | 130 | 43 | 23.9 | .262 | .149 |
| | | | .0022 | | | | 44 | | | .149 |

APPENDIX I. Amplitudes and Phases of Phase Averaged Data of Wall Shear Stress (Continued)

| No. of Run | $R_e$ | f(1/sec) | $\frac{\omega^+}{15}$ | $\theta_p$ | $\theta_{u_c}$ | $\theta_{\tau_w}$ | $(\theta_{\tau_w} - \theta_{u_c})$ | $\frac{a\left\|\frac{\partial \tilde{P}}{\partial x}\right\|}{\left\|\frac{d\bar{P}}{dx}\right\|}$ | $\frac{\|\tilde{\tau}_w\|}{\bar{\tau}_w}$ | $\hat{\tau}(0)$ |
|---|---|---|---|---|---|---|---|---|---|---|
| 2-8-83 | 40,400 | .324 | .0013 | 175 | 85 | 127 | 42 | 15.8 | .162 | .107 |
| 8-2-83 | 40,400 | .326 | .0013 | 176 | 86 | 132 | 46 | 15.1 | .151 | .104 |
| 8-12-83 | 40,000 | .325 | .0013 | 176 | 86 | 132 | 46 | 15.4 | .148 | .101 |
| | | | .0013 | | | | 45 | | | .104 |
| 2-8-83 | 50,400 | .325 | .00083 | 174 | 84 | 119 | 35 | 9.62 | .087 | .077 |
| 8-1-83 | 49,800 | .326 | .00090 | 176 | 86 | 121 | 35 | 10.3 | .097 | .082 |
| 8-12-83 | 49,600 | .325 | .00091 | 176 | 86 | 122 | 36 | 10.3 | .100 | .084 |
| 8-17-83 | 49,800 | .327 | .00091 | 176 | 86 | 121 | 35 | 9.90 | .098 | .086 |
| | | | .0089 | | | | 35 | | | .082 |
| 2-8-83 | 59,400 | .325 | .00066 | 173 | 83 | 108 | 25 | 6.45 | .059 | .068 |
| 8-1-83 | 57,500 | .322 | .00069 | 178 | 88 | 117 | 29 | 7.08 | .068 | .073 |
| 8-12-83 | 60,400 | .326 | .00065 | 177 | 87 | 105 | 18 | 6.59 | .061 | .068 |
| 8-17-83 | 60,400 | .325 | .00064 | 177 | 87 | 107 | 20 | 6.36 | .061 | .070 |
| 8-3-83 | 59,800 | .325 | .00065 | 178 | 88 | 113 | 25 | 6.75 | .068 | .074 |
| | | | .00066 | | | | 23 | | | .071 |
| 8-3-83 | 70,000 | .325 | .00050 | 176 | 86 | 103 | 17 | 4.75 | .051 | .069 |
| 8-17-83 | 69,800 | .325 | .00050 | 178 | 88 | 96 | 8 | 4.54 | .054 | .077 |
| | | | .00050 | | | | 13 | | | .073 |

APPENDIX I. Amplitudes and Phases of Phase Averaged Data of Wall Shear Stress (Continued)

| No. of Run | $R_e$ | f(1/sec) | $\frac{\omega^+}{15}$ | $\theta_p$ | $\theta_{u_c}$ | $\theta_{\tau_w}$ | $(\theta_{\tau_w} - \theta_{u_c})$ | $\frac{a\lvert\frac{\partial\tilde{P}}{\partial x}\rvert}{\lvert\frac{d\bar{P}}{dx}\rvert}$ | $\frac{\lvert\tilde{\tau}_w\rvert}{\bar{\tau}_w}$ | $\hat{\tau}(0)$ |
|---|---|---|---|---|---|---|---|---|---|---|
| 1-30-83 | 15,100 | .627 | .014 | 175 | 85 | 125 | 40 | 72.6 | .459 | .300 |
| 8-3-83 | 15,400 | .625 | .0135 | 179 | 89 | 124 | 35 | 74.3 | .481 | .301 |
| *8-3-83 | 15,400 | .625 | .0135 | 178 | 88 | 123 | 35 | 35.3 | .229 | .300 |
| 8-10-83 | 15,400 | .627 | .0135 | 177 | 87 | 124 | 37 | 72.2 | .468 | .303 |
| 8-17-83 | 15,600 | .624 | .0132 | 179 | 89 | 125 | 36 | 69.7 | .478 | .314 |
| | | | .0135 | | | | 37 | | | .304 |
| 2-10-83 | 19,400 | .625 | .0090 | 177 | 87 | 127 | 40 | 60.8 | .441 | .275 |
| 8-2-83 | 20,400 | .625 | .0083 | 180 | 90 | 127 | 37 | 63.6 | .445 | .254 |
| *8-2-83 | 20,500 | .624 | .0082 | 178 | 88 | 128 | 40 | 25.9 | .179 | .249 |
| 8-17-83 | 19,900 | .622 | .0086 | 179 | 89 | 127 | 38 | 60.6 | .425 | .268 |
| | | | .0085 | | | | 39 | | | .262 |
| 2-9-83 | 29,400 | .620 | .0043 | 177 | 87 | 124 | 37 | 45.1 | .323 | .187 |
| 1-27-83 | 30,000 | .623 | .0042 | 175 | 85 | 129 | 44 | 46.3 | .338 | .189 |
| 8-2-83 | 30,400 | .623 | .0041 | 180 | 90 | 130 | 40 | 46.7 | .348 | .190 |
| 8-10-83 | 29,900 | .627 | .0043 | 178 | 88 | 129 | 41 | 47.4 | .362 | .199 |
| 8-17-83 | 29,800 | .624 | .0043 | 179 | 89 | 128 | 39 | 46.1 | .336 | .190 |
| | | | .0042 | | | | 40 | | | .191 |

APPENDIX I. Amplitudes and Phases of Phase Averaged Data of Wall Shear Stress (Continued)

| No. of Run | $R_e$ | f(1/sec) | $\frac{\omega^+}{15}$ | $\theta_p$ | $\theta_{u_c}$ | $\theta_{\tau_w}$ | $(\theta_{\tau_w} - \theta_{u_c})$ | $\frac{a\lvert\frac{\partial \tilde{P}}{\partial x}\rvert}{\lvert\frac{d\bar{P}}{dx}\rvert}$ | $\frac{\lvert\tilde{\tau}_w\rvert}{\bar{\tau}_w}$ | $\hat{\tau}(0)$ |
|---|---|---|---|---|---|---|---|---|---|---|
| 2-8-83 | 40,400 | .623 | .0025 | 174 | 84 | 122 | 38 | 35.7 | .241 | .134 |
| 8-2-83 | 40,500 | .625 | .0025 | 177 | 87 | 132 | 45 | 36.3 | .264 | .145 |
| 8-12-83 | 40,000 | .626 | .0025 | 176 | 86 | 133 | 47 | 37.7 | .281 | .151 |
| | | | .0025 | | | | 43 | | | .143 |
| 2-8-83 | 50,400 | .625 | .0017 | 174 | 84 | 123 | 39 | 27.9 | .229 | .136 |
| 8-2-83 | 49,800 | .623 | .00173 | 177 | 87 | 128 | 41 | 30.2 | .211 | .116 |
| 8-12-83 | 49,400 | .624 | .00176 | 175 | 85 | 131 | 46 | 30.4 | .225 | .140 |
| 8-17-83 | 49,800 | .624 | .00176 | 178 | 88 | 128 | 40 | 30.8 | .233 | .125 |
| | | | .00174 | | | | 42 | | | .129 |
| 2-8-83 | 59,400 | .625 | .00127 | 163 | 73 | 117 | 44 | 21.6 | .154 | .102 |
| 8-1-83 | 57,500 | .625 | .00135 | 180 | 90 | 132 | 42 | 25.7 | .180 | .103 |
| 8-12-83 | 60,400 | .621 | .00123 | 179 | 89 | 123 | 34 | 22.3 | .156 | .098 |
| | | | .00128 | | | | 40 | | | .101 |
| 2-10-83 | 69,300 | .625 | .00097 | 178 | 88 | 119 | 31 | 16.6 | .098 | .074 |
| 8-3-83 | 70,000 | .625 | .00095 | 179 | 89 | 120 | 31 | 16.7 | .107 | .079 |
| 8-17-83 | 69,800 | .622 | .00096 | 179 | 89 | 118 | 29 | 16.3 | .096 | .073 |
| | | | .00096 | | | | 30 | | | .075 |

# APPENDIX II. Derivation of Finite Difference Methods for Variable Grids and Computer Programs.

## (A) Finite difference of variable grids.

A function of U(y) is approximated by a second order polynomial as

$$U(y) = a_j + b_j y + c_j y^2 , \quad y_{j-1} \le y \le y_{j+1} . \tag{II.1}$$

If the values of the function U(y) are known at $y_{j-1}$, $y_j$ and $y_{j+1}$, the coefficients $a_j$, $b_j$, $c_j$ can be determined by solving following system equations:

$$\begin{vmatrix} 1 & y_{j-1} & y_{j-1}^2 \\ 1 & y_j & y_j^2 \\ 1 & y_{j+1} & y_{j+1} \end{vmatrix} \begin{vmatrix} a_j \\ b_j \\ c_j \end{vmatrix} = \begin{vmatrix} U_{j-1} \\ U_j \\ U_{j+1} \end{vmatrix} \tag{II.2}$$

i.e.,

$$a_j = \frac{y_j\, y_{j+1}}{(y_{j-1} - y_j)(y_{j-1} - y_{j+1})} U_{j-1} + \frac{y_{j-1}\, y_{j+1}}{(y_j - y_{j-1})(y_j - y_{j+1})} U_j$$

$$+ \frac{y_j\, y_{j-1}}{(y_{j+1} - y_j)(y_{j+1} - y_{j-1})} U_{j+1}$$

$$b_j = - \frac{y_j + y_{j+1}}{(y_{j-1} - y_j)(y_{j-1} - y_{j+1})} U_{j-1} - \frac{y_{j-1} + y_{j+1}}{(y_j - y_{j-1})(y_j - y_{j+1})} U_j$$

$$- \frac{y_j + y_{j-1}}{(y_{j+1} - y_j)(y_{j+1} - y_{j-1})} U_{j+1}$$

$$c_j = \frac{1}{(y_{j-1} - y_j)(y_{j-1} - y_{j+1})} U_{j-1} + \frac{1}{(y_j - y_{j-1})(y_j - y_{j+1})} U_j$$

$$+ \frac{1}{(y_{j+1} - y_j)(y_{j+1} - y_{j-1})} U_{j+1} \qquad \text{(II.3)}$$

From (3.55) the differences between two adjacent grids are

$$Y_j - Y_{j-1} = \Delta Y_1 \, H^{j-2}$$

$$Y_{j-1} - Y_{j+1} = - \Delta Y_1 \, H^{j-2} \, (H + 1)$$

$$Y_{j+1} - Y_j = \Delta Y_1 \, H^{j-1} \qquad \text{(II.4)}$$

The first and second derivatives of U(Y) are then approximated as

$$\left.\frac{\partial U}{\partial Y}\right|_{Y_j} = b_j + 2C_j Y_j$$

$$= \left[ - \frac{U_{j+1}}{H(H + 1)} + \frac{(H - 1) U_j}{H} - \frac{H U_{j-1}}{H + 1} \right] \Big/ \; \Delta Y_1 \cdot H^{j-2} \, , \qquad \text{(II.5)}$$

and

$$\left.\frac{\partial^2 U}{\partial Y^2}\right|_{Y_j} = \left[ \frac{2 U_{j+1}}{H(H + 1)} - \frac{2 U_j}{H} + \frac{2 U_{j-1}}{H+1} \right] \Big/ \; \Delta Y_1 \, H^{j-2} \, . \qquad \text{(II.6)}$$

The computer programs calculating oscillating flow fields from Models A to D are as follows:

(B) Model A

```
c       this program solves quasi-laminar pulsating pipe flow using
c       cronk-niclson implicit scheme.
c       input: re  reynolds number
c              vis viscosity
c              fr  frequency of oscillation
c              ns  time steps per period
c              nprds  periods to be proceeded
c              bt  ratio of first grid size to the thickness of
c                  stokes layer.
c              hk  factor of geometric series of grid size
c        output:
c              for003.dat (x,2e13.5)  wall shear stress variation
c              for021.dat -- for028.dat  (x,2e13.6)
c                  velocity profile at 8 different phases
c              for071.dat(x,g13.6,x,g13.6)   y(j),amplitude
c              for072.dat(x,g13.6,x,g13.6)   y(j),phase
c              for073.dat(x,g13.6,x,g13.6)   y(j),zavg
c              for051.dat (x,2g13.6) -- on
c                  time variation of u at y(j)
        program moda
        dimension u(200),y(200),alfa(200),bata(200),duy(33)
        dimension uf(33,200),uff(33,2)
        pi=4.*atan(1.)
        print*,'type in re,vis,fr,ns/period,nprds'
        read*,re,vis,fr,ns,nprds
        print*,'enter radius of pipe'
        read*,r
        w=2.*pi*fr
        ymax=.099436*re**.875
        ustar=ymax/r
        print*,'enter bt,hk'
        read*,bt,hk
        h1=sqrt(2.*vis/w)*ustar/bt
        ni=alog10(ymax*(hk-1)/h1+1)/alog10(hk)+1
        print*,'ymax=',ymax,'jmax=',ni
        ymax=h1*(hk**(ni-1)-1)/(hk-1)
        h1=h1/ymax
c       initial condition
        do 10 i=1,ni
 10     y(i)=h1*(hk**(i-1)-1)/(hk-1)
        st=r*sqrt(w/vis)
        u(1)=0.
        do 40 i=2,ni-1
        tmp=-st*y(i)/sqrt(2.)
 40     u(i)=-sqrt(1./(1.-y(i)))*exp(tmp)*sin(tmp)
        u(ni)=u(ni-1)
        print*,u(1),u(2),u(3),u(4),u(5)
        dt=2.*pi/ns
        l=ns/32
        r=ymax/ustar
        st=sqrt(w/vis)*r
c
c       calculate velocity profile at new time level
        do 50 mt=1,nprds
        do 60 k=1,32
        do 70 i=1,l
        ip=(mt-1)*ns+(k-1)*l+i
        alfa(1)=0.
        bata(1)=0.
        call tri(2,ni-1,h1,hk,y,r,st,dt,alfa,bata,ip,u)
        u(ni)=bata(ni-1)/(1.-alfa(ni-1))
        do 80 j=1,ni-2
        n=ni-j
 80     u(n)=alfa(n)*u(n+1)+bata(n)
        u(1)=0.
 70     continue
```

```
      if(mt.ne.nprds) go to 60
      do 95 j=1,2
 95   uff(k,j)=u(j+1)
      do 90 j=1,ni
 90   uf(k,j)=u(j)
 60   continue
 50   continue
c
c     calculate shear stress variation at the wall
      do 100 k=1,32
      duy(k)=2.*uff(k,1)/(h1*st*st)
      deg=k*11.25
 100  write(3,110) deg,duy(k)
 110  format(x,2e13.5)
      duy(33)=duy(1)
      call datfit(duy,zavg,amag,angd)
      angd=90.+angd
      write(3,255) y(1),amag
      write(3,255) y(1),angd
      write(3,255) y(1),zavg
 255  format(x,g13.6,x,g13.6)
c     calculate amplitude and phase profile of oscillating
c     component of velocity.
      do 451 i=1,32
 451  u(i)=uf(i,ni)
      u(33)=u(1)
      call datfit(u,zavg,amag,angd)
      temp=angd
      do 190 j=2,ni
      do 195 i=1,32
 195  u(i)=uf(i,j)
      u(33)=u(1)
      call datfit(u,zavg,amag,angd)
      angd=angd-temp
      write(71,255) y(j),amag
      write(72,255) y(j),angd
      write(73,255) y(j),zavg
 190  continue
      print*,'do you want u profile in 8 phases ? 0 yes, 1 no'
      read*,ncr
      if(ncr.ne.0) go to 501
      print*,'enter y/r (the y where the profile ends)'
      read*,ys
      j=1
 186  if(y(j).gt.ys) go to 187
      j=j+1
      go to 186
 187  nk=j
      do 500 i=1,8
      ii=i*4
      n=20+i
      do 511 j=1,nk
      write(n,510) y(j),uf(ii,j)
 510  format(x,g13.6,x,g13.6)
 511  continue
 500  continue
 501  continue
c
      print*,'do you want time variation of u at y(j) ? 0 yes ,1 no'
      read*,nt1
      if(nt1 ne 0) go to 123
      n=50
 120  print*,'which y/r? type in j'
      read*,j
      n=n+1
      do 130 k=1,32
      u(k)=uf(k,j)
      u(k+1)=u(k)
      deg=k*11.25
 130  write(n,131) deg,u(k+1)
 131  format(x,2g13.6)
      print*,'go on ? yes 0,no 1'
      read*,ntst
      if(ntst.eq.0) go to 120
 123  continue
      stop
      end
```

(C) Model B

```
c       this program solves pulsating flow field by using model b.
c       crank-nicolson implicit scheme is used.
c
c       input.re     reynolds number.
c             vis    viscosity.
c             fr     frequency.
c             ns     time steps per reriod.
c             r0     radius of pipe.
c             bt     ratio of first grid size to the thickness of
c                    stokes layer.
c       output:
c             for021.dat(1x,f13.3,1x,4g13.6,i3) fr,wpp,amag,angd,
c                                               temp,itr2
c             results of wall shear stress.
c             fr      frequency.
c             wpp     dimensioless frequency(wplus/15).
c             amag    amplitude.
c             angd    phase(related to central velocity).
c             temp    phase of central velocity(related to
c                     pressure gradient).
c             itr2    number of iteration
c             for071.dat (x,g13.6,x,g13.6) y(j),amag
c                        amplide profile.
c             for072.dat (x,g13.6,x,g13.6) y(j),angd
c                        phase profile
c
c
      program modb
      dimension u(300),y(300),alfa(300),bata(300),du(33),old(130)
      dimension uf(160,300),a(300),b(300),c(300),strss(160)
      dimension vt1(300),vt2(300),f1(300),df1(300),dy(300),fra(2)
      dimension v(300),f2(300),df2(300),fi1(300),fi2(300),reyd(20)
      pi=4.*atan(1.)
      print*,'type in bata'
      read*,bt
      print*,'type in re,vis,fr,ns,hk'
      read*,re,vis,fr,ns,hk
      print*,'type in radius of pipe '
      read*,r0
      r=r0
      w=2.*pi*fr
      ymax=.099436*re**.875
      us=ymax/r0
      h1=sqrt(2.*vis/w)*us/bt
      ni=alog10(ymax*(hk-1)/h1+1)/alog10(hk)+1
      ymax=h1*(hk**(ni-1)-1)/(hk-1)
      h1=h1/ymax
c     initial condition
      do 10 i=1,ni
 10   y(i)=h1*(hk**(i-1)-1)/(hk-1)
      st=r0*sqrt(w/vis)
      u(1)=0.
      do 50 i=2,ni-1
      tmp=-st*y(i)/sqrt(2.)
 50   u(i)=-sqrt(1./(1.-y(i)))*exp(tmp)*sin(tmp)
      u(ni)=u(ni-1)
      do 55 i=2,ni
 55   dy(i)=h1*hk**(i-2)
      hk1=1./(hk+1.)
      hkk1=1./(hk*(hk+1))
      dt=2.*pi/ns
      l=ns/32
      r=ymax/us
      st=sqrt(w/vis)*r
      call vt(y,us,r,min1,min2,ni,vis,vt1,vt2,f1)
      do 65 j=1,min1
 65   f1(j)=vt1(j)
      do 60 j=min1+1,ni-1
 60   f1(j)=vt2(j)
```

```
      do 70 j=2,ni-1
      fi1(j)=f1(j)
 70   continue
      f1(1)=0.
      fi1(1)=0.
      f1(ni)=f1(ni-1)
      fi1(ni)=f1(ni-1)
      do 80 j=2,ni-1
      df1(j)=(hkk1*f1(j+1)-hk*hk1*f1(j-1)+(hk-1)*f1(j)/hk)
     z /dy(j)
 80   continue
      do 90 j=2,ni-1
      df1(j)=(df1(j)-(1.+f1(j))/(1.-y(j)))/(st*st)
      f1(j)=(1.+f1(j))/(st*st)
 90   continue
      ufr=us*vis
      wp=w*vis/(ufr*ufr)
      wpp=wp/15.
      ub=re*vis/(2.*r)
      alfap=wp/15.
      do 160 j=2,ni-1
      tmp1=f1(j)/(dy(j)*dy(j))
      tmp2=df1(j)/(2.*dy(j))
      a(j)=-dt*hkk1*(tmp1+tmp2)
      b(j)=1.+(tmp1-tmp2*(hk-1))*dt/hk
      c(j)=dt*hk1*(-tmp1+hk*tmp2)
 160  continue
      itr2=1
      do 171 i=1,ns
 171  old(i)=0.
 170  do 180 k=1,32
      do 190 i=1,1
      ip=(k-1)*1+i
      do 400 j=2,ni-1
      d=dt*cos((ip-.5)*dt)-a(j)*u(j+1)+(2.-b(j))*u(j)-c(j)*u(j-1)
      alfa(j)=-a(j)/(b(j)+c(j)*alfa(j-1))
      bata(j)=(d-c(j)*bata(j-1))/(b(j)+c(j)*alfa(j-1))
 400  continue
      u(ni)=bata(ni-1)/(1.-alfa(ni-1))
      do 410 j=1,ni-2
      n=ni-j
 410   u(n)=alfa(n)*u(n+1)+bata(n)
       kk=(k-1)*1+i
       do 420 j=1,ni
 420   uf(kk,j)=u(j)
 190   continue
 180   continue
c     calculate shear stress variation at the wall from eqmod
      do 430 i=1,ns
 430  strss(i)=2.*uf(i,2)/(h1*st*st)
      do 440 i=1,ns
      def=strss(i)-old(i)
      if(def.gt..00001)go to 445
 440  continue
      do 451 i=1,32
      ii=i*1
 451  du(i)=uf(ii,ni)
      du(33)=du(1)
      call datfit(du,zavg,amag,angd)
      temp=angd
      do 450 i=1,32
      ii=i*ns/32
 450  du(i)=strss(ii)
      du(33)=du(1)
      call datfit(du,zavg,amag,angd)
      amag=amag*5.02836*(st*r0/r)**2/re**.875
      angd=angd-temp
      write(21,255) fr,wpp,amag,angd,temp,itr2
      go to 476
```

```
 445    do 442 i=1,ns
 442    old(i)=strss(i)
        itr2=itr2+1
        go to 170
 255    format(1x,f13.3,1x,4g13.6,i3)
c       profile of amplitude and phase of u
 476    do 475 j=2,ni
        do 470 i=1,32
        ii=i*1
 470    du(i)=uf(ii,j)
        du(33)=du(1)
        call datfit(du,zavg,amag,angd)
        angd=angd-temp
        write(71,161) y(j),amag
        write(72,161) y(j),angd
 161    format(x,g13.6,x,g13.6)
 475    continue
        stop
        end
```

(D) Model C

```
c       this program solves pulsating flow field by using model c.
c       crank-nicolson implicit scheme is used.
c       input:  re     reynolds number.
c               vis    viscosity.
c               fr     frequency.
c               ns     time steps per period.
c               r0     radius of pipe.
c               bt     ratio of first grid size to the thickness
c                      of stokes layer.
c
c       output:
c               for021.dat (x,f13.3,x,4g13.6,i3)
c                          fr,wpp,amag,angd,temp,itr2
c               results of wall shear stress.
c               fr     frequency.
c               wpp    dimesionless frequency(wplus/15).
c               amag   amplitude.
c               angd   phase(relative to central velocity).
c               temp   phase of central velocity(relative to the
c               pressure gradient).
c               itr2   number of iteration.
c
c
        program modc
        dimension u(300),y(300),alfa(300),bata(300),du(33),old(130)
        dimension uf(160,300),a(300),b(300),c(300),strss(160)
        dimension vt1(300),vt2(300),f1(300),df1(300),dy(300),fra(2)
        dimension v(300),f2(300),df2(300),fi1(300),fi2(300),reyd(20)
        pi=4.*atan(1.)
        print*,'type in k1'
        read*,k1
        print*,'type in bata'
        read*,bt
        print*,'type in re,vis,fr,ns/perod,crt'
        read*,re,vis,fr,ns,crt
        print*,'type in radius of pipe and ampl. of velocity'
        read*,r0,gama
        r=r0
        w=2.*pi*fr
        ymax=.099436*re**.875
        us=ymax/r0
        h1=sqrt(2.*vis/w)*us/bt
        hk=1.05
        ni=alog10(ymax*(hk-1)/h1+1)/alog10(hk)+1
        ymax=h1*(hk**(ni-1)-1)/(hk-1)
        h1=h1/ymax
```

```
c       initial condition
        do 10 i=1,ni
 10     y(i)=h1*(hk**(i-1)-1)/(hk-1)
        st=r0*sqrt(w/vis)
        u(1)=0.
        do 50 i=2,ni-1
        tmp=-st*y(i)/sqrt(2.)
 50     u(i)=-sqrt(1./(1.-y(i)))*exp(tmp)*sin(tmp)
        u(ni)=u(ni-1)
        do 55 i=2,ni
 55     dy(i)=h1*hk**(i-2)
        hk1=1./(hk+1.)
        hkk1=1./(hk*(hk+1))
        dt=2.*pi/ns
        l=ns/32
        r=ymax/us
        st=sqrt(w/vis)*r
        call vt(y,us,r,min1,min2,ni,vis,vt1,vt2,f1)
        do 60 j=min2+1,ni
 60     f1(j)=2*vt2(ni-1)
        do 70 j=2,ni-1
        yp=y(j)*us*r
        tmp1=exp(-yp/26.)
        tmp=(1.-tmp1)
        x1=.4*y(j)*r*tmp
        duy=vt1(j)*vis/(x1*x1)
        bb=2.*x1*(duy*duy)*tmp1*.4*y(j)*r*yp/26.
        tmp=bb/(2.*(1.-y(j))*(us*vis)**2)
        f2(j)=bb*2.*r*r/(vis*vis*gama*re*(1.-tmp))
        fi1(j)=f1(j)
        fi2(j)=f2(j)
 70     continue
        f1(1)=0.
        f2(1)=0.
        fi1(1)=0.
        fi2(1)=0.
        f1(ni)=f1(ni-1)
        f2(ni)=f2(ni-1)
        fi1(ni)=f1(ni-1)
        fi2(ni)=f1(ni-1)
        do 80 j=2,ni-1
        df1(j)=(hkk1*f1(j+1)-hk*hk1*f1(j-1)+(hk-1)*f1(j)/hk)
     z  /dy(j)
        df2(j)=(hkk1*f2(j+1)-hk*hk1*f2(j-1)+(hk-1)*f2(j)/hk)
     z  /dy(j)
 80     continue
        do 90 j=2,ni-1
        f2(j)=(df2(j)-f2(j)/(1.-y(j)))/(st*st)
        df1(j)=(df1(j)-(1.+f1(j))/(1.-y(j)))/(st*st)
        F1(J)=(1.+F1(J))/(ST*ST)
 90     continue
        ufr=us*vis
        wp=w*vis/(ufr*ufr)
        wpp=wp/15.
        ub=re*vis/(2.*r)
        alfap=wp/15.
        pc=-gama*wp*ub/ufr
        do 160 j=2,ni-1
        tmp1=f1(j)/(dy(j)*dy(j))
        tmp2=df1(j)/(2.*dy(j))
        a(j)=-dt*hkk1*(tmp1+tmp2)
        b(j)=1.+(tmp1-tmp2*(hk-1))*dt/hk
        c(j)=dt*hk1*(-tmp1+hk*tmp2)
 160    continue
        itr2=1
        do 171 i=1,ns
 171    old(i)=0.
 170    do 180 k=1,32
        do 190 i=1,l
        ip=(k-1)*l+i
```

```
      do 400 j=2,ni-1
      d=dt*cos((ip-.5)*dt)-a(j)*u(j+1)+(2.-b(j))*u(j)-c(j)*u(j-1)
     z -.5*dt*f2(j)*k1*pc*cos((ip-.5)*dt)
      alfa(j)=-a(j)/(b(j)+c(j)*alfa(j-1))
      bata(j)=(d-c(j)*bata(j-1))/(b(j)+c(j)*alfa(j-1))
  400 continue
      u(ni)=bata(ni-1)/(1.-alfa(ni-1))
      do 410 j=1,ni-2
      n=ni-j
  410  u(n)=alfa(n)*u(n+1)+bata(n)
       kk=(k-1)*l+i
       do 420 j=1,ni
  420  uf(kk,j)=u(j)
  190  continue
  180  continue
c     calculate shear stress variation at the wall from eqmod
      do 430 i=1,ns
  430 strss(i)=2.*uf(i,2)/(h1*st*st)
      do 440 i=1,ns
      def=strss(i)-old(i)
      if(def.gt..00001)go to 445
  440 continue
      do 451 i=1,32
      ii=i*l
  451 du(i)=uf(ii,ni)
      du(33)=du(1)
      call datfit(du,zavg,amag,angd)
      temp=angd
      do 450 i=1,32
      ii=i*ns/32
  450 du(i)=strss(ii)
      du(33)=du(1)
      call datfit(du,zavg,amag,angd)
      amag=amag*5.02836*(st*r0/r)**2/re**.875
      angd=angd-temp
      write(21,255) fr,wpp,amag,angd,temp,itr2
      go to 476

  445 do 442 i=1,ns
  442 old(i)=strss(i)
      itr2=itr2+1
      go to 170
  255 format(1x,f13.3,1x,4g13.6,i3)
c     profile of amplitude and phase of u
  476 do 475 j=2,ni
      do 470 i=1,32
      ii=i*l
  470 du(i)=uf(ii,j)
      du(33)=du(1)
      call datfit(du,zavg,amag,angd)
      angd=angd-temp
      write(71,161) y(j),amag
      write(72,161) y(j),angd
  161 format(x,g13.6,x,g13.6)
  475 continue
      stop
      end
```

(E) Model D

```
c       this program solves turbulent pulsating flow in a pipe
c       by model d.
c       input: re       reynolds number
c              vis      viscosity
c              fr       frequency
c              ns       time steps per period
c              nprds    periods to be proceeded
c              bt       ratio of first grid size to the thickness
c                       of stokes layer.
c              hk       factor of geometric series of grid size
c              k1       constant in model d
c              k1       relaxation constant in model d
c       output.for002.dat(x,i3,4g13.6) j,y(j),vt1(j),vt2(j),fi(j)
c                       eddy viscosities
c              for003.dat(x,2g13.6) deg,stress
c                       shear stress variaation at the wall
c              for004.dat(x,2g13.6) deg,p(eff)
c                       effective pressure gradient variation in time
c              for021.dat(x,4g13.6) y(j),mean,amag,angd
c                       profile of mean ,ampl. and phase
c              for022.dat(x,2g13.6) y(j),u(ii,j)
c                       profile of u in 8 phases
c              for023.dat(x,2g13.6) deg,u(ii,j)
c                       u variation in time at y(j)
c              for024.dat(x,2g13.6) y(j),b(j) (re. stress)
c                       profile of reynolds stress
        program mod2
        dimension u(300),y(300),alfa(300),bata(300),du(33)
        dimension uf(160,300),a(300),b(300),c(300),strss(160)
        dimension vt1(300),vt2(300),f1(300),df1(300),dy(300)
        dimension v(300),f2(300),df2(300),fi1(300),fi2(300)
        pi=4.*atan(1.)
        print*,'type in re,vis,fr,ns/period,nprds'
        read*,re,vis,fr,ns,nprds
        print*,'type in radius of the pipe and amplitude of velocity '
        read*,r0,gama
        print*,'type in converge criteria'
        read*,crt
        r=r0
        w=2.*pi*fr
        ymax=.099436*re**.875
        us=ymax/r
c
c       select grid size
        print*,'bata,hk'
        read*,bt,hk
        aa=26.
        ck=.4
        h1=sqrt(2.*vis/w)*us/bt
        ni=alog10(ymax*(hk-1)/h1+1)/alog10(hk)+1
        print*,'ymax=',ymax,'jmax=',ni,'h1=',h1
        ymax=h1*(hk**(ni-1)-1)/(hk-1)
        h1=h1/ymax
        print*,'h1=',h1,'ymax=',ymax
c
c       initial condition
        do 10 i=1,ni
 10     y(i)=h1*(hk**(i-1)-1)/(hk-1)
        st=r*sqrt(w/vis)
        u(1)=0.
        do 50 i=2,ni-1
        tmp=-st*y(i)/sqrt(2.)
 50     u(i)=-sqrt(1./(1.-y(i)))*exp(tmp)*sin(tmp)
        u(ni)=u(ni-1)
        do 55 i=2,ni
 55     dy(i)=h1*hk**(i-2)
        hk1=1./(hk+1.)
        hkk1=1./(hk*(hk+1))
        dt=2.*pi/ns
        l=ns/32
        r=ymax/us
        st=sqrt(w/vis)*r
```

```
c
c       calculate u at new time level
        call vt(y,us,r,min1,min2,ni,vis,vt1,vt2,f1,aa,ck)
        do 60 j=min2+1,ni
 60     f1(j)=2*vt2(ni-1)
        do 70 j=2,ni-1
        yp=y(j)*us*r
        tmp1=exp(-yp/aa)
        tmp=(1.-tmp1)
        x1=ck*y(j)*r*tmp
        duy=vt1(j)*vis/(x1*x1)
        bb=2.*x1*(duy*duy)*tmp1*ck*y(j)*r*yp/aa
        tmp=bb/(2.*(1.-y(j))*(us*vis)**2)
        f2(j)=bb*2.*r*r/(vis*vis*gama*re*(1.-tmp))
        fi1(j)=f1(j)
        fi2(j)=f2(j)
 70     continue
        f1(1)=0.
        f2(1)=0.
        fi1(1)=0.
        fi2(1)=0.
        f1(ni)=f1(ni-1)
        f2(ni)=f2(ni-1)
        fi1(ni)=f1(ni-1)
        fi2(ni)=f2(ni-1) .
        do 80 j=2,ni-1
        df1(j)=(hkk1*f1(j+1)-hk*hk1*f1(j-1)+(hk-1)*f1(j)/hk)
     z  /dy(j)
        df2(j)=(hkk1*f2(j+1)-hk*hk1*f2(j-1)+(hk-1)*f2(j)/hk)
     z  /dy(j)
 80     continue
        do 90 j=2,ni-1
        f2(j)=(df2(j)-f2(j)/(1.-y(j)))/(st*st)
        df1(j)=(df1(j)-(1.+f1(j))/(1.-y(j)))/(st*st)
        f1(j)=(1.+f1(j))/(st*st)
 90     continue
        ufr0=.099436*re**.875*vis/r
        wp=w*vis/(ufr0*ufr0)
        ub=re*vis/(2.*r)
        alfap=wp/15.
c
c       calculate effective pressure gradient
        print*,'type in k1,k1'
        read*,k1,k1
        pc=-gama*wp*ub/ufr0
        alfap=2*alfap*k1
        pk=(k1*dt)/(alfap+dt)
        vk=(alfap-dt)/(alfap+dt)
        v(1)=0.
        itr=1
 105    continue
        do 100 i=2,ns+1
        ii=(itr-1)*ns+i-1
 100    v(i)=pk*pc*(cos(ii*dt)+cos((ii-1)*dt))+vk*v(i-1)
        v(1)=v(ns+1)
        do 120 i=1,ns
        dlta=abs(v(i)-df2(i))
        if(dlta.gt.crt) go to 130
 120    continue
        go to 145
 130    do 140 i=1,ns
 140    DF2(I)=V(I)
        itr=1+itr
        go to 105
 145    do 146 i=1,32
        ii=i*1
        deg=i*11.25
        du(i)=v(ii)
 146    write(4,150) deg,du(i)
 150    format(x,2g13.6)
        du(33)=du(1)
        call datfit(du,zavg,amag,angd)
        write(4,151) zavg,amag,angd
 151    format(/,x,'mean=',g13.6,x,'ampl=',g13.6,x,'phas=',g13.6)
        print*,'itr=',itr
```

```
      do 160 j=2,ni-1
      tmp1=f1(j)/(dy(j)*dy(j))
      tmp2=df1(j)/(2.*dy(j))
      a(j)=-dt*hkk1*(tmp1+tmp2)
      b(j)=1.+(tmp1-tmp2*(hk-1))*dt/hk
      c(j)=dt*hk1*(-tmp1+hk*tmp2)
 160  continue
      do 170 m=1,nprds
      do 180 k=1,32
      do 190 i=1,l
      ip=(k-1)*l+i
      do 400 j=2,ni-1
      d=dt*cos((ip-.5)*dt)-a(j)*u(j+1)+(2.-b(j))*u(j)-c(j)*u(j-1)
     z -.5*dt*f2(j)*(v(ip)+v(ip+1))
      alfa(j)=-a(j)/(b(j)+c(j)*alfa(j-1))
      bata(j)=(d-c(j)*bata(j-1))/(b(j)+c(j)*alfa(j-1))
 400  continue
      u(ni)=bata(ni-1)/(1.-alfa(ni-1))
      do 410 j=1,ni-2
      n=ni-j
 410   u(n)=alfa(n)*u(n+1)+bata(n)
       if(m.ne.nprds) go to 190
       kk=(k-1)*l+i
       do 420 j=1,ni
 420   uf(kk,j)=u(j)
 190   continue
 180   continue
 170   continue
c     calculate shear stress variation at the wall from mod2
      do 430 I=1,NS
 430  strss(i)=2.*uf(i,2)/(h1*st*st)
      do 450 i=1,32
      II=I*L
 450  du(i)=strss(ii)
      du(33)=du(1)
      do 460 i=1,32
      deg=i*11.25
 460  write(3,150) deg,du(i)
      call datfit(du,zavg,amag,angd)
      angd=90.+angd
      write(3,151) zavg,amag,angd
      amag=amag*5.02836*(st*r0/r)**2/re**.875
      print*,'t(0)=',amag
c
c     profile of amplitude and phase of u
      do 451 i=1,32
      ii=i*l
 451  du(i)=uf(ii,ni)
      du(33)=du(1)
      call datfit(du,zavg,amag,angd)
      temp=angd
      do 475 j=2,ni
      do 470 i=1,32
      ii=i*l
      du(i)=uf(ii,j)
 470  continue
      du(33)=du(1)
      call datfit(du,zavg,amag,angd)
      angd=angd-temp
      write(21,161) y(j),zavg,amag,angd
 161  format(x,4g13.6)
475   continue
c
      print*,'do you want u profile in 8 phases ? 0 yes, 1,no'
      read*,ncr
      if(ncr.ne.0) go to 501
      print*,'enter y/r (the y where the profile ends)'
      read*,ys
      j=1
 186  if(y(j).gt.ys) go to 187
      j=j+1
      go to 186
 187  nk=j-1
```

```
      do 500 i=1,8
      ii=i*ns/8
      do 511 j=1,nk
      write(22,150) y(j),uf(ii,j)
 511  continue
 500  continue
 501  continue
c
      print*,'do you want time variation of u at y(j) ? 0 yes , 1 no'
      read*,nt1
      if(nt1.ne.0) go to 123
 121  print*,'which y/r ? type in j'
      read*,j
      do 131 i=1,32
      ii=i*1
      deg=i*11.25
 131  write(23,150) deg,uf(ii,j)
      print*,'go on ? 0 yes , 1 no'
      read*,ntst
      if(ntst.eq.0) go to 121
 123  continue
c
      print*,'do you want reynolds stress profile at 8 phases ?'
      print*,'0 yes, 1 no'
      read*,nt2
      if(nt2.ne.0) go to 521
      do 520 i=1,8
      ii=i*ns/8
      do 530 j=2,nk
      a(j)=(uf(ii,j+1)*hkk1-hk*hk1*uf(ii,j-1)+(hk-1)*uf(ii,j)/hk)
     z /dy(j)
 530  b(j)=-(fi1(j)*a(j)-fi2(j)*v(ii))*gama/re
      b(1)=0.
      do 525 j=1,nk
525   write(24,150) y(j),b(j)
 520  continue
 521  continue
      stop
      end
```

(F) Subroutines

```
c
      subroutine tri(m,n,h1,hk,y,r,st,dt,alfa,bata,i,u)
      dimension u(200),alfa(200),bata(200),y(200)
      hk1=1./(hk+1)
      hkk1=1./(hk*(hk+1))
      do 300 j=m,n
      dy=h1*hk**(j-2)
      stdy=dt/(st*st*dy*dy)
      stdyym=dt/(2.*st*st*dy*(1-y(j)))
      a=(-stdy+stdyym)*hkk1
      b=1.+(stdy+stdyym*(hk-1))/hk
      c=(-stdy-stdyym*hk)*hk1
      d=dt*cos((i-1+0.5)*dt)-a*u(j+1)+(2.-b)*u(j)-c*u(j-1)
      alfa(j)=-a/(b+c*alfa(j-1))
      bata(j)=(d-c*bata(j-1))/(b+c*alfa(j-1))
 300  continue
      return
      end
```

```
c
      subroutine vt(y,us,r,min1,min2,ni,vis,vt1,vt2,fi)
      dimension vt1(200),vt2(200),fi(200),y(200)
      defm1=10000.
      defm2=10000.
      do 132 j=2,ni-1
      yp=y(j)*us*r
      tmp1=exp(-yp/26.)
      vt1(j)=.5*(-1.+sqrt(1.+.64*yp**2*(1.-tmp1)**2*(1.-y(j))))
      tmp2=(2.-y(j))*(1+2.*(1.-y(j))**2)
      vt2(j)=.4*yp*tmp2/6.
      x1=.4*r*y(j)*(1.-tmp1)
      x11=.2*r*y(j)*tmp1*yp/(26.*(1.-y(j))*(us*vis)**2)
      dmvy=vis*vt1(j)/(x1*x1)
      tmp=2.*x1*x11*dmvy**2
      if(j.gt.20)go to 132
  132 fi(j)=(2.*vt1(j)+tmp)/(1.-tmp)
      do 134 j=20,ni-1
      def1=abs(vt1(j)-vt2(j))
      def2=abs(fi(j)-2*vt2(ni-1))
      if(def1.ge.defm1) go to 133
      defm1=def1
      min1=j
  133 if(def2.ge.defm2) go to 134
      defm2=def2
      min2=j
  134 continue
      return
      end

c
c
      subroutine datfit(z,zavg,amag,angd)
      dimension a(2,2),b(2),z(33),x(33)
      np=33
      pi=4*atan(1.)
      n=2
      do 210 i=1,33
  210 x(i)=i*.03125*2*pi
      do 1 i=1,n
      do 2 j=1,n
    2 a(i,j)=0.
    1 b(i)=0
      sumavg=0.
      do 250 i=1,32
  250 sumavg=sumavg+z(i)
      zavg=sumavg/(np-1)
      do 5 m=1,np
      ii=0
      do 6 jj=1,n,2
      ii=ii+1
      b(jj)=b(jj)+(z(m)-zavg)*sin(x(m)*ii)
      b(jj+1)=b(jj+1)+(z(m)-zavg)*cos(x(m)*ii)
      mm=0
      do 7 kk=1,n,2
      mm=mm+1
      a(jj,kk)=a(jj,kk)+sin(x(m)*ii)*sin(x(m)*mm)
      a(jj,kk+1)=a(jj,kk+1)+sin(x(m)*ii)*cos(x(m)*mm)
      a(jj+1,kk)=a(jj+1,kk)+cos(x(m)*ii)*sin(x(m)*mm)
      a(jj+1,kk+1)=a(jj+1,kk+1)+cos(x(m)*ii)*cos(x(m)*mm)
    7 continue
    6 continue
    5 continue
c
      delt=a(1,1)*a(2,2)-a(1,2)*a(2,1)
      delt1=b(1)*a(2,2)-b(2)*a(1,2)
      delt2=b(2)*a(1,1)-b(1)*a(2,1)
      b(1)=delt1/delt
      b(2)=delt2/delt
      amag=sqrt(b(1)**2+b(2)**2)
      bb=-b(1)
      bbb=b(2)
      ang=atan2(bb,bbb)
      angd=ang*360./(2.*pi)
      return
      end
```

# APPENDIX III. Sampling Programs in LSI-11

(A) Sampling program for steady flow.

```
C*****************************************************
C           PROGRAM MCRTS
C           THIS IS THE FORTRAN CONTROLLER PROGRAM
C           FOR ANALOG TO DIGITAL CONVERSION OF
C           MULTIPLE CHANNELS AT SPEEDS UP TO
C           20000 CHANNELS PER SECOND.THIS
C           PROGRAM SETS THE OUTPUT FILE,THE ERROR
C           FLAGS,THE DATA ARRAY AND CALLS THE
C           MACRO SUBROUTINE MCRTSB.MAC WHICH
C           STARTS THE CLOCK, AND COLLECTS THE DATA.
C
C           THE OUTPUT FILE IS SPECIFIED USING THE
C           GETSTR COMMAND, THIS MUST BE COMPILED
C           USING THE NOSWAP OPTION.
C
C           THE OUTPUT FILE IS FORMATTED I5,I5
C           WITH THE FIRST A DATA POINT NUMBER
C           AND THE SECOND, THE VALUE OF THE DATA
C           POINT IN 2'S COMPLEMENT.
C           A SEPARATE PROGRAM IS NECESSARY TO
C           CONVERT THESE NUMBERS TO VOLTAGES.
C           THIS SAVES MEMORY SPACE IN THE
C           COLLECTION PROGRAM FOR THE LARGEST
C           NUMBER OF DATA POINTS.
C
C           THE NUMBER OF CHANNELS AND THE NUMBER
C           OF DATA POINTS ARE READ FROM THE
C           TERMINAL AND ARE TRANSFERED TO THE
C           SUBROUTINE.
C
C           THE CLOCK SPEED,THE DATA AQUISITION RATE,
C           IS SET BY SELECTING THE MULTIPLE
C           OF 10000/SEC DESIRED.
C           I.E. RATE= MULTIPLE/10000
C           MULTIPLE MUST BE A POSITIVE INTEGER
C           AND IF FINER INTERVAL SPLITTING IS NEEDED
C           THE MACRO PROGRAM CAN BE EDITED TO
C          ALLOW DIVSIONS OF 10**5 OR 10**6/SEC.
C
C*****************************************************
C
C
            PROGRAM MCRTS
C
            INTEGER*2 DATA(12000)
            DATA      DATA/12000*0/
            LOGICAL*1  DATFIL(12),ERR
            COMMON  /AD/ DONE,ERCLK,ERADC      !DONE FLAG,ERROR FLAGS
C
            DONE=0
            ERCLK=0
            ERADC=0
C
 1            WRITE(7,10)
 10         FORMAT(1X,'TYPE IN THE NAME OF THE OUTPUT FILE')
C
            CALL GETSTR(5,DATFIL,11,ERR)
            IF(ERR) GO TO 1
C
            OPEN(UNIT=3,NAME=DATFIL,TYPE='NEW')    !WRITING WITH
C                                                  !DEVICE 3 WILL
C                                                  !NOW GO INTO OUTPUT FILE
```

```
C
C
            WRITE(7,20)
 20         FORMAT(1X,'TYPE IN THE NUMBER OF CHANNELS
     Z      AND THE NUMBER OF POINTS PER CHANNEL')
            READ(5,*) NCHS,NPTS
C
            WRITE(7,30)
 30         FORMAT(1X,'TYPE IN THE MULTIPLE OF 10000/SEC
     Z      FOR THE SAMPLING RATE')
C
            READ(5,*) MULT
C
            WRITE(7,40)

 40         FORMAT(1X,'DATA AQUISITION IN PROGRESS')
C
            CALL MCRTSB(NPTS,NCHS,MULT,DATA)
C
 99         IF (DONE.EQ.0) GO TO 99
C
            IF (ERCLK.LT.1) GO TO 89
            WRITE(7,50)
 50         FORMAT(1X,'CLOCK OVERFLOW ERROR')
C
 89         IF (ERADC.LT.1) GO TO 79
            WRITE(7,60)
 60         FORMAT(1X,'A/D CONVERTER ERROR')
C
 79         WRITE(7,70)
 70         FORMAT(1X,'DATA COLLECTION COMPLETE')
C
            DO 100 I=1,NPTS*NCHS
                   WRITE(3,*) DATA(I)
C                   WRITE(3,80)I,DATA(I)
C 80                FORMAT(I5,I5)
100         CONTINUE
C
            STOP
            END

;*************************************************************
;
;
;           SUBROUTINE MCRTSB.MAC
;           THIS SUBROUTINE IS CALLED FROM MCRTS.FOR.
;           CALL MCRTSB(NPTS,NCHS,MULT,DATA)
;
;           WHERE:      NPTS= NUMBER OF DATA POINTS PER CHANNEL
;                       NCHS= NUMBER OF CHANNELS
;                       MULT= MULTIPLE OF 10000/SEC
;                       DATA= DATA ARRAY
;
;           REGISTER 4 IS USED TO POINT TO THE DATA ARRAY
;           REGISTER 5 IS THE POINTER FOR THE ARGUMENTS IN
;                      THE FORTRAN CALL
;           THE OTHER REGISTERS ARE NOT USED.
;
;*****************************************************************
;
            .SBTTL MCRTSB.MAC
            .GLOBL MCRTSB
            .GLOBL COLOOP
;
            ADSTAT=177000               ;THE ADDRESS OF THE A/D BOARD
            ADBUF=ADSTAT+2              ;THE ADDRESS OF THE DATA REGISTER
;
            CLSTAT=170420               ;THE ADDRESS OF THE CLOCK
            CLBUF=CLSTAT+2              ;THE ADDRESS OF THE CLOCK COUNTER
;
            CLVEC=440                   ;THE CLOCK INTERUPT VECTOR
            PR7=340                     ;INTERUPT PRIORITY IS 7
```

```
;
            DEVPRI=5                    ;DEVICE PRIORITY IS 5
            .PSECT AD,RW,D,GBL,REL,OVR
DONE:       .WORD 0
ERCLK:      .WORD 0
ERADC:      .WORD 0                     ;SET UP FLAGS IN /AD/ COMMON
;
            .PSECT $DATA RW,D,LCL,REL,CON
DATA:       .WORD 0
NCHS:       .WORD 0
NPTS:       .WORD 0
MULT:       .WORD 0
;
            .PSECT $CODE RW,I,LCL,REL,CON
            .MCALL .INTEN               ;LOWERS PRIORITY ON INTERUPT
;
MCRTSB:     MOV @(R5)+,R0               ;IGNORE NUMBER OF ARGUMENTS
            MOV @(R5)+,NPTS             ;GET NUMBER OF POINTS
            MOV @(R5)+,NCHS             ;GET NUMBER OF CHANNELS
            MOV @(R5)+,MULT             ;GET MULTIPLE FOR CLOCK
            MOV  (R5)+,DATA             ;GET ADDRESS OF DATA ARRAY
;
            MOV #COLOOP,@#CLVEC         ;LOAD INTERUPT LOCATION
            MOV #PR7,@#CLVEC+2          ;AND PRIORITY
            CLR @#ADSTAT
            TST @#ADBUF
;
            CLR @#CLSTAT                ;INITIALIZE CLOCK
            NEG MULT                    ;CHANGE MULT TO 2'S COMPLEMENT
            MOV MULT,@#CLBUF            ;MOV MULT INTO CLOCK COUNTER
            MOV #133,@#CLSTAT           ;START CLOCK 10000/SEC
;                                       ;INTERUPT ENABLED
;
;
            RTS PC                      ;RETURN TO MAIN PROGRAM TO
;
;                                       ;WAIT FOR INTERUPT
;
;
COLOOP:     .INTEN DEVPRI               ;LOWER DEVICE PRIORITY
            BIC #200,@#CLSTAT           ;CLEAR CLOCK OVERFLOW BIT
            MOV NCHS,R5                 ;SAVE NUMBER OF CHANNELS

            MOV DATA,R4                 ;MOVE DATA ADDRESS TO R4
            MOV #1,@#ADSTAT             ;LOAD CHANNEL 0 AND START CONVERSION
1$:         TSTB @#ADSTAT               ;WAIT UNTIL COMPLETE
            BPL 1$
            MOV @#ADBUF,(R4)+           ;SAVE DATA POINT
            DEC NCHS
            BEQ 3$
22$:        ADD #401,@#ADSTAT         ;SET SEQUENTIAL MODE
2$:         TSTB @#ADSTAT               ;TEST IF DONE
            BPL 2$
            MOV @#ADBUF,(R4)+           ;SAVE NEXT DATA POINT
            DEC NCHS                    ;DECREMENT NCHS
            BNE 22$                      ;ANY MORE CHANNELS
3$:         DEC NPTS                    ;NO DECREMENT POINTS
            BEQ EXIT                    ;EXIT IF DONE
            MOV R4,DATA                 ;SAVE DATA
            MOV R5,NCHS                 ;SAVE CHANNEL COUNT
            RTS PC                      ;RETURN FOR MORE DATA
;
;
EXIT:       CLRB @#CLSTAT               ;STOP CLOCK
            BIT #10000,@#CLSTAT         ;CHECK CLOCK ERROR BIT
            BEQ 10$                     ;NO SET CONTINUE
            MOV #2,ERCLK                ;SET CLOCK ERROR
10$:        TST @#ADSTAT                ;AD ERROR BIT SET ?
            BPL RETURN                  ;NO RETURN
            MOV #2,ERADC                ;SET A/D ERROR
RETURN:     MOV #1,DONE                 ;SET DONE
            RTS PC
            .END
```

(B) Sampling program for time interval between two trigger signals.

```
C*************************************************************
C       PROGRAM TTMF.FOR

C       THIS IS A FORTRAN DRIVER FOR MEASURING MEAN TIME
C       INTERVAL BETWEEN TWO EXTERNAL TRIGGER SIGNALS.
C       NPTS     NUMBER OF PERIODS TO BE MEASURED.
C       NN       NUMBER OF POINTS TO BE USED IN DATCL.FOR
C                FOR A PERIOD.
C       MULT     SAMPLINIG RATE TO BE USED IN DATCL.FOR.
C       BEFORE RUN THIS PROGRAM,LINK IT WITH TTM.MAC.
C*************************************************************

        PROGRAM TTMF
        INTEGER*2 DATA(500)
        DATA DATA/500*0/
        LOGICAL*1 DATFIL(12),ERR
        COMMON /AD/DONE,ERCLK
C
        DONE=0
        ERCLK=0
C
  1     WRITE(7,10)
  10    FORMAT(1X,'TYPE IN THE NAME OF THE OUTPUT FILE')
C
        CALL GETSTR(5,DATFIL,11,ERR)
        IF(ERR) GO TO 1
        OPEN(UNIT=3,NAME=DATFIL,TYPE='NEW')
C
        WRITE(7,20)
  20    FORMAT(1X,'TYPE THE NUMBER OF PERIODS AND POINTS PER PERIOD')
        READ(5,*) NPTS,NN
        WRITE(7,30)
  30    FORMAT(1X,'PERIOD MEASUREMENT IN PROGRESS')
        CALL TTM(DATA,NPTS)
   99   IF(DONE.EQ.0) GO TO 99
        IF(ERCKL.LT.1) GO TO 89
        WRITE(7,40)
  40    FORMAT(1X,'CLOCK OVERFLOW ERROR')
  89    WRITE(7,50)
  50    FORMAT(1X,'PERIOD MEASUREMERNT IS OVER')
        SUM=0
        DO 100 I=1,NPTS
  100   SUM=SUM+DATA(I)
        COUNT=SUM/NPTS
        MULT=COUNT/NN
        STDV=0
        DO 200 I=1,NPTS
  200   STDV=STDV+(DATA(I)-COUNT)**2
        STDV=SQRT(STDV/NPTS)/COUNT
        WRITE(3,*) COUNT,STDV,MULT
C  110   FORMAT(1X,'COUNT=',I6,'STDV=',F8.4)
        STOP
        END


;*************************************************************************
;          SUBROUTINE TTM.MAC
;          THIS SUBROUTINE IS CALLED FROM TTMF.FOR.
;          CALL TTM(DATA,NPTS)
;          WHERE  DATA=DATA ARRAY.
;                 NPTS=PERIODS TO BE AVERAGED
;*************************************************************************
           .SBTTL TTM.MAC
           .GLOBL TTM
;
           CLSTAT=170420            ;THE ADDRESS OF THE CLOCK
           CLBUF=CLSTAT+2           ;THE ADDRESS OF THE CLOCK COUNTER
```

```
;
            CLVEC=444                   ;THE CLOCK INTERRUPT VECTOR
            PR7=340                     ;INTERRUPT PRIORITY IS 7
;
            DEVPRI=5                    ;DEVICE PRIORITY IS 5
            .PSECT AD,RW,D,GBL,REL,OVR
DONE:       .WORD 0
ERCLK:      .WORD 0
;
            .PSECT $DATA RW,D,LCL,REL,CON
DATA:       .WORD 0
NPTS:       .WORD 0
FLAG:       .WORD 0
;
            .PSECT $CODE RW,I,LCL,REL,CON
            .MCALL .INTEN
;
TTM:        MOV @(R5)+,R0               ;IGNORE NUMBER OF ARGUMENT
            MOV (R5)+,DATA              ;GET ADDRESS OF DATA
            MOV @(R5)+,NPTS             ;GET NUMBER OF POINTS
            MOV #0,FLAG                 ;SET FLAG ZERO
            MOV #CLKISR,@#CLVEC         ;LOAD INTERRUPT LOCATION
            MOV #PR7,@#CLVEC+2          ;AND PRIORITY
;
            CLR @#CLSTAT                ;INITIALIZE CLOCK
            MOV #60036,@#CLSTAT         ;SET CLOCK,ST2 GO ENABLE,
                                        ;INTERRUPT ON ST2,10KHZ,MODE 3
            RTS PC                      ;RETURN TO MAIN PROGRAM TO WAIT
                                        ;FOR INTERRUPT
;
CLKISR:     .INTEN DEVPRI               ;LOWER DEVICE PRIORITY
            TST FLAG                    ;TEST FLAG
            BNE 1$                      ;IGNORE FIRST ST2 EVENT
            MOV #1,FLAG                 ;SET FLAG ONE
            BIC #100000,@#CLSTAT        ;CLEAR ST2 FLAG
            RTS PC                      ;RETURN TO MAIN PROGRAM TO WAIT
                                        ;FOR NEXT ST2 EVENT
;
1$:         MOV DATA,R0
            MOV @#CLBUF,(R0)+           ;SEND COUNTS TO DATA ARRAY
            MOV R0,DATA
            BIC #100000,@#CLSTAT        ;CLEAR ST2 FLAG
            DEC NPTS                    ;DECREMENT NUMBER OF POINTS
            BEQ EXIT                    ;NO MORE POINT,GO TO EXIT
            RTS PC                      ;MORE POINTS,RETURN TO MAIN PROGRAM
                                        ;TO WAIT FOR NEXT ST2 EVENT
;
EXIT:       BIC #20000,@#CLSTAT         ;UNABLE ST2 GO BIT
            BIC #1,@#CLSTAT             ;STOP CLOCK
            BIT #10000,@#CLSTAT         ;CHECK CLOCK ERROR BIT
            BEQ RETURN                  ;NO ERROR,GO TO RETURN
            MOV #2,ERCLK                ;ERROR,SET ERCLK 2
;
RETURN:     MOV #1,DONE                 ;SET DONE 1,FINISH SAMPLING
            RTS PC
            .END
```

(C) Sampling program for oscillating flow.

```
C*********************************************************
C           PROGRAM DATCL
C           THIS IS A FORTRAN DRIVER FOR COLLECTING DATA AND
C           WRITTING THEM DIRECTLY TO A DISK. THIS PROGRAM
C           STARTS TO TAKING DATA WHEN AN OUTER TRIGGER SIGNAL
C           OCCURS,THEN SWEEPS ALL CHANNELS AT EACH SAMPLING
C           POINT UNTIL THE REQUIRED PERIODS ARE REACHED.
C           DATA ACQUISITION RATE IS 2000 POINTS/SEC FOR MULTIPLE
C           CHANNELS.
C           NCHS       NUMBER OF CHANNELS
C           NPTS       NUMBER OF POINTS PER CHANNEL PER PERIOD
C           NPRDS      NUMBER OF PERIODS
C           DIMENSION OF IX      NCHS*NPTS
C           BEFORE RUN THIS PROGRAM, LINK IT WITH DATCLT.MAC.
C
C*************************************************************
            PROGRAM DATCL
            INTEGER IX(192)
            LOGICAL*1  DATFIL(12),ERR
C
 1            WRITE(7,10)
 10         FORMAT(1X,'TYPE IN THE NAME OF THE OUTPUT FILE')
C
            CALL GETSTR(5,DATFIL,11,ERR)
            IF(ERR) GO TO 1
C
C
C           OPEN THE DATA FILE,USE DEVICE 3 TO WRITE
C
            OPEN(UNIT=3,NAME=DATFIL,TYPE='NEW',ERR=1
     Z      ,FORM='UNFORMATTED',RECORDSIZE=50)
C
C
            WRITE(7,20)
 20         FORMAT(1X,'TYPE IN THE NUMBER OF CHANNELS
     Z      AND THE NUMBER OF POINTS PER CHANNEL AND NUMBER OF PERIODS')
            READ(5,*) NCHS,NPTS,NPRDS
C
            WRITE(7,30)
 30         FORMAT(1X,'TYPE IN THE MULTIPLE OF 10000/SEC
     Z      FOR THE SAMPLING RATE')
C
            READ(5,*) MULT
C
            WRITE(7,40)
 40         FORMAT(1X,'DATA AQUISITION IN PROGRESS')
            CALL DATCLT(NPTS,NCHS,MULT,32767)
C
C           THIS SECTION GETS DATA AND WRITES IT TO DISK
            DO 120 K=1,NPRDS
            DO 130 I=1,NPTS*NCHS
 130        CALL GETW(IX(I))
 120        WRITE(3) IX
C
            CALL CLEAN
            CLOSE(UNIT=3)
 79         WRITE(7,70)
 70         FORMAT(1X,'DATA COLLECTION COMPLETE')
C
C
            STOP
            END
```

```
;*************************************************************

;           SUBROUTINE DATCLT.MAC
;           THIS SUBROUTINE IS CALLED FROM DATCL.FOR.
;           CALL DATCLT(NPTS,NCHS,MULT,32767)
;*************************************************************
;
            .SBTTL DATCLT.MAC
            .GLOBL DATCLT
            .GLOBL COLOOP
            .GLOBL GETW
            .GLOBL CLEAN
;
            ADSTAT=177000               ;THE ADDRESS OF THE A/D BOARD
            ADBUF=ADSTAT+2              ;THE ADDRESS OF THE DATA REGISTER
            CLSTAT=170420               ;THE ADDRESS OF THE CLOCK
            CLBUF=CLSTAT+2
            STVEC=444                   ;ST2 INTERRUPT VECTOR
            CLVEC=440                   ;THE CLOCK INTERRUPT VECTOR
            PR7=340                     ;INTERRUPT PRIORITY IS 7
;
            .PSECT $DATA RW,D,LCL,REL,CON
            BUFSIZ=32767
NCHS:       .WORD 0
NPTS:       .WORD 0
MULT:       .WORD 0
LIMIT::     .WORD 0
TEMP:        .BLKW 1
INPTR::       .WORD BUF
OUTPTR::      .WORD BUF
COUNT::       .WORD 0
BUF::         .BLKW BUFSIZ

;
DATCLT:     MOV @(R5)+,R0               ;IGNORE NUMBER OF ARGUMENTS
            MOV @(R5)+,NPTS             ;GET NUMBER OF POINTS
            MOV @(R5)+,NCHS             ;GET NUMBER OF CHANNELS
            MOV @(R5)+,MULT             ;GET MULTIPLE FOR CLOCK
            MOV @(R5)+,LIMIT
;
            MOV #COLOOP,@#STVEC         ;LOAD ST2 INTERRUPT LOCATION
            MOV #PR7,@#STVEC+2          ;AND PRIORITY
            MOV #COLOOP,@#CLVEC         ;LOAD INTERUPT LOCATION
            MOV #PR7,@#CLVEC+2          ;AND PRIORITY

            CLR @#ADSTAT
            MOV #0,R1
1$:         SOB R1,1$
;
            CLR @#CLSTAT                ;INITIALIZE CLOCK
            MOV #BUF,INPTR
            MOV #BUF,OUTPTR
            NEG MULT                    ;CHANGE MULT TO 2'S COMPLEMENT
            MOV MULT,@#CLBUF            ;MOV MULT INTO CLOCK COUNTER
            MOV NPTS,TEMP
            MOV #60132,@#CLSTAT         ;ST2 START CLOCK 10000/SEC,REPEATED MODE
;                                       ;INTERUPT ENABLED
            TST @#ADBUF
;
;
            RTS PC                      ;RETURN TO MAIN PROGRAM TO
;
```

```
;                                       ;WAIT FOR INTERUPT
COLOOP:     MOV #0,@#ADSTAT             ;LOAD CHANNEL 0 AND START CONVERSION
            BIC #200,@#CLSTAT
            MOV R0,-(SP)                ;SAVE R0
            MOV R4,-(SP)                ;SAVE R4
            MOV NCHS,R4                 ;SAVE NUMBERS OF CHANNELS
1$:         TSTB @#ADSTAT               ;WAIT UNTIL COMPLETE
            BPL 1$
            MOV @#ADBUF,R0          ;SAVE DATA POINT
            DEC R4
            BEQ 3$
            BIS #40000,@#ADSTAT         ;SET SEQUENTIAL MODE
            JSR PC,PUTW                 ;SAVE DATA IN BUFFER
2$:         TSTB @#ADSTAT               ;TEST IF DONE
            BPL 2$
            MOV @#ADBUF,R0          ;SAVE NEXT DATA POINT
            INCB @#ADSTAT               ;LOAD NEXT CHANNEL
            JSR PC,PUTW               ;SAVE DATA IN BUFFER

            DEC R4                     ;DECREMENT NCHS
            BNE 2$                      ;ANY MORE CHANNELS
3$:         DEC TEMP                      ;NO DECREMENT POINTS
            BEQ EXIT                    ;EXIT IF DONE
            MOV (SP)+,R4
            MOV (SP)+,R0
            RTI                         ;RETURN FROM INTERRUPT
EXIT:       MOV (SP)+,R4
            MOV (SP)+,R0
            MOV NPTS,TEMP
            MOV #60132,@#CLSTAT
            RTI                         ;NO,BACK FOR ANOTHER ST2 EVENT;
;
            .PSECT PUTW
PUTW::      CMP COUNT,LIMIT
            BGE 2$
            MOV R0,@INPTR
            INC COUNT
            ADD #2,INPTR
            CMP INPTR,#BUF+(BUFSIZ*2)
            BLO 1$
            MOV #BUF,INPTR
1$:         RTS PC
2$:         BIC #100,@#CLSTAT
            RTS PC
;
;           THIS SECTION IS CALLED FROM FORTRAN PROGRAM AND MOVES DATA FROM
;           BUFFER TO THE RETURN CALL STATEMENT. THE FORTRAN PROGRAM THEN WRITES
;           DATA POINTS TO DISK
            .PSECT GETW
GETW::      CMP #1000,COUNT
            BGE GETW
            MOV @OUTPTR,@2(R5)
            DEC COUNT
            ADD #2,OUTPTR
            CMP OUTPTR,#BUF+(BUFSIZE*2)
            BLO 1$
            MOV #BUF,OUTPTR
1$:         RTS PC
CLEAN::     CLR COUNT
            CLR @#CLSTAT
            CLRB @#ADSTAT
            RTS PC
            .END
```

## APPENDIX IV. Pulsating Pump Curve

A schematic drawing of a pulsating pum is shown in Figure IV.1. Point 0 represents the shaft of the motor. Point C, the position of the piston, is moving along axis oc. Term $L_s$ is the stroke length and $L_a$ is the length of the arm which connects the piston in one end and the storke in the another end.

At any moment, the position of the piston C is expressed as

$$x = L_s \cos \omega t + \sqrt{L_a^2 - L_s^2 \sin^2 \omega t} \quad , \tag{IV.1}$$

where $\omega$ is angular frequency. The velocity of the piston is then

$$u = \frac{dx}{dt}$$

$$= L_s \omega \sin \omega t \left[ -1 - \frac{L_s}{L_a} \frac{\cos \omega t}{\sqrt{1 - \left(\frac{L_s}{L_a}\right)^2 \sin^2 \omega t}} \right] . \tag{IV.2}$$

Therefore, the pressure gradient can be expressed as $-\frac{1}{\rho}\frac{dP}{dx} = \frac{du}{dt}$ and plotted in Figure IV.2 for $L_s$ = 7.62 cm, $L_a$ = 55.25 cm and f = 0.325 Hz. The least square fit of a cosine curve is also plotted in dashed line. It is seen that when $\frac{L_s}{L_a}$ is not negligible the movement of the piston starts to deviate from a sinusoidal variation.

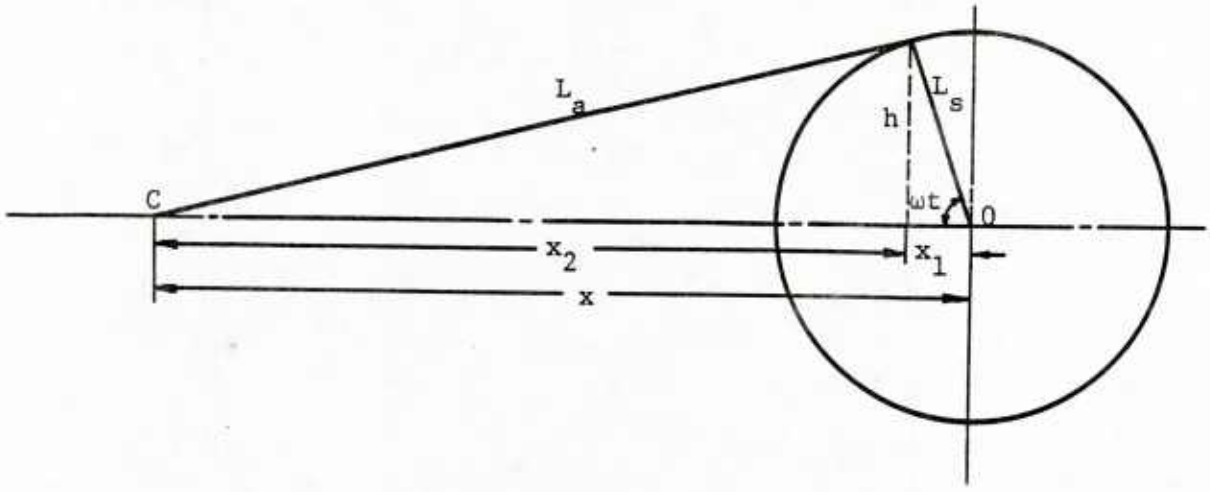


Figure IV.1 Schematic of pulsating pump

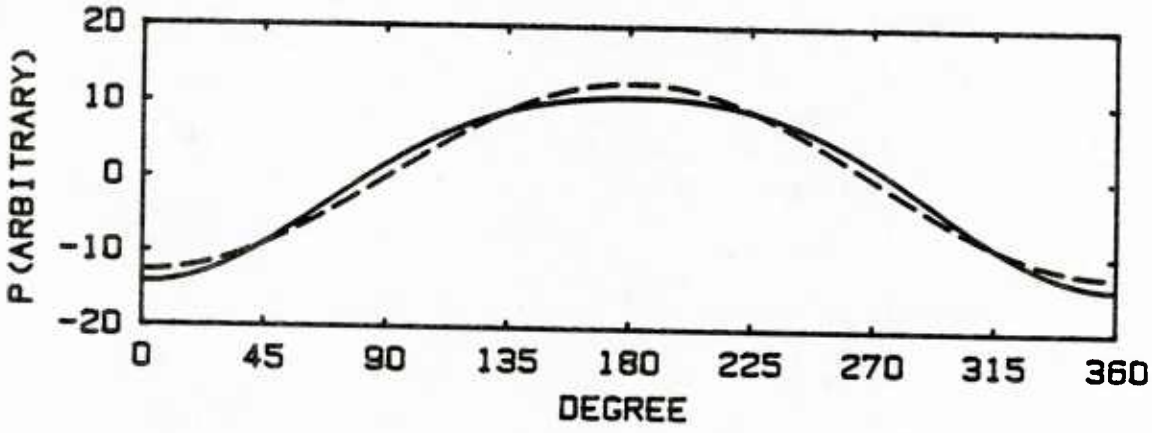


Figure IV.2 Pressure gradient calculated from the movement of the piston

($L_s$ = 7.62 cm, $L_a$ = 55.25 cm and f = 0.325 Hz)

# NOMENCLATURE

| Symbol | | Unit |
|---|---|---|
| $a$ | Amplitude of pressure gradient | $g/cm\text{-}sec^2$ |
| $a_0$ | Dimensionless amplitude of flow oscillation | |
| $A$ | Amplitude correction factor for frequency response of the probe; Van Driest damping constant | |
| $A_e$ | Area of electrode | $cm^2$ |
| $B$ | Factor defined in (3.43) | |
| $c_1$ | Dimensionless time dependent concentration defined in (4.10) | |
| $C$ | Concentration | $mole/cm^3$ |
| $C_b$ | Bulk concentration | $mole/cm^3$ |
| $D$ | Pipe diameter | cm |
| $D_m$ | Damping function in Van Driest formula | |
| $f$ | Frequency | 1/sec |
| $F$ | Faraday's constant, 96,500 | $\frac{\text{abs-coul}}{\text{q-equivalent}}$ |
| $H$ | Ratio of two consequent grid sizes | |
| $I$ | Current flowing in the electrochemical cell | amp |
| $k$ | Von Karman constant 0.4; Time dependent component of mass transfer coefficient | cm/sec |
| $k_I$ | Imaginary part of k | |
| $k_L$ | Relaxation constant defined in (3.47) | |
| $k_R$ | Real part of k | |
| $k_s$ | Pseudosteady approximation of k | cm/sec |
| $k_1, k_2$ | Coefficients defined in (3.46) | |
| $K$ | Mass transfer coefficient | cm/sec |
| $\ell$ | Mixing length | cm |
| $L$ | Length of electode (in x direction) | cm |

| Symbol | | Unit |
|---|---|---|
| $L_s$ | Stroke length of pulse generator | cm |
| $n_e$ | Number of electrons transferred in electrochemical reaction | |
| N | Number of total samples; Rate of mass transfer per unit area | mole/cm$^2$-sec |
| p | Pressure | g/cm-sec$^2$ |
| r | Coordinate in radial direction | cm |
| $r_0$ | Pipe radius | cm |
| Re | Reynolds number | |
| s | Time dependent component of velocity gradient at the wall | cm/sec$^2$ |
| $s_x$ | Streamwise velocity gradient fluctuation at the wall | cm/sec$^2$ |
| S | Velocity gradient at the wall | cm/sec$^2$ |
| Sc | Schmidt number | |
| $S_x$ | Streamwise velocity gradient at the wall | cm/sec$^2$ |
| t | Time | sec |
| T | Dimensionless time defined in (3.53) | |
| u | Streamwise velocity | cm/sec |
| $u^*$ | Friction velocity | cm/sec |
| $u_b$ | Bulk velocity in pipe | cm/sec |
| $u_c$ | Central velocity | cm/sec |
| U | Dimensionless oscillation velocity | |
| U' | Dimensionless time averaged velocity | |
| v | Radial velocity | cm/sec |
| w | Spanwise velocity | cm/sec |
| W | Width of the electrode | cm |
| x | Coordinate in the flow direction | cm |
| X | Dimensionless x (X = x/L) | |

| Symbol | | Unit |
|---|---|---|
| $y$ | Coordinate normal to the wall | cm |
| $y^+$ | Dimensionless y. ($y^+ = y u^*/\nu$) | |
| $y^*$ | Dimensionless y. ($y^* = y^+ Sc^{1/3}/L^{+1/3}$) | |
| $Y$ | Dimensionless Y. ($Y = y/r_0$) | |

| Greek Symbol | | |
|---|---|---|
| $\alpha$ | Diffusivity;<br>Wave number of wavy surface | $cm^2/sec$<br>1/cm |
| $\alpha^+$ | Dimensionless wave number. ($\alpha^+ = \alpha\nu/u^*$) | |
| $\beta$ | Coefficient defined in (4.33) | |
| $\delta_c$ | Concentration boundary thickness | cm |
| $\delta_s$ | Stokes layer thickness | cm |
| $\delta_v$ | Viscous sublayer thickness | cm |
| $\eta$ | Dimensionless length defined in (4.6) | |
| $\theta$ | Phase degree | degree |
| $\lambda$ | Wave length of wavy surface | cm |
| $\mu$ | Molecular viscosity | g/cm-sec |
| $\nu$ | Kinematic viscosity | $cm^2/sec$ |
| $\nu_t$ | Turbulent eddy viscosity | $cm^2/sec$ |
| $\rho$ | Density of fluid | $g/cm^3$ |
| $\tau$ | Shear stress | $g/cm\text{-}sec^2$ |
| $\tau^{(t)}$ | Turbulent shear stress | $g/cm\text{-}sec^2$ |
| $\tau_w$ | Wall shear stress | $g/cm\text{-}sec^2$ |
| $\hat{\tau}(0)$ | Dimensionless amplitude of wall shear stress, defined in (4.25) | |
| $\phi_1$ | Coefficient defined in (3.45) | |
| $\phi_2$ | Coefficient defined in (3.51) | |

| Greek Symbol | | Unit |
|---|---|---|
| $\omega$ | Angular frequency | 1/sec |
| $\omega^+$ | Dimensionless $\omega$ ($\omega^+ = \omega\nu/u^{*2}$) | |
| $\omega^*$ | Dimensionless $\omega$ ($\omega^* = \omega^+ Sc^{1/3}$) | |
| $\Omega$ | Frequency parameter ($\Omega = \sqrt{\omega/\nu}\, r_0$) | |

Overline and brackets:

| | |
|---|---|
| $\tilde{}$ | Peoretical component |
| $\bar{}$ | Time average |
| $< >$ | Phase average |
| $\lvert\hat{}\rvert$ | Amplitude |

Superscripts:

| | |
|---|---|
| + | Nondimensionlized with firction velocity $u^*$ and kinematic viscosity $\nu$ |
| (t) | Turbulent component |

# REFERENCES

Abrams, J., K. A. Fredrick and T. J. Hanratty. 1981 "Interaction between a Turbulent Flow and a Wavy Surface." presented at National Meeting of the AIChE. Detroit, Michigan.

Abrams, J. 1984 "Turbulent Flow Over Small Amplitude Solid Waves," Ph.D. thesis in Chameical Engineering, University of Illinois, Urbana.

Acharya, M. and W. C. Reynolds. 1975 "Measurements and Predictions of a Fully Developed Turbulent Channel Flow with Imposed Controlled Oscillations." Report TF-8, Thermosciences Div., Dept. of Mech. Engrg., Stanford University, Stanford, California.

Bendat, J. S. and A. G. Piersol. 1971 "Radom Data: Analysis and Measurement Procedures." John Wiley & Sons.

Binder, G. and J. L. Kueny. 1982 "Measurements of the Periodic Velocity Oscillations Near the Wall in Unsteady Turbulent Channel Flow." in Turbulent Shear Flow 3 (ed. L.J.S. Bradbury et al.) Springer-Verlag, pp. 6-17).

Cousteix, J., A. Desopper and R. Houdeville. 1977 "Structure and Development of a Turbulent Boundary Layer in an Oscillatory External Flow." Turbulent Sehar Flow I, Springer-Verlag, pp. 154-171.

Cousteix, J., R. Houdevill and J. Javelle. 1981 "Response of a Turbulent Boundary Layer to Pulsation of the External Flow with and without Adverse Pressure Gradient." Unsteady Turbulent Shear Flows, Springer-Verlag, pp. 120-144.

Cousteix, J., J. Javelle and R. Houdeville. 1982 "Influence of Strouhal Number on the Structure of Flat Plate Turbulent Boundary Layer." Turbulent Shear Flows 3, Springer-Verlag, pp. 46-59.

Davis, S. H. 1976 "The Stability of Time-periodic Flows." Annual Review of Fluid Mechanics, 8, p. 57.

Fortuna, G. and T. J. Hanratty. 1971 "Frequency Response of the Boundary Layer on Wall Transfer Probes." Int. J. Heat Mass Transfer, 14, pp. 1499.

Gerrard, J. H. 1971 "An Experimental Investigation of Pulsating Turbulent Water Flow in a Tube." J. Fluid Mech. 46, pp. 43-46.

Hanratty, T. J., L. G. Chorn and D. T. Hatziavramidis. 1977 "Turbulent Fluctuations in Viscous Wall Region for Newtonian and Drag Reducing Fluids." The Physics of Fluids, 20(10),S112-119.

Hanratty, T. J. and J. A. Campbell. 1983 "Measurement of Wall Shear Stress." in Fluid Mechanics Measurements (ed. R. J. Goldstein) pp. 559, Washington, New York, London: Hemisphere.

Hussain, A.K.M.F. and W. C. Reynolds. 1970 "The Mechanics of an Organized Wave in Turbulent Shear Flow." 41, part 2, pp. 241-258.

Jayaraman, R., P. G. Parikh and W. C. Reynolds. 1982 "An Experimental Study of Dynamics of an Unsteady Trubulent Boundary Layer." Report TF-18, Thermosciences Div., Dept. of Mech. Engrg., Stanford University, Stanford, California.

Karlsson, S.K.F. 1959 "An Unsteady Turbulent Boundary Layer" J. Fluid Mech., 5, p. 622-636.

Kirmse, R. E. 1979 "Investigations of Pulsating Turbulent Pipe Flow." Transactions of the ASME, J. Fluids Engineering, 101, pp. 436-442.

Kita, Y., Y. Adachi and K. Hirose. 1980 "Periodically Oscillating Turbulent Flow in a Pipe." Bulletin of the JSME, 23, pp. 656-664.

Lighthill, M. H. 1954 "The Response of Laminar Skin Friction and Heat Transfer to Fluctuations in the Stream Velocity." Proc. R. Soc. 224A, pp. 1.

Loyd, R. J., R. J. Moffat and W. M. Kays. 1970 "The Turbulent Boundary Layer on a Porous Plate: an Experimental Study of the Fluid Dynamics with Strong Favorable Pressure Gradients and Blowing." Report HMT-13, Thermosciences Div., Dept. of Mech. Engrg. Stanford University, Stanford, California.

Lu, S-Z. 1973 "Pulsating Turbulent Water Flow in a Tube," Ph.D. thesis, Clarkson College of Technology.

Mao, Z.-X. and T. J. Hanratty. 1984 "The Use of Scalar Transport Probes to Measure Wall Shear Stress in a Flow with Imposed Oscillations." to be published in Experiments in Fluids.

Mizushina, T., T. Maruyama and Y. Shiozaki. 1973 "Pulsating Trubulent Flow in a Tube." Jounral of Chem. Engrg. of Japan, 6, pp. 487-494.

Mizushina, T., T. Maruyama and H. Hirasawa. 1975 "Structure of the Turbulence in Pulsating Pipe Flows." Journal of Chem. Engrg. of Japan, 8, pp. 210-216.

Nikolaides, C. and T. J. Hanratty. 1983 "A Study of the Coherent Stuctures in the Viscous Wall Region of a Trubulent Flow." to be published.

Nikuradse, J. 1932 "Gesetzmässigkeit der trubulenten Strömung in glatten Rohren." Forschg. Arb. Ing.-Wes. No. 346. (or from Schilichting, H: Boundary-Layer Theory. 1979, pp. 598).

Ohmi, M., T. Usui, O. Tanaka and M. Toyama. 1976 "Pressure and Velocity Distributions in Pulsating Trubulent Pipe Flow. part 2 Experimental Investigations," Bulletin of JSME, 19, pp. 951-957.

Ohmi, M., S. Kyomen and T. Usui. 1978 "Analysis of Velocity Distribution in Pulsating Turbulent Pipe Flow with Time-Dependent Friction Velocity." Bulletin of JSME, 21, pp. 1137-1143.

Parikh, P. G., W. C. Reynolds, R. Jayaraman and L. W. Carr. 1981 "Dynamic Behavior of an Unsteady Turbulent Boundary Layer." Unsteady Turbulent Shear Flows, Springer-Verlag, pp. 35-46.

Parikh, P. G., R. Jayaraman and W. C. Reynolds. 1982 "Dynamics of an Unsteady Turbulent Boundary Layer." Turbulent Shear Flows 3, Springer-Verlag, pp. 34-45.

Ramaprian, B. R. and S. W. Tu. 1980 "An experimental Study of Oscillatory Pipe Flow at Transitional Reynolds Numbers" J. Fluid Mech. 100, pp. 513-544.

Ramaprian, B. R. and S. W. Tu. 1982 "Study of Periodic Turbulent Pipe Flow." IIHR Report 238, Iowa Institute of Hydraulic Research, The University of Iowa, Iowa City, Iowa.

Ramaprian, B. R. and S. W. Tu. 1983 "Fully Developed Periodic Turbulent Pipe Flow. Part 2. The Detailed Structure of the Flow." J. Fluid Mech. 137, pp. 59-81.

Rayleigh, Lord. 1911 "On the Motion of Solid Bodies Through Viscous Liquids." Phil. Mag. 21, 697-711; also Sci. Papers VI, 29.

Reiss, L. P. and T. J. Hanratty. 1963 "An Experimental Study of the Unsteady Nature of the Viscous Sublayer." A.I.Ch.E.J. 9, p. 154.

Reynolds, W. C. 1974 "Recent Advances in the Computation of Turbulent Flows." Adv. Chem. Eng. 9, 193-246.

Reynolds, W. C. 1976 "Computation of Turbulent Flows." Annual Rev. Fluid Mech. 8, 183-208.

Sarpkaya, T. 1966 "Experimental Determination of the Critical Reynolds Number for Pulsating Poiseuille Flow." J. Basic Eng. Trans. ASME Ser. D88, p. 589.

Schlichting, D. 1979 "Boundary-Layer Theory" pp. 93-94, pp. 408-445 McGraw-Hill Book Company.

Sexl, Th. 1930 "Über den von E. G. Richardson entdeckten 'Annulareffekt'." Z. Phys. 61, 349.

Shemer, L. and I. Wygnaski 1981 "On the Pulsating Flow in a Pipe" In Proceedings of the 3rd Symposium on Turbulent Shear Flows, Davis CA (University of California, Davis, CA, 1981) p. 8.13.

Simpson, R. L., B. G. Shivaprasad and Y.-T. Chew. 1981 "Some Features of Unsteady Separating Turbulent Boundary Layers." Unsteady Turbulent Shear Flows, Springer-Verlag., pp. 109-119.

Simpson, R. L., B. G. Shivaprasad and Y.-T. Chew. 1983 "The Structure of a Separating Turbulent Boundary Layer. Part 4. Effect of Periodic Free-Stream Unsteadiness." J. Fluid Mech. 127, pp. 219-261.

Simpson, R. L., B. G. Shivaprasad. 1983 "The Structure of a Separating Turbulent Boundary Layer. Part 5. Frequency Effects on Periodic Unsteady Free-Stream Flows." J. Fluid Mech. 131, pp. 319-339.

Sirkar, K. K. 1969 "Turbulence in the Immediate Vicinity of a Wall and Fully Developed Mass Transfer at High Schmidt Numbers." Ph.D. thesis, University of Illinois at Champaign-Urbana.

Sirkar, K. K. and T. J. Hanratty. 1970 "The Limiting Behavior of the Turbulent Transverse Velocity Component Close to a Wall." J. Fluid Mech., 44, pp. 605-614.

Stokes, G. G. 1851 "On the effect of the internal friction of fluids on the motion of pendulums." Cambr. Phil. Trans. IX, 8; Math. and Phys. Papers, Cambridge, III, 1-141 (1901).

Thorsness, C. B. 1975 "Transport Phenomena Associated with Flow Over a Solid Wavy Surface." Ph.D. thesis in Chemical Engineering, University of Illinois, Urbana.

Thorsness, C. B., P. E. Morrisroe and T. J. Hanratty. 1978 "A Comparison of Linear Theory with Measurements of the Variation of Shear Stress Along a Solid Wave." Chemical Engineering Science, 33, pp. 579-592.

Tu, S. W. and B. R. Ramprian. 1983 "Fully Developed Periodic Turbulent Pipe Flow. Part 1. Main Experimental Results and Comparison with Predictions." J. Fluid Mech. 137, pp. 31-58.

Uchida, S. 1956 "The Pulsating Viscous Flow Superposed on the Steady Laminar Motion of Incompressible Fluid in a Circular Pipe." ZAMP 7, 403-422.

Distribution List

Professor W. W. Willmarth
The University of Michigan
Department of Aerospace Engineering
Ann Arbor, MI 48109

Office of Naval Research
Code 481
800 N. Quincy Street
Arlington, VA 22217

Professor Richard W. Miksad
The University of Texas at Austin
Department of Civil Engineering
Austin, TX 78712

Professor Stanley Corrsin
The Johns Hopkins University
Department of Mechanics and
Materials Sciences
Baltimore, MD 21218

Professor Paul Lieber
University of California
Department of Mechanical Engineering
Berkeley, CA 94720

Professor P. S. Virk
Massachusetts Institute of Technology
Department of Chemical Engineering
Cambridge, MA 02139

Professor E. Mollo-Christensen
Massachusetts Institute of Technology
Department of Meteorology
Room 54-1722
Cambridge, MA 02139

Professor Patrick Leehey
Massachusetts Institute of Technology
Department of Ocean Engineering
Cambridge, MA 02139

Professor Eli Reshotko
Case Western Reserve University
Department of Mechanical and
Aerospace Engineering
Cleveland, OH 44106

Professor S. I. Pai
University of Maryland
Institute of Fluid Dynamics
and Applied Mathematics
College Park MD 20742

Computation and Analyses Laboratory
Naval Surface Weapons Center
Dahlgren Laboratory
Dahlgren, VA 22448

Dr. Robert H. Kraichnan
Dublin, NH 03444

Professor Robert E. Falco
Michigan State University
Department of Mechanical Engineering
East Lansing, MI 48824

Professor E. Rune Lindgren
University of Florida
Department of Engineering Sciences
231 Aerospace Engineering Building
Gainesville, FL 32611

Mr. Dennis Bushnell
NASA Langley Research Center
Langely Station
Hampton, VA 23365

Dr. A. K. M. Faz Hussain
University of Houston
Department of Mechanical Engineering
Houston, TX 77004

Professor John L. Lumley
Cornell University
Sibley School of Mechanical
and Aerospace Engineering
Ithaca, NY 14853

Professor K. E. Shuler
University of California, San Diego
Department of Chemistry
La Jolla, CA 92093

Dr. E. W. Montroll
Physical Dynamics, Inc.
P. O. Box 556
La Jolla, CA 92038

Librarian Station 5-2
Coast Guard Headquarters
NASSIF Building
400 Seventh Street, SW
Washington, DC 20591

Library of Congress
Science and Technology Division
Washington, DC 20540

Dr. A. L. Slafkosky
Scientific Advisor
Commandant of the Marine Corps
Code AX
Washington, DC 20380

Maritime Administration
Office of Maritime Technology
14th & E Streets, NW
Washington, DC 20230

Maritime Administration
Division of Naval Architecture
14th & E Streets, NW
Washington, DC 20230

Dr. G. Kulin
National Bureau of Standards
Mechanics Section
Washington, DC 20234

Naval Research Laboratory
Code 2627
Washington, DC 20375 6 copies

Library
Naval Sea Systems Command
Code 09GS
Washington, DC 20362

Mr. Thomas E. Peirce
Naval Sea Systems Command
Code 03512
Washington, DC 20362

Dr. Gary Chapman
Ames Research Center
Mail Stop 227-4
Moffett Field, CA 94035

Dr. Louis Schmidt
Assistant for Engineering Technology
Assistant Secretary of the Navy (RE&S)
Department of Navy
Washington, D.C. 20310

Mr. Stanley W. Doroff
Mechanical Technology, Inc.
2731 Prosperit Avenue
Fairfax, VA 2 031

Dr. Charles Wa..kins
Head, Mechanica Engineering Department
Howard University
Washington, DC 20059

Dr. Denny R. S. Ko
Dynamics Technology, Inc.
22939 Hawthorne Boulevard, Suite 200
Torrance, CA 90505

Air Force Office of Scientific
Research/NA
Building 410
Bolling AFB
Washington, DC 20332

Professor Hsien-Ping Pao
The Catholic University of America
Department of Civil Engineering
Washington, DC 20064

Dr. Phillip S. Klebanoff
National Bureau o Standards
Mechanics Section
Washington, DC 20234

Dr. G. Kulin
National Bureau of Standards
Mechanics Section
Washington, DC 20234

Dr. J. O. Elliot
Naval Research Laboratory
Code 8310
Washington, DC 20375

Mr. R. J. Hansen
Naval Research Laboratory
Code 8441
Washington, DC 20375

Library
Naval Weapons Center
China Lake, CA 93555

Technical Library
Naval Surface Weapons Center
Dahlgren Laboratory
Dahlgren, VA 22418

Technical Documents Center
Army Mobility Equipment Research Center
Building 315
Fort Belvoir, VA 22060

Technical Library
Webb Institute of Naval Architecture
Glen Cove, NY 11542

Dr. J. P. Breslin
Stevens Institute of Technology
Davidson Laboratory
Castle Point Station
Hoboken, NJ 07030

Professor Louis Landweber
The University of Iowa
Institute of Hydraulic Research
Iowa City, IA 52242

R. E. Gibson Library
The Johns Hopkins University
Applied Physics Laboratory
Johns Hopkins Road
Laurel, MD 20810

Lorenz G. Straub Library
University of Minnesota
St. Anthony Falls Hydraulic Laboratory
Minneapolis, MN 55414

Library
Naval Postgraduate School
Monterey, CA 93940

Technical Library
Naval Underwater Systems Center
Newport, RI 02840

Engineering Societies Library
345 East 47th Street
New York, NY 10017

The Society of Naval Architects and
Marine Engineers
One World Trade Center, Suite 1369
New York, NY 10048

Technical Library
Naval Coastal System Laboratory
Panama City, FL 32401

Professor Theodore . Wu
California Institute of Technology
Engineering Science Department
Pasadena, CA 91125

Director
Office of Naval Research Western Regional
1030 E. Green Street Office
Pasadena, CA 91101

Technical Library
Naval Ship Engineering Center
Philadelphia Division
Philadelphia, PA 19112

Army Research Office
P. O. Box 12211
Research Triangle Park, NC 27709

Editor
Applied Mechanics Review
Southwest Research Institute
8500 Culebra Road
San Antonio, TX 78206

Technical Library
Naval Ocean Systems Center
San Diego, CA 92152

ONR Scientific Liaison Group
American Embassy - Room A-407
APO San Francisco 96503

Librarian
Naval Surface Weapons Center
White Oak Laboratory
Silver Spring, MD 20910

Defense Research and Development Attache
Australian Embassy
1601 Massachusetts Avenue, NW
Washington, DC 20036

Dr. Steven A. Orszag
Cambridge Hydrodynamics, Inc.
54 Baskin Road
Lexington, MA 02173

Professor Tuncer Cebeci
California State University
Mechanical Engineering Department
Long Beach, CA 90840

Dr. C. W. Hirt
University of California
Los Alamos Scientific Laboratory
P. O. Box 1663
Los Alamos, NM 87544

Professor Frederick K. Browand
University of Southern California
University Park
Department of Aerospace Engineering
Los Angeles, CA 90007

Professor John Laufer
University of Southern California
University Park
Department of Aerospace Engineering
Los Angeles, CA 90007

Professor T. R. Thomas
Teesside Polytechnic
Department of Mechanical Engineering
Middlesbrough TS1 3BA, England

Dr. Arthur B. Metzner
University of Delaware
Department of Chemical Engineering
Newark, DE 19711

Professor Harry E. Rauch
The Graduate School and University
Center of the City University of
New York
Graduate Center: 33 West 42 Street
New York, NY 10036

Mr. Norman M. Nilsen
Dyntec Company
5301 Laurel Canyon Blvd., Suite 201
North Hollywood, CA 91607

Professor L. Gary Leal
California Institute of Technology
Division of Chemistry and Chemical
Engineering
Pasadena, CA 91125

Professor H. W. Liepmann
California Institute of Technology
Graduate Aeronautical Laboratories
Pasadena, CA 91125

Professor A. Roshko
California Institute of Technology
Graduate Aeronautical Laboratories
Pasadena, CA 91125

Dr. Leslie M. Mack
Jet Propulsion Laboratory
California Institute of Technology
Pasadena, CA 91103

Professor K. M. Agrawal
Virginia State College
Department of Mathematics
Petersburg, VA 23803

Technical Library
Naval Missile Center
Point Mugu, CA 93041

Dr. Joseph H. Clarke
Brown University
Division of Engineering
Providence, RI 02912

Professor J. T. C. Liu
Brown University
Division of Engineering
Providence, RI 02912

Chief, Document Section
Redstone Scientific Information Center
Army Missile Command
Redstone Arsenal, AL 35809

Dr. Jack W. Hoyt
Naval Ocean Systems Center
Code 2501
San Diego, CA 92152

Professor Richard L. Pfeffer
Florida State University
Geophysical Fluid Dynamics Institute
Tallahassee, FL 32306

Defense Technical Information Center
Cameron Station
Alexandria, VA 22314 12 copies

Professor Bruce Johnson
U.S. Naval Academy
Engineering Department
Annapolis, MD 21402

Library
U.S. Naval Academy
Annapolis, MD 21402

Technical Library
David W. Taylor Naval Ship Research
and Development Center
Annapolis Laboratory
Annapolis, MD 21402

Professor C. -S. Yih
The University of Michigan
Department of Engineering Mechanics
Ann Arbor, MI 48109

Professor T. Francis Ogilvie
The University of Michigan
Department of Naval Architecture
and Marine Engineering
Ann Arbor, MI 48109

Office of Naval Research
Code 200B
800 N. Quincy Street
Arlington, VA 22217

Office of Naval Research
Code 438
800 N. Quincy Street
Arlington, VA 22217 3 copies

Office of Naval Research
Code 473
800 N. Quincy Street
Arlington, VA 22217

NASA Scientific and Technical
Information Facility
P. O. Box 8757
Baltimore/Washington International
Airport
Maryland 21240

Professor Paul . Naghdi
University of California
Department of Mechanical Engineering
Berkeley, CA 94720

Librarian
University of California
Department of N al Architecture
Berkeley, CA 94720

Professor John V. Wehausen
University of California
Department of Naval Architecture
Berkeley, CA 94720

Library
David W. Taylor Naval Ship Research
and Development Center
Code 522.1
Bethesda, MD 20084

Mr. Justin H. McCarthy, Jr.
David W. Taylor Naval Ship Research
and Development Center
Code 1552
Bethesda, MD 20084

Dr. William B. Morgan
David W. Taylor Naval Ship Research
and Development Center
Code 1540
Bethesda, MD 20084

Director
Office of Naval Research Eastern/Central
Building 114, Section D Regional Office
666 Summer Street
Boston, MA 02210